2017

Impact of spatial variability of subsoil stiffness on immersed tunnels

Xinhang Wu

No. 4521285

2017-10-30

TU Delft

Impact of spatial variability of subsoil stiffness on immersed tunnels

By

Xinhang Wu

in partial fulfilment of the requirements for the degree of

Master of Science

in Civil Engineering

at the Delft University of Technology,

to be defended publicly on Monday October 30, 2017 at 13:30 PM.

Supervisor:	Dr. ir. W. Broere	TU Delft
Thesis committee:	Prof. dr. M. A. Hicks,	TU Delft
	Ir. K. Reinders,	TU Delft
	Ing. M. de Kant,	Royal HaskoningDHV

TU Delft

Royal HaskoningDHV
Enhancing Society Together

PREFACE

Time flies, a two-year master student life came to the end after finishing this final thesis research.

In January, I started my research at Royal HaskoningDHV, in Amersfoort. The topic “Impact of spatial variability of subsoils stiffness on immersed tunnels” is based on the project HZMB immersed tunnel in China. I am very lucky to work on such an interesting and challenging topic as a Chinese.

First, I would like to thank my supervisor Wout Broere, who gave me this rare opportunity and introduced me to such an excellent company. I am thankful for his patience and the valuable recommendations.

I would like to thank my supervisor in Royal HaskoningDHV, Martin de Kant, for giving me a chance to work on a topic I love. I am extremely grateful for his guidance during these 10 months.

I would like to thank Michael Hicks for his comments in understanding probabilistic theories and his suggestions on my research.

I would like to thank Kristina Reinders for her precious advices and her feed backs on my report.

During the time I spent in Royal HaskoningDHV, everyone there is friendly and always be ready to help. Especially thank to Rene Kuiper, for his critical suggestions for me to understand the detailed theory of immersed tunnel design.

I am grateful to my friends, my girlfriend and family for keeping me motivated and supporting me during this period.

Xinhang Wu

Delft, October 2017

ABSTRACT

Due to increased traffic density, there is a tendency to construct larger immersed tunnels with larger tunnel elements both in transversal and longitudinal direction resulting in a more critical design of the joints. Especially for those tunnels with relatively soft foundation and high siltation, there is no mature experience for reference. This not only requires a more detailed analyze of the joint itself, but also of the total behavior of the tunnel and its interaction with the subsoil.

Conventional deterministic designing procedure is based on average soil characteristics with sensitivity analyses including upper and lower boundaries of soil stiffness. The mentioned above trend of larger structures requires a more sophisticated probabilistic approach with deeper understanding of uncertainties and insight in probability of exceedance of requirements in serviceability limit state.

In this paper, a probabilistic analysis approach has been implemented to understand the shear behavior of tunnel joints. The biggest contributor for tunnel joints shear behavior is differential settlement between adjacent parts of the tunnel structure. Two probabilistic methods, Point Estimate Method and Monte Carlo Simulation are performed on settlement determination. The former is more efficient and with a considerable accuracy while, the latter is extremely accurate with high computational costs. For simple cases, Monte Carlo Simulations are commonly used to solve soil structure interaction problems due to its straightforward process and easily understandable theory. While for large and complex soil-structure interaction problem, it is computationally intensive to complete even a single run. Such practical disadvantage can be solved by modifying the algorithm or by performing computationally efficient probabilistic methods.

The soil-structure interaction analysis is researched by models set up in PLAXIS 2D. Python scripts are programmed in cooperation with PLAXIS models to perform Monte-Carlo Simulation in determination of shear forces in tunnel joints. The function of Python scripts is helping PLAXIS to select properties automatically and to storing the output after every single run.

The reliability analysis is done for different conditions in 3 models. Comparison shows that reliability significantly influenced by the distribution and correlation length of soil parameters.

Content

NOMENCLATURE

μ	mean
σ	standard deviation
σ^2	variance
COV	coefficient of variation
θ	scale of fluctuation
θ_h	horizontal scale of fluctuation
ρ	correlation coefficient
τ	absolute distance
e	void ratio
H	thickness
C_c	compression index
C_r	recompression index
E_s	secant modulus
E_{ur}	unloading-reloading modulus
E_q	equivalent stiffness
EI	bending stiffness
EA	normal stiffness
S	settlement
q_c	cone resistance
P	load
Γ	reduction function
P_f	probability of failure
Φ	cumulative standard normal distribution
R	reliability
n_f	number of failure
n	number of total simulations

PEM	point estimate method
MCS	Monte Carlo simulation
SLS	serviceability limit state
ULS	ultimate limit state
SOF	scale of fluctuation

1. Introduction

1.1 Research context

Immersed tunnels are mainly built for river, canal, or open sea crossing where the subsoil is regularly soft. Due to increased traffic density, there is a tendency to construct larger immersed tunnels with larger tunnel elements both in transversal and longitudinal direction resulting in a more critical design of the joints. This not only requires a more detailed analyze of the joint itself, but also of the total behavior of the tunnel and its interaction with the subsoil. Conventional deterministic designing procedure is based on average soil characteristics with sensitivity analyses including upper and lower boundaries of soil stiffness. The mentioned above trend of larger structures requires a more sophisticated probabilistic approach with deeper understanding of uncertainties and insight in probability of exceedance of requirements in serviceability limit state.

This thesis starts with a general qualitative assessment of uncertainties such as sub soil conditions, and the impact of these uncertainties on tunnel design. The uncertainty with largest impact on the design depends on the project, while for an immersed tunnel in soft soil conditions the spatial variability of the subsoil is expected to be the largest contributor. This aspect is then further elaborated. Based on the soil investigation data from the HZMB tunnel project in China, the spatial variability of the soil stiffness is assessed and its effect on the tunnel structure.

1.2 Research problem

In nature, soils are often inherently anisotropic due to the manner, in which they are deposited. It has been observed that the performance of foundations is considerably affected by the inherent spatial variability of the soil properties. The most likely problem is differential settlement, where soft zones of subsoil will settle more than stiff zones. For most immersed tunnels, the tunnel length is much bigger compared with its width, leading to more uncertainties in longitudinal direction which may cause shear failure in tunnel joints.

However, the uncertainties in transversal direction can also be considerable, which may possibly cause torsion failure to tunnel joints. Immersed tunnels usually have a length of thousands of meters, so it is hard to determine the exact soil stiffness and spatial stiffness distribution along the whole tunnel line.

Soil investigation is often limited due to scheduling and economic reasons, so assumptions have to be made based on interpolation of singular data points and on geological models if any.

Thus, in another word, uncertainties of soil always exist. How these uncertainties of soil stiffness will influence differential settlement as well as tunnel structure behavior will be further analyzed in this thesis.

1.3 Goal and Aim

Analyze the spatial variability of subsoil and estimate the reliability of shear forces in tunnel joints against Serviceability Limit State (SLS), in the form of excessive differential settlements, taking the HZMB immersed tunnel project as an example case.

1.4 Research Questions

From the above-mentioned problems, it is interesting to have an understanding on the behavior of inhomogeneous soils under immersed tunnel. Therefore, a list of research questions is asked.

- What are the influence factors of differential settlement in immersed tunnel foundation?
- How uncertainties of soil stiffness will impact on differential settlement?
- How gravel bed will influence on immersed tunnel settlement?
- What is the criterion of tunnel joints design regarding shear force?
- What is the reliability of shear forces in tunnel joints against SLS, taking spatial variability of the soil into account?

1.5 Research Method

To achieve the goal and aim of the report, a soil structure model is needed to set up to simulate the shear forces in tunnel joints and analyze the reliability against Serviceability Limit State. The results from this thesis need to be able to answer the mentioned above research questions. Based on the aim and research question, the main methodology of this research is shown as follow.

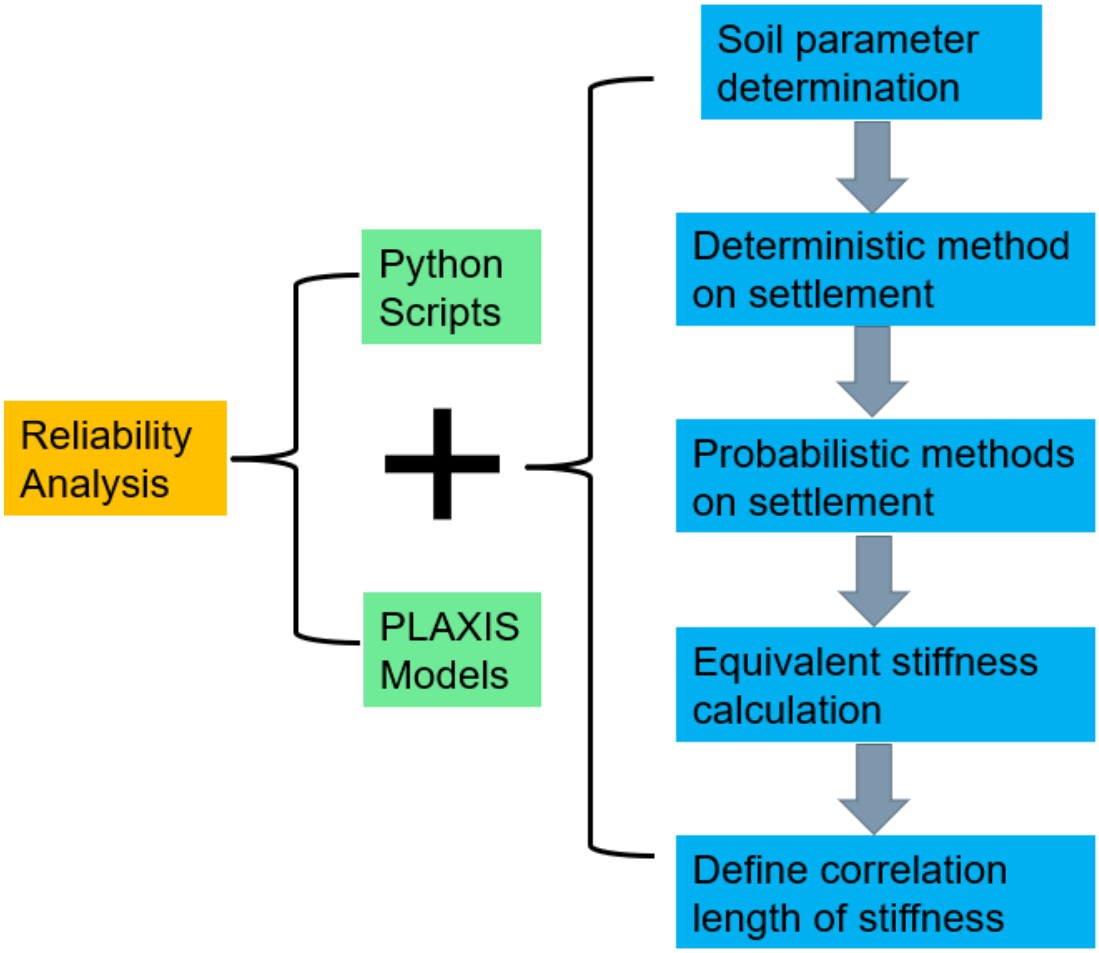

The “blue blocks” on the right of the above flow chart are on the purposes of determine the inputs in PLAXIS model, and Python scripts are programmed to perform Monte-Carlo Simulation in cooperation with PLAXIS.

1.6 Thesis Outline

This thesis presents the impact of these uncertainties on immersed tunnel joints design. The report includes six main chapters listed as follow

1. Introduction
2. Project background
3. Literature study
4. Probabilistic methods on settlement
5. Soil structure interaction and reliability analysis
6. Conclusions and Recommendations

In Chapter 2, the background of this case project in China will be introduced. An overview of the

site is provided to give an idea of the locations of the project and the dimension of the research area.

In Chapter 3, the relevant literature for this research is summarized. The literature study includes the influence factors on settlement of immersed tunnel and the basic principles analytical methods for settlement calculation. Furthermore, the principles of probabilistic methods applied in this research are introduced. Finally, basic theory of “beam-spring model” is summarized.

Chapter 4 starts with determinations of the stochastic properties of subsoil in the research area. Afterwards, Point Estimate Method and Monte Carlo simulations are performed on settlement calculation, the results are compared and discussed. Followed by analysis of influence of gravel bed on settlement. Finally, the equivalent stiffness of the subsoils is back calculated, and its correlation length is determined.

In Chapter 5, soil-structure interaction models are carried out in PLAXIS, in cooperation with Python coding, Monte-Carlo Simulations are performed on determination of the shear forces in tunnel joints. The reliability of tunnel joints against Serviceability Limit State of shear force is analyzed.

In the end, the results and discussions are summarized and concluded in Chapter 6, some recommendations are given.

2. Project Background

2.1 Introduction

The Hong Kong-Zhuhai-Macao Bridge (HZMB) is located at the entrance of the Pearl River, crossing the Lingding Bay in the South China Sea. This HZMB project, worth ¥80 billion, connects three metropolises in the south coast of China (Figure 2.1). It consists of designs and constructions of three navigable bridges, two artificial islands, and one immersed tunnel, including non-navigable and ramp bridges. As a key element of the HZMB project, the immersed tunnel crossing of Lingding West and Tonggu Fairway has a service life of 120 years (Hu, 2015).

This HZMB Tunnel (5990m), completed in 2016, exceeded the current record of BART tunnel (5825m) in the United States, although it will soon be overtaken by the 19km Fehmarn Tunnel between Denmark and Germany that is to be completed in 2020. The HZMB Tunnel is composed by a 5664 m underwater tunnel and two 326 m cut and cover sections, facing greater challenges that ever previously experienced.

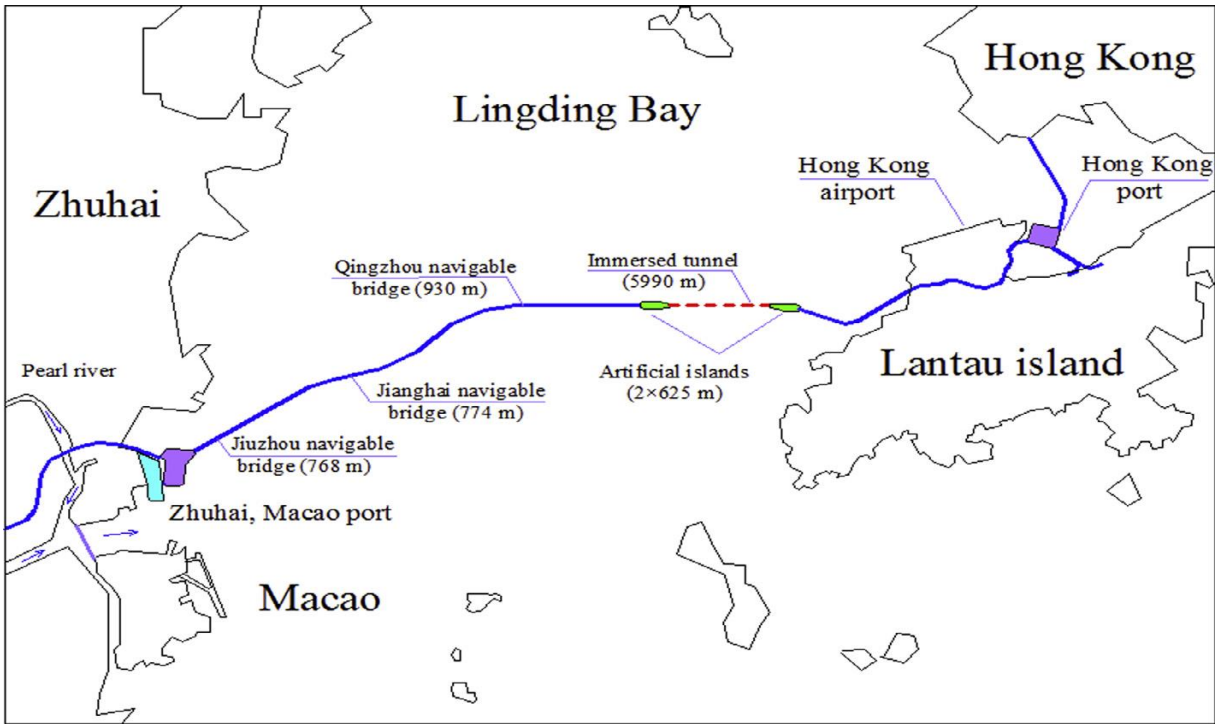

Figure 2.1 Location of HZMB immersed tunnel

Comparison of the length of existing immersed tunnels in the world is shown in Table 2.1 (Lunniss&Baber, 2013)

No.	Tunnel	Length(m)	Structure	Country
1	Hong Kong-Zhuhai-Macao Bridge	5990	Reinforce concrete	China
2	BART in San Francisco	5825	Single steel concrete	United States
3	Resund Link Strait Crossing	3510	Reinforce concrete	Denmark and Sweden
4	Busan-Geoje	3384	Reinforce concrete	Korea
5	Rotterdam Metro	2855	Reinforce concrete	Netherlands
6	Jurong Strait Utility	2600	Reinforce concrete	Singapore

Table 2.1 Length of immersed tunnels existing in the world (Lunniss and Baber, 2013)

2.2 Tunnel structure

The underwater tunnel consists of 33 rectangular concrete elements, with a standard length of 180 m each. Each element (shown in Figure 2.2) is 37.95 m wide and 11.40 m high, and the reinforced concrete box is 1.50 m thick. The bottom of the structure is about 45 m below the mean water lever, which makes it the third deepest immersed tunnel in the world after the Marmaray tunnel (58m) and Busan-Geoje tunnel (50 m) (Ingerslev, 2005).

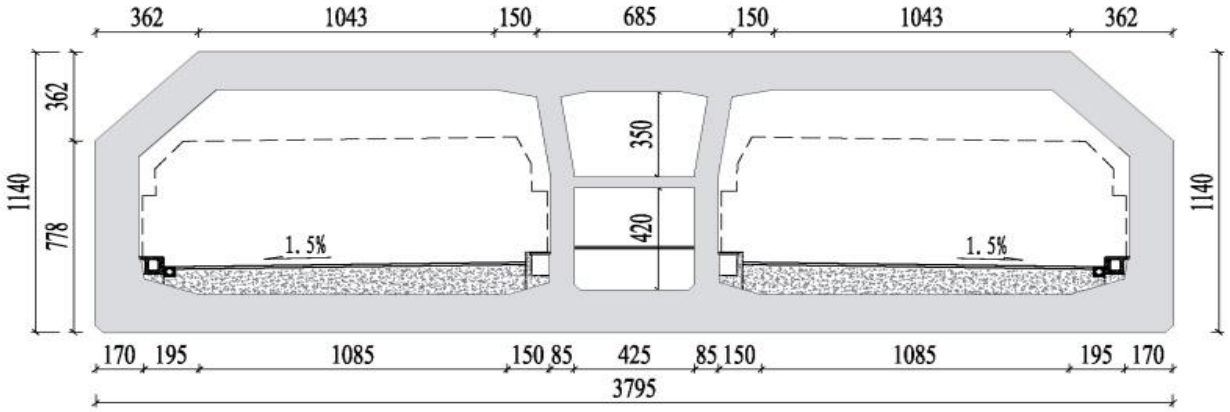

Figure 2.2 Cross section of HZMB immersed tunnel element

2.3 Geotechnical conditions

Figure 2.3 indicates the geotechnical and geomorphic profile along the tunnel alignment. The terrain of the tunnel site slopes gently, and the water depth is about 10-18m. Holocence deposits of a thickness from 10-25 m are found below the seabed surface. These soils consist of muck, mucky clay mixed with sand and can be classified as very soft, highly compressible and normally consolidated. Under the Holocene deposits, Late Pleistocene deposits are found, with a thickness that varies between 37m and 102m (locally). The Pleistocene deposits appear to be over consolidated and mainly consist of clay, silty sand, sand and gravel. The sand and gravel generally underlay the cohesive soils. Underneath the Pleistocene deposits, the bedrock mainly composed by mixed granite is encountered.

Seismic activity is not active in the tunnel site and destructive earthquakes have never happened before. According to the records, earthquakes ever happened at this site were smaller that magnitude 4.7. The detailed subsoil properties below tunnel elements are listed in **APPENDIX A**.

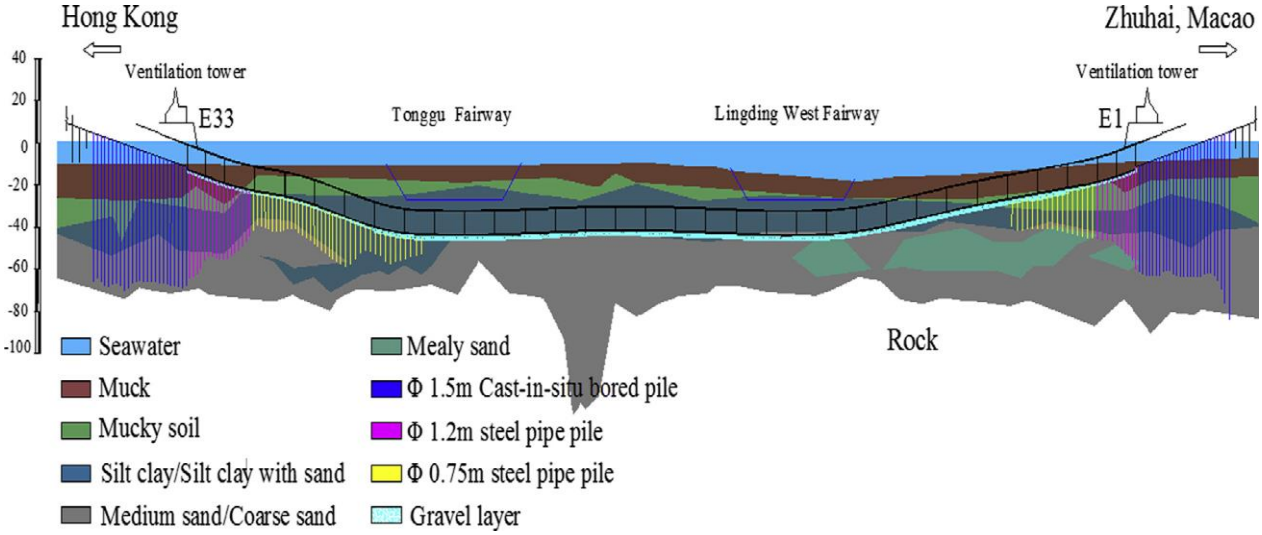

Figure 2.3 Soil strata in construction area

2.4 Immersed tunnel foundation

The structure-soil interaction is one of the governing factors in immersed tunnel design. The HZMB Tunnel is placed mainly on muck and silty clay at both ends and on silty clay or sand in the middle. As a consequence, differential settlements along the tunnel will definitely occur without ground improvement measures. In this project ground treatment is required over a considerable part of the tunnel alignment. The objective of the ground treatment is to improve the foundation conditions for the tunnel, in this way, the settlements and differential settlements can be limited and therefore also the internal forces in the tunnel.

Two design approaches were adopted for this project：

1） Improvement of the ground properties in terms of strength and stiffness and to increase the uniform behavior of the ground by means of.

- Replacement of soft soils by mean of sandy gravels or gravel.

- Settlement Reduction Piles in soft cohesive layers
- Cement deep mixing piles in soft cohesive layers
- Sand compaction piles

2） Foundation Piles on bearing ground layers in case the ground is too week or too unpredictable (close to the artificial islands where large reclamations are carried out)

The terminal sections (E1 and E33) are placed on 1.2 diameter steel pipe piles, while transition sections are applied 0.75m diameter steel pipe piles and a 2.0m gravel layer to transit settlements between the terminal and natural ground sections.

The middle parts of the tunnel (Element10-Element24) which placed on natural foundation are paved with a 1.3 m gravel layer made of 20-75mm sized gravels with a stiffness of 50Mpa.The cross section of tunnel element in middle part is indicated in Figure 2.4

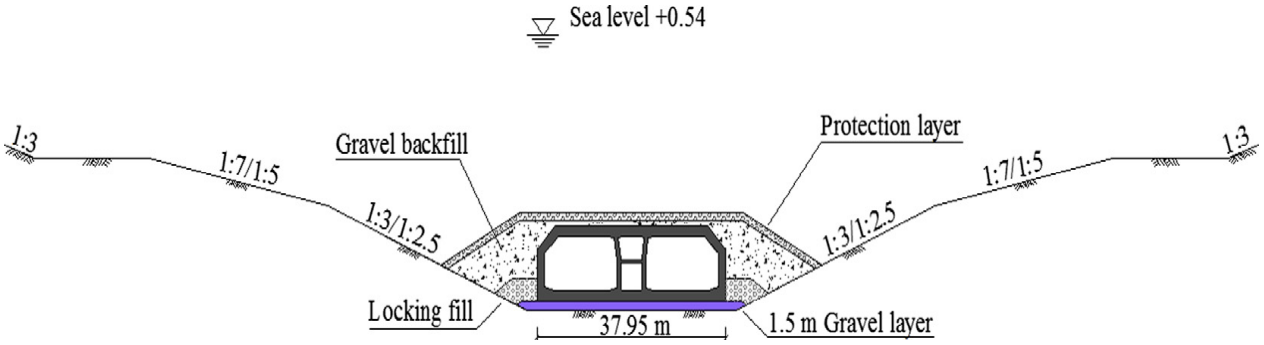

Figure 2.4 Cross section of tunnel element

The material and thickness of the subsoil are discontinuous along the tunnel alignment, which may cause uneven settlements after back filling. The mechanism of soil settlement is complex during construction and relevant to time in the operation phase. A portion of the soils under the tunnel will be recompressed after tunnel installation and backfilling. Detailed locations for tunnel elements are indicated in Figure 2.5.

In this report, settlement analysis is only based on the natural ground sections, which is from Element 10 to Element 24 (research area marked in Figure 2.5), and the acting load are estimated after placement of tunnel elements, backfilling and siltation. Detail information of loads on subsoils corresponding to the above element are listed in Table 2.2.

Element No	Load (kPa)	Element No	Load (kPa)	Element No	Load (kPa)
10	188.1	**15**	246.0	**20**	257.6
11	218.9	**16**	254.8	**21**	263.8
12	227.4	**17**	256.8	**22**	272.8
13	208.9	**18**	258.4	**23**	272.3
14	230.2	**19**	257.8	**24**	263.6

Table 2.2 Load acting on the subsoils based on each element

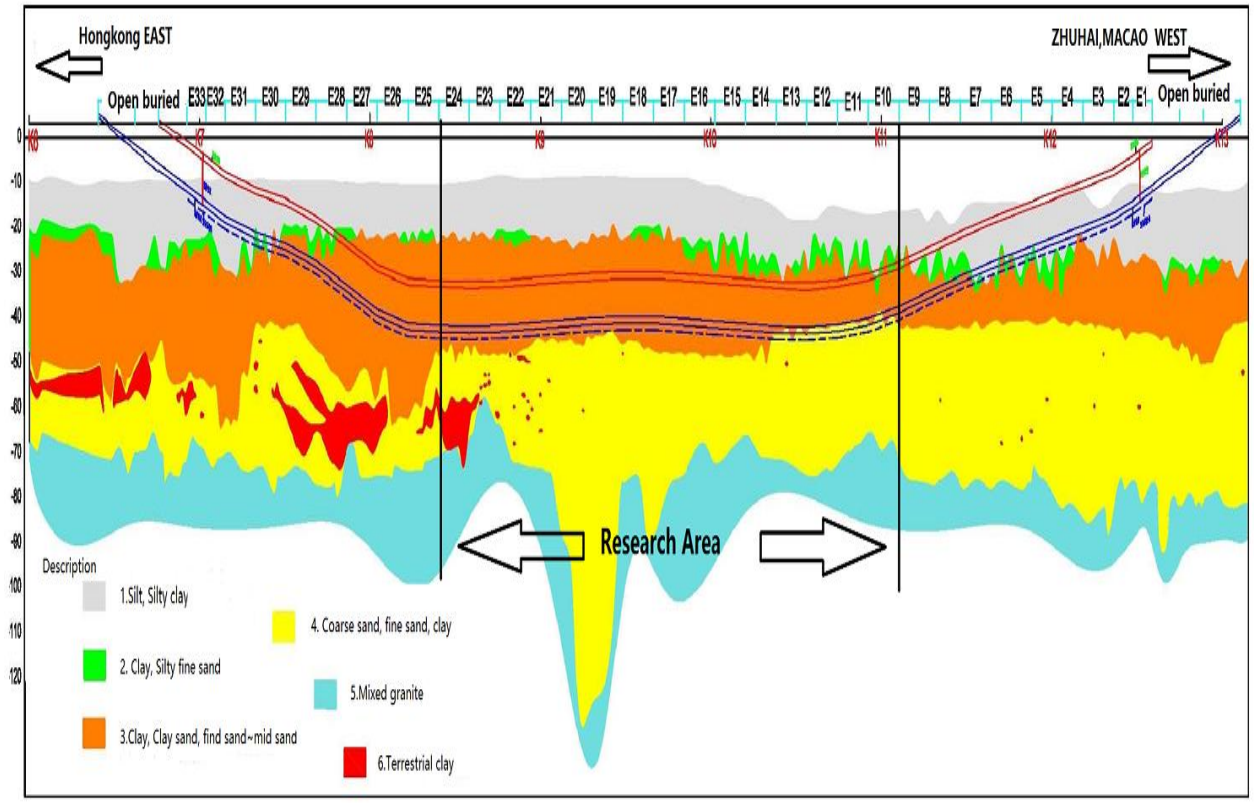

Figure 2.5 Location of research area

3. Literature study

In this chapter a theoretical background is given and previous research is summarized. Firstly, a summary of settlement behavior in immersed tunnel has been made, including the causes of settlement and descriptions of settlement mechanism and differential settlements. Then calculations for settlements of foundations on clay and sand are presented respectively, the relationship between CPT values and soil deformation properties is introduced. Finally, probabilistic methods in geotechnical engineering are discussed and a simplified soil-structure interaction model is illustrated.

3.1 Settlement of immersed tunnel

3.1.1 Causes of settlement of immersed tunnel

To estimate the total settlement caused by tunnel element after it is put on the bottom of its dredged trench and covered over with backfill materials, there are numbers of factors that should be taken into account which are presented below. Some can be determined by calculation, others only by judgement and experience.

Subsoil conditions

Because of the weight of a fully ballasted element is only approximately 10% heavier than water and much less than the submerged weight of the soil it replaces (Walter, 2001), it is somewhat surprising how much settlement can occur when the element is backfilled. The single most important factor (apart from any exceptionally heavy surcharge) to influence the magnitude of settlement of an immersed element, is the stiffness of the supporting soil layers. Relatively little settlement occurs and final stable grades are quickly reached if consolidated sands and silts with little or no rebound are encountered. The change in grade from placement of the element to full surcharge under these conditions is mostly limited to ‘nestling’ of the element into the screeded or pumped sand foundation. On the other hand, if the subsoils consist of thick layers of compressible soils with considerable rebound, the magnitude of settlement is likely to be several times as much, and may take much longer to stabilize.

Settlements expected as a result of seismic consolidation or potential liquefaction is generally unacceptable and some forms of ground modification may be required.

Siltation

Siltation is the sediment back filling the trench after dredging process and after installation of the tunnel. It plays an important role in immersed tube tunnel settlement either in construction or operation. In construction, over siltation affect the safety and accuracy of the tube sinking; in operation, uneven siltation can cause overload lead to uneven settlement, which must be dredged from time to time, however, the cyclical silting and dredging disturbs the foundation and original soil. (Gang, 2012)

This is especially troublesome in the case of tunnel elements supported on jacks prior to installing

a jetted sand or sand flow foundation where the interface becomes inaccessible. For a carefully graded gravel bed, a build-up of sand or silt can be also a serious problem. Even every effort is made to carry out the final screeding and sounding check just hours before placing the element, siltation can occur unexpectedly. For example, a carelessly operated contractor's tugboat can blast sand onto the bedding with its propeller. When the element is found to rest too high or somewhat rolled transversely, to raise and lower the element in its proper attitude, the excess silt is either flushed out from under the element, or made to conform to the irregularities of the bottom plate. Removing it to an anchorage location and re-screeding the bedding surface might not be possible, careful airlifting may be the method to remove the excess material.

Trench dredging methods

(Walter, 2001) mentioned that it is difficult to quantify the relative effect of different kinds of dredging equipment on later settlements. Normally, hydraulic cutter-head suction dredges and/or clamshell bucket dredges are used to excavate the tunnel trench. The first type is generally used in shallower water followed by the second type in deeper water. Often both are utilized for the trenches that exceed the normal operating depth of the ladders of available cutter-head dredges. In sands, there would seem to be little difference between the two methods. In stiff clays, the disruption of the bottom might be less with the cutter-head than with a grab bucket. The latter may tend to leave a more irregular bottom with larger voids that can take longer for the foundation material to fill and stabilize. Where the trench is excavated by blasting methods in rock and a sand/gravel foundation course is later screeded or pumped over the blasted surfaces, long-term settlements might result from the gradual migration of foundation materials into the fissures and broken rock left in the bottom of the trench.

Deficiency during construction

Deficiency during construction like the treatment of the foundation not dense enough, the gap between the foundation and tunnel element is too large, dredging disturbs the original soil too much, irregular over break etc. can be not negligible factors considering the settlement. They affect the settlement together with the factors describe before and enlarged the influence.

3.1.2 Settlement mechanism

Immersed tunnel settlement is mainly caused by compression deformation of foundation layer and recompression deformation of original soil. When analyze settlement mechanism of a non-pile foundation immersed tunnel, the changing of foundation load in construction processes should be considered. The construction process of an immersed tunnel is as follows:

a) original soil excavation and unloading

b) cleaning siltation (happens immediately after trench dredging)

c) placement of foundation layer

d) installation of tunnel element

e) refilling of overlaying soil

Research shows that weak soil is mainly produced in process (a) and (b), by disturbance and

siltation.

Settlement mechanism will be analyzed from aspect of original soil and foundation layer as follow.

a) To original layer, it is a mechanical process of unloading-reloading in construction process, unloaded by excavation and recompressed by tunnel placement and siltation. From the point of soil stress history, since the tunnel element itself is only slightly heavier than water, so after placement of the elements, the subsoil is still under over-consolidation state. In operation period, with the increase of external load, the pressure on original soil increases and may exceeds the pre-consolidation state. Then the original soil comes to be normal-consolidated. And with further consolidation, the further settlement is accumulated. Whether the soil stress state will be excessed or not, depends on the over-consolidation ratio determined after construction process.

b) To the foundation layer, during construction period, the layer is subjected to several kinds of load by placing tunnel elements, backfilling the cover soil and operating. The particles of foundation layer are rearranged and the void ratio decreases.

3.1.3 Differential settlements

The differential settlement between one part on a structure and another is of greater significance to the stability of the structure than the magnitude of the total settlement. If the whole structure settles to the same extent, there is no big influence on the tunnel joints. If however, there is relative movement between various parts of the tunnel, stresses are set up in the structure. Serious cracking, damaging of the tunnel joints, may occur while the differential movements are excessive.

Differential settlements between parts of an immersed tunnel may occur as a result of the following:

a) Variations in strata.

1. One elements of the tunnel may be placed on a compressible soil and the other on incompressible or relative stiffer material.
2. In areas of irregular bedrock surface, parts of a tunnel may be founded on shallow rock and others on soil or compressible weathered rock. Or the layer thickness between the element bottom and the bedrock may also be different.

b) Variations on foundation loading.

In ideal condition, the load acting on tunnel elements are similar with each other. While in the reality, the tunnel line is not paralleled to the sea level, which means, those elements with deeper elevation, will suffer larger siltation after construction. Then the load acting on these elements are obviously larger than others.

c) Variation in site conditions.

One part of the tunnel area may have been occupied by a heavy structure which had been removed or demolished; or on a sloping site it may be necessary to remove a considerable thickness of overburden to form a level site. These variations results in different stress state both before and after loading with consequent differential settlement or swelling.

3.2 Estimation of settlements of foundations on clay

3.2.1 One dimensional consolidation settlement

Void ratio and settlement changes under a constant load

The initial volume of a soil is $V = 1 + e_0$, where e_0 is the initial void ratio.

The change in volume of the soil is equal to the change in void ratio. Then the volumetric strain can be calculated from the change in void ratio as

$$\varepsilon_p = \frac{\Delta z}{H_0} = \frac{\Delta e}{1+e_0} \tag{3.1}$$

Where, H_0 is the initial height of the soil layer. The Equation can be rewritten as

$$\Delta z = H_0 \frac{\Delta e}{1+e_0} \tag{3.2}$$

Here S is going to be used to denote consolidation settlement rather than Δz , so

$$S = H_0 \frac{\Delta e}{1+e_0} \tag{3.3}$$

The void ratio at any time under load P is

$$e = e_0 - \Delta e = e_0 - \frac{\Delta z}{H_0}(1+e_0) \tag{3.4}$$

Effects of vertical stress on consolidation

Applying additional loads to the soil and for each load increment we can calculate the final void ratio from Equation (3.4) and plot the results, as shown by segment AB in Figure 3.1. Three types of graph are shown is Figure 3.1 to illustrate three different arbitrary ways of plotting the data from test. Figure 3.1a is an arithmetic plot of the void ratio versus vertical effective stress. Figure 3.1b is a similar plot except the vertical effective stress is plotted on a logarithmic scale. Figure 3.1 c is an arithmetic plot of the vertical strain versus vertical effective stress. The segment AB in Figure 3.1a and c are not linear because the settlement that occurs for each increment of loading brings the soil to a denser state from its initial state, and the permeability of soil decreases. Therefore, doubling the load from a previous increment, for example, would not cause a twofold increase in settlement. The segment AB is called normal consolidation line (NCL). In a plot of stress (log scale) versus void ratio, the NCL is approximately a straight line.

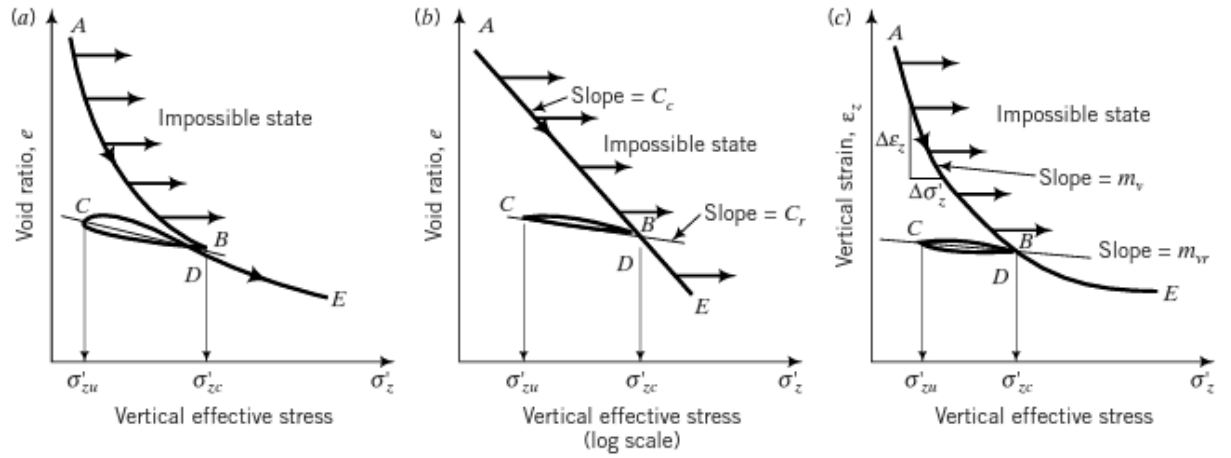

Figure 3.1 Stress vs void ratio (Tawfiq, 2010)

When an increment of load is removed, the soil will start to swell by absorbing water. The void ratio increases, but the increase is much less than the decrease in void ratio for the same magnitude of loading that was previously applied.

The reloading path CD is convex compared with the concave unloading path BC. One reason for this is the evolving soil structure (soil particles arrangement) during loading and unloading. At each loading/unloading stage, the soil particles are reorganized into a different structural frame work to resist the load. The average slopes of the unloading path and the reloading path are not equal, but the difference is assumed to be small. We will represent the unloading–reloading path by an average slope BC and refer to it as the recompression line or the unloading–reloading line (URL).

Once the past maximum vertical effective stress σ'_{zc} is exceeded, the slope of the path followed by the soil, DE, is approximately the same as that of the initial loading path (line AB). Unloading and reloading the soil at any subsequent vertical effective stress would result in a soil's response similar with paths BCDE.

3.2.2 Primary Consolidation Parameters

The primary consolidation settlement of the soil (settlement that occurs along path AB in Figure 3.1) can be expressed through the slopes of the curves. Two slopes are going to be defined for primary consolidation. One is called the coefficient of compression or compression index Cc and is obtained from the plot of e versus $\log\sigma'_z$ (Figure 3.1) as

$$Cc = -\frac{e_2 - e_1}{\log\dfrac{(\sigma'_z)_2}{(\sigma'_z)_1}} \qquad \text{(no units)} \tag{3.5}$$

where the subscripts 1 and 2 denote two arbitrarily selected points on the NCL.

Similarly, slope BC can be determined in Figure 3.1b as the recompression index Cr, which can be expressed as

$$Cr = -\frac{e_2 - e_1}{\log \frac{(\sigma_z^{'})_2}{(\sigma_z^{'})_1}} \tag{3.6}$$

where the subscripts 1 and 2 denote two arbitrarily selected points on the URL (unloading-reloading line).

3.2.3 Procedure to calculate primary consolidation settlement

The procedure to calculate primary consolidation settlement is as follows (Tomlinson, 2001):

1. Calculate the current vertical effective stress ($\sigma_{z0}^{'}$) and the current void ratio (e_0)

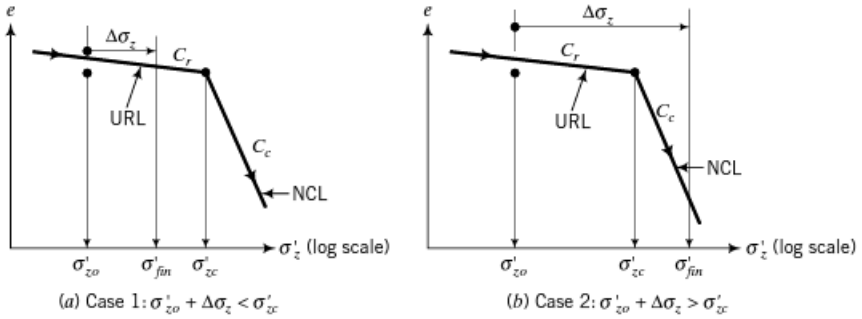

Figure 3.2 Two cases to consider for over consolidated soil settlement

2. Calculate the applied vertical stress increase ($\Delta\sigma_z$) at the center of the soil layer.
3. Calculate the final vertical effective stress $\sigma_{fin}^{'} = \sigma_{z0}^{'} + \Delta\sigma_z$
4. Calculate the primary consolidation settlement

a) If the soil is normally consolidated (OCR=1), the primary consolidation settlement is

$$S = \frac{H_0}{1+e_0} Cc \log \frac{\sigma_{fin}^{'}}{\sigma_{z0}^{'}} \tag{3.7}$$

b) If the soil is over-consolidated and $\sigma_{fin}^{'} < \sigma_{zc}^{'}$ (the maximum effective stress before unloading) the primary consolidation settlement is

$$S = \frac{H_0}{1+e_0} Cr \log \frac{\sigma_{fin}^{'}}{\sigma_{z0}^{'}} \tag{3.8}$$

c) If the soil is over-consolidated and $\sigma'_{fin} > \sigma'_{zc}$, the primary consolidation settlement is

$$S = \frac{H_0}{1+e_0}(Cr \log \frac{\sigma'_{zc}}{\sigma'_{z0}} + Cc \log \frac{\sigma'_{fin}}{\sigma'_{zc}}) \quad (3.9)$$

Where， H_0 is the thickness of the soil layer.

3.3 Estimation of settlements of foundations on sands and gravels

Settlements of foundations on sands and gravels take place almost immediately when the foundation loading is imposed on them. The Schmertmann equation for calculating the settlement of foundations on cohesionless soil is

$$S = C_1 C_2 \Delta_p \sum_0^{2B} \frac{I_z}{E_s} \Delta_z \quad (3.10)$$

Where

C_1 = depth correction factor

C_2 = creep factor

Δ_p = net increase of load on soil at foundation level due to applied loading

B = width of loaded area

I_z = vertical strain influence factor (Figure 3.3)

E_s = a secant Young's modulus

Δ_z =thickness of soil layer

(Schemertmann, 1970) suggested that value of Young's modulus could be determined using the cone penetration resistance of the soils at the site. In the case of normally loaded cohesionless materials, the modulus of the sand Es is related to the cone end resistance qc for each soil layer by $\mathrm{Es} = \alpha \mathrm{qc}$. The value α , based on the shape of foundation, consolidation state and loading magnitude.

Where

α=2.5 for a square foundation (L/B = 1)

α= 3.5 for a strip foundation (L/B>10)

These values are in the case of a load increment from 100 to 300 kN/m^2. While the Young's modulus Es, for either mechanically over consolidated or aged sands can be significantly higher.

The depth correction factor is given by

$$C_1 = 1 - 0.5\left(\frac{\sigma'_{vo}}{\Delta_p}\right) \tag{3.11}$$

Where σ'_{vo} = effective overburden pressure at foundation level.

Although settlements on cohesionless soil are considered as immediate, observations frequently show long-term creep (Schemertmann, 1970), which can be calculated by the factor

$$C_2 = 1 + 0.2\log_{10}\left(\frac{time_{years}}{0.1}\right) \tag{3.12}$$

The vertical strain factor is obtained from one of the two curves from Figure 3.3.

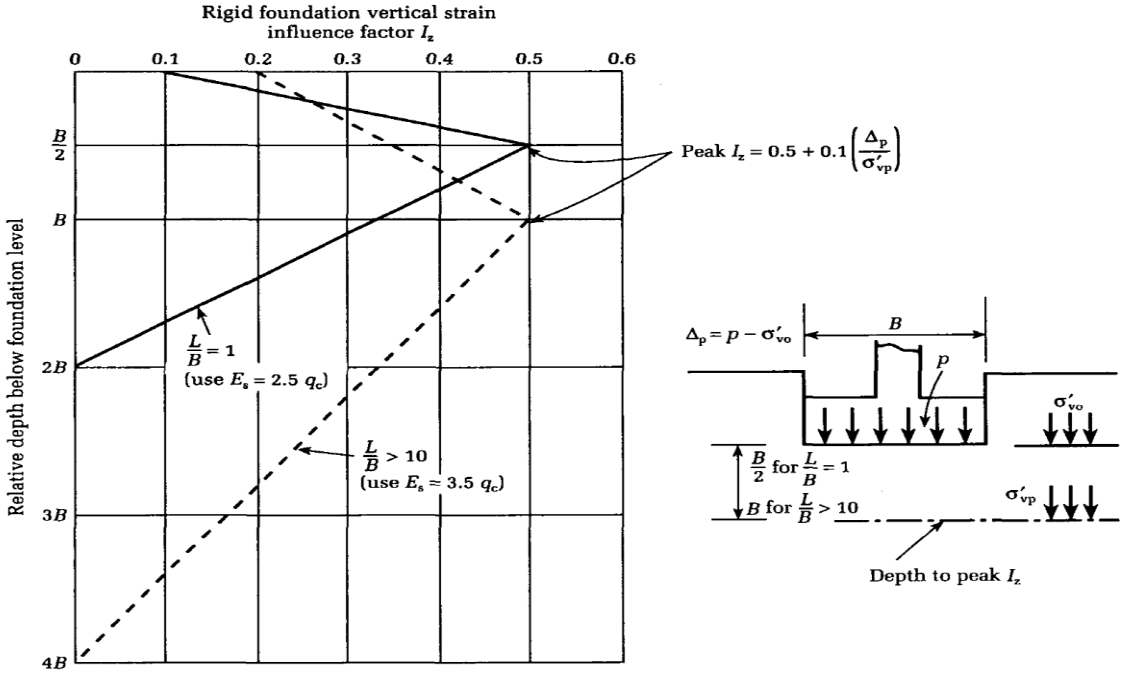

Figure 3.3 Vertical strain influence factor diagrams (Schmertmann, 1978)

Since HZMB immersed tunnel has a dimension with 5990m in length, and 37.95m in width, which means that L/B is much bigger than 10.

From the figure, the dashed line L/B>10 is used, the calculation depth should be the distance from the bottom of the element until 4B theoretically. While, 4B is way larger than the distance from bottom of the element to the bedrocks which are considered uncompressible, thus, vertical strain factor is then determined by the equation:

$$I_z = 0.2 + 0.008 * d$$

Where, “d” is the distance from the top of the foundation layers until bedrocks, equaling to approximately 30 meters.

3.4 Uncertainties

Geotechnical designs are seriously influenced by different kinds of uncertainties, in which, the most significant uncertainty is the spatial variability of soil. Since, it is not possible to take these uncertainties into account in traditional deterministic design, a proper probabilistic analysis is needed which provides the possibility of including uncertainties and making a better assessment of the reliability of a structure.

3.4.1 Soil uncertainties

According to (Kulhawy, 1992), uncertainty in soil can be attributed to three different sources (Figure 3.4) :

- Variability of soil parameters
- Measurement errors
- Transformation errors and uncertainty.

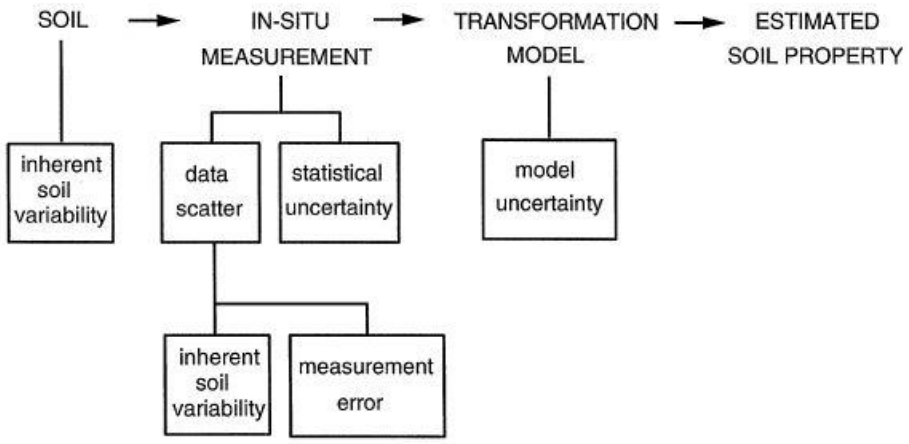

Figure 3.4 Sources of uncertainties (Kulhawy, 1992)

Most relevant categories are aleatory and epistemic uncertainty, which coincide in most geotechnical practical applications (Baecher, 2005). The aleatory uncertainty is associated with the natural variability of soil properties. This inherent variability of soil can be attributed to the deposition processes that lead to the formation of the soil, and ongoing geological processes that continue to alter the soil body. It is often modelled with random variables and can be quantified by soil investigation measurements, statistical approximations and engineering experience.

Measurement errors on the other hand arise from equipment error and other random effects. Measurement error can be improved upon and therefore falls under epistemic uncertainty. Inherent variability and measurement errors together can be characterized as data scatter. The last source of uncertainty is attributed to the transformation of results from in situ and lab parameters to design parameters which is also categorized as epistemic.

3.4.2 Coefficient of variation

In this research, inherent soil variability is considered, probabilistic analyses can be used to take this type of variability into account. With these analyses uncertain variables are introduced as stochastic variables, described by their mean (μ), and standard deviation (σ). Coefficient of variation (COV) is a non-dimensional statistical parameter that can describe the dispersion of a probabilistic distribution relative to mean, it is defined as the ratio of standard deviation over the mean of a parameter ($\mathrm{COV} = \sigma/\mu$). It is considered the most straightforward and widely used parameter to describe the uncertainty of soil properties and is used to make an approximation of the range of occurring soil properties.

In optimal geotechnical design situations, the coefficient of variation can be determined by sufficient soil investigation data. When this kind of data is unavailable, estimations on the range of COV can be obtained from literature and design standards.

In this research, based on the local soil investigation report, the mean values of COV's for all input variables are calculated and listed in Table 3.1.

Soil property	Symbol	Averaged Cov	Unit
Thickness of sand layer	hs	0.16	[m]
Thickness of clay layer	hc	0.15	[m]
Void ratio	e	0.11	[--]
Recompression index	Cr	0.28	[--]
Reloading Modulus	Eur	0.19	[MPa]

Table 3.1 Coefficient of variation of different variables

In probabilistic analysis, it is important to choose a probability distribution properly based on the values of COV of this variable. Assuming inappropriate distribution may lead to unrealistic values for soil properties in some cases. For example, in normal distributions, the values at lower boundary can be minus infinite, a small possibility exist that negative values occur.

Above mentioned problems frequently occur in case that variables have high COV's ($COV \geq 0.3$). To solve this problem, a lognormal distribution or other non-negative distributions should be used to avoid the possibility of negative values (Schnerder, 2012).

However, due to variance reduction in the cases of large soil volumes, it is often still acceptable to assume a normal distribution. For small coefficients of variation (($COV \leq 0.15$) the results are very similar between normal and lognormal distribution, and the probability of negative values is close to zero (S.P.Kamp, 2016). As indicated in Table 3.1, the COVs for all variables are less than 0.3, thus a normal distribution should be suitable in this paper.

3.4.3 Scale of fluctuation

In the conventional analyses of geotechnical engineering problems, the soil profile is usually modeled by homogenous layers in which the soil property is assumed to be deterministic and know at every point. However even within these homogenous layers, the soil property can show considerable variation from one location to another. This variability is associated with geology and the conditions during soil deposition. Considering the variability of soil, the probabilistic modeling of soil profiles was put forward by (Vanmarcke, 1977). Reliability of a structure is determined as a function of both point statistics (COV, discussed in previous section) and a spatial correlation property or autocorrelation function.

The autocorrelation function is usually expressed in terms of an exponential decaying function referred to as the scale of fluctuation (θ). θ is defined as the distance beyond which the correlation between soil properties becomes negligible. In other words, it is the measure of distance between adjacent strong and weak zones (Hicks, 2016). Scale of fluctuation, θ, can be classified further into θ_v and θ_h ,which are vertical and horizontal scale of fluctuation, respectively. Due to deposition processes, the value of θ_h is much higher than that of θ_v, which shows the anisotropy of soil heterogeneity.

Calculation of scale of fluctuation

Supposing one-dimensional homogeneous normal random field Y(z), its stochastic integral on [z, z+h] is

$$Y_h(z) = \frac{1}{h}\int_z^{z+h} Y(z)dz \tag{3.13}$$

Where h is the average length. Obviously,

$$\{E[Y]_h(z)] = E\left[\frac{1}{h}\int_z^{z+h} Y(z)dz\right] = \frac{1}{h}\int_z^{z+h} E[Y(z)]dz = 0 \tag{3.14}$$

That is to say, the local average of the random field is the same as the average of the original random field.

Supposing the variance of the random field is σ^2,the correlation function is $\rho(\tau)$, and the variance of $Y_h(z)$ is

$$\mathrm{Var}[Y_h(z)] = \sigma^2\left[\frac{2}{h}\int_0^h \left(1-\frac{\tau}{h}\right)\rho(\tau)d\tau\right] \tag{3.15}$$

Where, τ is the sample interval, standing for the distance to calculate the correlation function.

Considering that the variance reduction function is as follow:

$$\Gamma^2(\mathrm{h}) = \frac{Var[Y_h(z)]}{\sigma^2} = \frac{2}{h}\int_0^h \left(1-\frac{\tau}{h}\right)\rho(\tau)d\tau \tag{3.16}$$

The function above reflects the relationship between the variance reduction function and correlation function. The variance reduction function can be calculated by integration in case the correlation function form is determined.

In 1977, (Vanmarcke, 1977), put forward that

$$\lim_{h\to\infty} \mathrm{h}\cdot\Gamma^2(\mathrm{h}) = 2\lim_{h\to\infty}\int_0^h \left(1-\frac{\tau}{h}\right)\rho(\tau)d\tau = 2\int_0^h \rho(\tau)d\tau = \theta \tag{3.17}$$

Where θ is the scale of fluctuation, within the region, the soil properties are correlated; on the contrary, the soil properties are uncorrelated. When h is large enough, there exists:

$$\mathrm{h}\cdot\Gamma^2(\mathrm{h}) = \theta \tag{3.18}$$

Many methodologies have been developed to determine the scale of fluctuation, in this research, Space average method is introduced and later used in Chapter 4 to determine the scale of fluctuation of soil stiffness.

The space average method is to obtain the scale of fluctuation through the variance reduction function. In this method, h and sample interval Δz are taken as times of the sample distance Δz_0 , i.e., $\mathrm{h} = \Delta z = i\Delta z_0$. When the averages of adjacent samples are taken as new samples, and their variance can be worked out, then the variance reduction function can be written as

$$\Gamma^2(\mathrm{i}) = \frac{Var(\mathrm{i})}{\sigma^2} \tag{3.19}$$

The scale of fluctuation is a constant when the value of h is large enough, which indicates that in the curve of $\Gamma(\mathrm{i})—i$, $\Gamma(\mathrm{i})$ is stable when the value of i is larger than some value. Taking this i as n^*, which is named as the stable point, the scale of fluctuation can be derived according to

$$\theta = n^*\Delta z_0\Gamma^2(n^*) \tag{3.20}$$

This method is simple to be implemented, however, the stable point is usually hard to obtain due to the quality of data or the shortage of samples.

3.5 Probabilistic/ Reliability analysis methods

The ultimate limit state evaluation of a safety of a structure in its simplest form is expressed as the resistance of a structure (R) versus its load (S). This can be expressed in terms of a limit state Z where

$$\mathrm{Z} = \mathrm{R} - \mathrm{S} \tag{3.21}$$

Failure of the structure will occur when S > R or in other words Z < 0. A general formation for the limit state Z is

$$\mathrm{g(X)} = \mathrm{Z} = 0 \tag{3.22}$$

Where g is the limit state function and the vector X consists of n variables such as material properties, loads and geometric properties. Some of these are random variables and therefore must be considered with a probabilistic distribution. On the other hand, some variables have little or no variability in time and space, and therefore can be considered deterministic. Let $\mathrm{fx(x)}$ be the n dimensional PDF for the n variables X_i, the probability of failure can therefore be defined as

$$P_f = \int_{g(x)<0} fx(x)dx \tag{3.23}$$

If the number of dimensions is 2 (n=2), then the probability of failure can be determined with the use of joint probability distribution of R and S. The failure probability corresponds to the area where g(x)<0.

Reliability is the compliment of probability of failure and it expresses the probability of a safe structure. Reliability index β, is used as a measure of safety and was defined by (Cornell, 1969) as

$$\beta = \frac{0-\mu_z}{\sigma_z} = \frac{1}{COV_z} \tag{3.24}$$

Where COV_z refers to the coefficient of variation of Z. β is directly related to probability of failure and P_f can be expressed as

$$P_f = \Phi(-\beta) \tag{3.25}$$

Where, Φ is a cumulative standard normal distribution. Methods to elaborate the reliability of a structure can be divided into three different levels

Level I: semi-probabilistic methods：

Similar with engineering codes (e.g. Eurocode 7), uncertain parameters are modelled with used of partial factors and only characteristic value for S and R.

Level II: approximation methods:

Uncertainties are modeled with the use of their first two points statistics (variance and mean) and cross-correlation. A straightforward method is the Point Estimate Method, which will be elaborated in the next section.

Level III: fully probabilistic methods:

These methods use the full probability density functions of all uncertain parameters without simplifications and approximations of the model. An example of these reliability methods is crude Monte Carlo Simulation, also introduced in next section.

3.5.1 Point Estimate Method

Point Estimate Method (PEM) is a relatively simple method to evaluate the reliability of a structure. This method is a computationally straightforward approach to explicitly account for uncertainty of input parameters. PEM is able to estimate the statistical moments, i.e. mean and variance, of the output. The general idea is to simplify the entire distribution of a variable by a discrete equivalent distribution. This is done by assigning the same three first statistical from the complete original distribution to the new equivalent distribution. Before performing calculations with PEM, evaluations points need to be defined. Generally, two evaluations points are defined, located at one standard deviation on either side of the mean value. This is done for each stochastic input parameter. Next the performance function is calculated for every possible combination of the evaluation points. This results in 2n calculations, where n is the number of included stochastic variables.

One disadvantage is that PEM does not provide a complete output distribution as in the case with Monte Carlo. On the other hand, PEM requires little know about probability knowledge, and can be applied for any probability distribution.

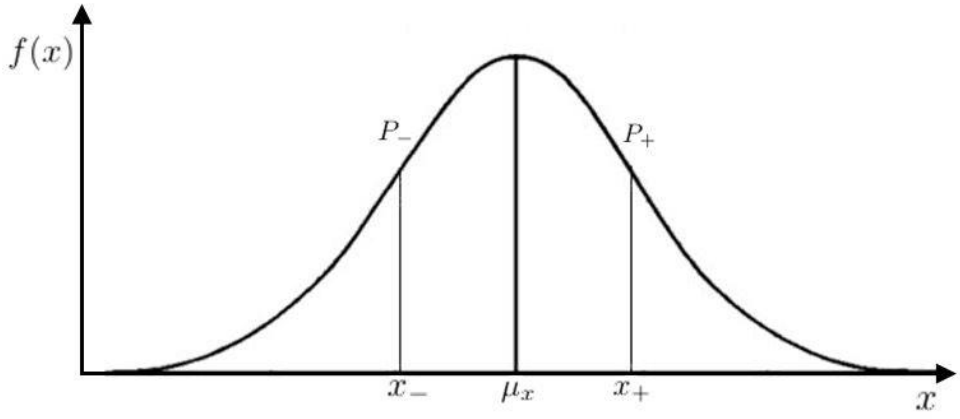

Figure 3.5 Evaluation points on probability density function

The basis of the PEM developed by (Rosenblueth, 1975), deals with three cases:

1. When Y is a function of one variable X, whose mean, variance, and standard deviation are known.
2. When Y is a function of one variable X，whose distribution is symmetrical and approximately Gaussian.
3. When Y is a function of n variables，X_1, X_2, …, X_n, whose distributions are symmetric and which may be correlated.

Commonly calculations are made at two evaluation points:

$$E[Y] \approx P_+ y_+ + P_- y_- \tag{3.26}$$

Where Y is a deterministic function of X, $E[Y^m]$ is the expected value of Y, y_+ is a value of Y evaluated at point x_+ which is greater than the mean, y_- is a value of Y evaluated at point x_- which is less than the mean, P_+ and P_- are the weights.

Case 1

In the first case, 3 conditions must be satisfied for the first statistic moments:

$$P_+ + P_- = 1 \tag{3.27}$$

$$P_+ x_+ + P_- x_- = \mu_x \tag{3.28}$$

$$P_+ (x_+ - \mu_x)^2 + P_- (x_- - \mu_x)^2 = \sigma^2 \tag{3.29}$$

When the distribution of the variables X is symmetric, the solutions become:

$$P_+ = P_- = \frac{1}{2}; x_+ = \mu_x + \sigma_x; \quad x_- = \mu_x - \sigma_x \tag{3.30}$$

Case 2

In Case 2, when the distribution X is symmetrical and approximately normal, the evaluation points x can be estimated at more than two points. For three points this involves a central point at the mean μ_x and two points at x_+ and x_- which are symmetrically distributed about the mean. The weight for the central point is defined as P and the other two notation stay the same, therefore：

$$2P_+ + P = 1 \tag{3.31}$$

$$2P_+(x_+ - \mu_x)^2 = \sigma_x^2 \tag{3.32}$$

$$2P_+(x_+ - \mu_x)^4 = 3\sigma_x^3 \tag{3.33}$$

The solutions for these equations are:

$$P = \frac{2}{3} \quad P_+ = P_- = \frac{1}{6} \tag{3.34}$$

$$x_\pm = \mu_x \pm \sqrt{3}\sigma_x \tag{3.35}$$

Case 3

Case 3 is the most widely used application of Rosenblueth's method. This is a generalization of Case 1, In this procedure calculations are done at 2^n points, so that the value of each variable is at one standard deviation below or above the mean. For two variables, four calculations are done at the points $(\mu_{x1}-\sigma_{x1}, \mu_{x2}-\sigma_{x2})$, $(\mu_{x1}-\sigma_{x1}, \mu_{x2}+\sigma_{x2})$, $(\mu_{x1}+\sigma_{x1}, \mu_{x2}-\sigma_{x2})$, $(\mu_{x1}+\sigma_{x1}, \mu_{x2}+\sigma_{x2})$ .If the variables are uncorrelated , the weight of each point is $P_i = 0.25$

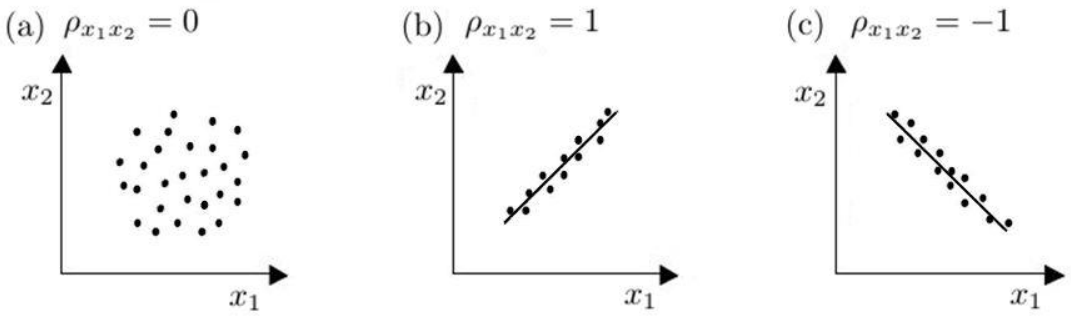

Figure 3.6 Example evaluations points and weights of correlated soil properties

There may be also correlation between the input variables. The principle of correlation is schematized for two correlated variables in Figure 3.6. If two variables are correlated with the correlation coefficient ρ， the points are still located at one standard deviation below or above the mean, but the weights are adjusted. For the same evaluation points the weights become $(1+\rho)/4$ and $(1-\rho)/4$, as shown in Figure 3.7 point and weights for two (left) and three (right) variablesFigure 3.7 (left), PEM also allows more than two variables to be included as correlated, which is illustrated in Figure 3.7 (right). To obtain a clear definition of the weights, (Rosenblueth, 1975) used a set of + and - as subscripts. When three correlated variables X are considered, the first sign refers to X_1, the second to X_2, and the third to X_3. The sign is positive when the evaluation point is considered one standard deviation above the mean value. For three correlated variables, where ρ_{12} is the correlation coefficient between X_1 and X_2, and so on, the weights are defined as:

$$P_{+++} = P_{---} = \frac{1}{8}(1+\rho_{12}+\rho_{23}+\rho_{31}) \tag{3.36}$$

$$P_{++-} = P_{--+} = \frac{1}{8}(1+\rho_{12}-\rho_{23}-\rho_{31}) \tag{3.37}$$

$$P_{+-+} = P_{-+-} = \frac{1}{8}(1-\rho_{12}-\rho_{23}+\rho_{31}) \tag{3.38}$$

$$P_{+--} = P_{-++} = \frac{1}{8}(1-\rho_{12}+\rho_{23}-\rho_{31}) \tag{3.39}$$

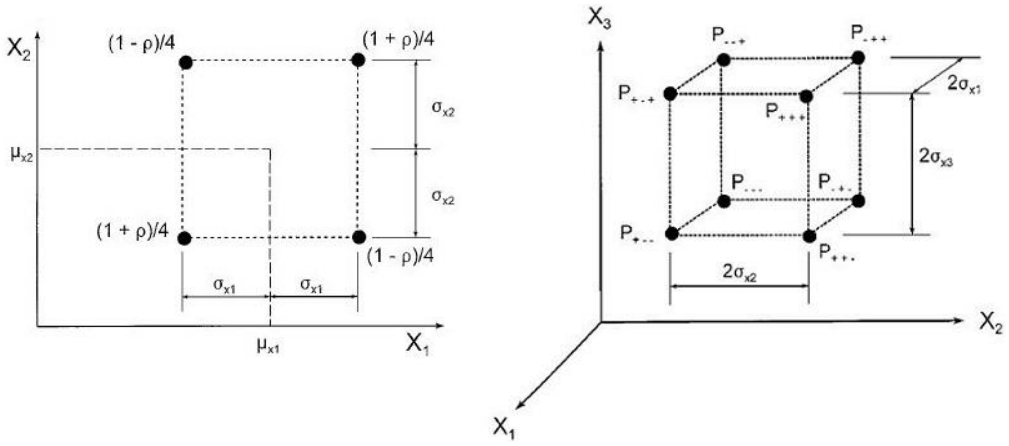

Figure 3.7 (Rosenblueth, 1975) point and weights for two (left) and three (right) variables

When for two variables the evaluation points are both at the same side of the mean (e.g. both one standard deviation above the mean), the sign of the correlation coefficient is positive. If the location of the two points is opposite, the sign is negative. For n variables, 2^n points are required to include all possible combinations with each variable one standard deviation above and below the mean. With n variables, the weights are:

$$P_{(s1s2,\ldots,sn)} = \frac{1}{2^n}[1+\sum_{i=1}^{n-1}\sum_{j=i+1}^{n}(s_i)(s_j)\rho_{ij}] \tag{3.40}$$

Where s_i is positive when the value of the i th variable is one standard deviation above the mean and negative when the value is one standard deviation below the mean, y_i is the value of Y evaluated at x_i ,and i is an appropriate combination of $+$ and $-$ signs indication the location of x_i . For uncorrelated variables the equation reduces to $P_i = 1/2^n$.

After all input variables are defined and the calculation has been performed, the output statistics can be computed. Typical output statistics of PEM are the mean (μ_{xi}), standard deviation (σ_{xi}). The first moment, or μ_{xi}, is calculated as follows:

$$\mu_{xi} = \sum_{i=1}^{2^n} P_i y_i \tag{3.41}$$

The second central moment, or variance σ_{xi}^2, is defined as:

$$\sigma_{xi}^2 = \sum_{i=1}^{2^n} P_i (y_i - \mu)^2 \tag{3.42}$$

A more common quantification of the output deviation is the standard deviation, which is calculated as the square root of the variance:

$$\sigma_{xi} = \sqrt{\sum_{i=1}^{2^n} P_i (y_i - \mu)^2} \tag{3.43}$$

3.5.2 Monte Carlo Simulation

As reliability related issues are becoming more critical in engineering design and analysis, proper assessment of stochastic behavior of an engineering system is essential. The true distribution for the system response subject to parameter uncertainty should be derived, if possible. However, due to the complexity of physical systems and mathematical functions, derivation of the exact solution for the random characteristics of the system response is difficult. In such cases, Monte Carlo simulation is a viable tool to provide numerical estimations of the stochastic features of the system response.

Monte Carlo simulation is like to repeatedly measuring the system response of interest under various parameter sets generated from the known or assumed probabilistic laws. It offers a practical approach to reliability analysis because the stochastic behavior of the system response can be probabilistically duplicated. The problem is evaluated analytically. The frequency of each outcome can be plotted by means of a histogram. When sufficient simulations have been performed a probability density function can be fitted on the output histogram. In advance a limit state is determined, for example terms of the factor of safety (S.P.Kamp, 2016). By counting the total number of simulations and the number of simulations that failed, it is possible to calculate the probability of failure.

$$P_f = \frac{nf}{n} \tag{3.44}$$

Where n is the total number of simulations and nf is the number of failures. In order to obtain sufficient accuracy, the following requirement is given for the number of simulations (Ching, 2011):

$$\mathrm{n} > \left(\frac{100}{P_f}\right) \tag{3.45}$$

The number of failure is counted as follows:

$$\mathrm{nf} = \sum_{i=1}^{n} I(X_1, X_2, \dots, X_n) \tag{3.46}$$

Where $I(X_1, X_2, \dots, X_n)$ is a function defined as :

$$I(X_1, X_2, \dots, X_n) = \begin{cases} 1 & if\ I(X_1, X_2, \dots, X_n) \leq 0 \\ 0 & if\ I(X_1, X_2, \dots, X_n) \geq 0 \end{cases} \tag{3.47}$$

Two major concerns in practical applications of Monte Carlo simulation are: (1) The requirement of tremendous computations for generating random variates; and (2) the response of correlation among stochastic system parameters. In fact, the former concern is diminishing as the computing power increases. As for the second concern, it has been pointed out that neglecting correlation could have significant effect on the result of reliability analysis (Thoft-Christensen and Baker 1982). Therefore, a proper assessment of joint probability density function (PDF) for the

correlated parameters is necessary in the generation of multivariate random variables. Compared with a variety of univariate random generators, generating multivariate random variable is much more restricted to a few joint distributions such as multivariate normal, multivariate lognormal and multivariate gamma. If the random variables involved are correlated with a mixture of marginal distributions, the multivariate PDF is difficult to formulate.

Proposed multivariate Monte Carlo simulation procedure

In many practical engineering analyses, random variables are often statistically and physically dependent, Furthermore, distribution types for random variables involved cam ne a mixture of different distributions. To properly replicate such systems, Monte Carlo simulation should be able to preserve the correlation relationship among the stochastic parameters and their distributions.

However, derivation of the joint CDF which describes the complete multivariate characteristics of random variables is generally difficult. This is difficulty, in both theory and practice increases with the number of random variables and the type of corresponding distributions. As a practical alternative, this section describes procedure to generate multivariate random variates that preserves the marginal distributions and correlation of the random variables involved. In doing so, the difficulty of determination of complete joint PDF in multivariate Monte Carlo simulation is avoided.

Steps to generate normal distributed correlated variables

Since the normal distribution has the unique properties of keeping distribution law under linear transformation, the generation of correlated normal distributed random variables can be achieved by linear transformation of independent random variables through Cholesky decomposition of the covariance matrix.

Suppose that $X_{m\times n}=(X_1,X_2,...,X_n)$ is n-dimensional correlated normal distributed variables, each variable X_i (i=1,2,…,n) is a column vector consisting of m random samples (m is the number of calculation times in Monte Carlo simulation, normally $m\gg n$), which has a mean value of $\mu=(\mu_1,\mu_1,...,\mu_n)$. And the covariance matrix of these variables is:

$$v_{n\times n}=\begin{pmatrix} v11 & \cdots & v1n \\ \vdots & \ddots & \vdots \\ vn1 & \cdots & vnn \end{pmatrix}$$

Then, the steps of generation of correlated normal distributed variables are listed as:

- Create an n-dimensional independent standard normal distributed random sample set $Y_{m\times n}=(Y_1,Y_2,...,Y_n)$, each variable consists of m samples.
- Define the covariance matrix of these variables, and apply Cholesky decomposition of the matrix $v_{n\times n}$. (in fact, the covariance matrix is always positive definite. So the performance of Cholesky decomposition is always doable), $v_{n\times n}=C_v^T\bullet C_v$, and $C_{v,n\times n}$ is a upper triangular matrix.
- Perform a linear transformation, let $X_{m\times n}=Y_{m\times n}\cdot C_{v,n\times n}+\mu_{m\times n}$.

It is also feasible to generate the correlated normal distributed variables based on known correlation coefficient matrix. If the n-dimensional correlated normal distributed sample set has a correlation coefficient $R_{n\times n}$.

$$R_{n\times n}=\begin{pmatrix} 1 & r_{12} & \cdots & r_{1n} \\ r_{21} & 1 & & r_{2n} \\ \vdots & & \ddots & \vdots \\ r_{n1} & r_{n2} & \cdots & 1 \end{pmatrix}$$

Perform Cholesky decomposition to $R_{n\times n}$, resulting in $R_{n\times n}=C_r^T \bullet C_r$, then

$$X'_{m\times n}=Y_{m\times n}\cdot C_{r,n\times n} \tag{3.48}$$

And $X'_{m\times n}$ is the standard normal distributed sample set, which has a fixed correlation coefficient matrix $R_{n\times n}$. Let

$$X_i=\sigma_i\times X'_i+\mu_i,\quad i=1,2,\ldots,n \tag{3.49}$$

This procedure can also result in a correlated normal distributed sample set X_i, which has standard deviation σ_i and mean value μ_i. And $R_{n\times n}$ is the correlation coefficient matrix of all X_i.

3.6 Beam on elastic foundations

The computational model of a beam or a plate on an elastic foundation, such as that in Figure 3.8, is often used to describe a lot of engineering problems and has application in geotechnics, road, railroad and marine engineering. The key issue in the analysis is modelling the contact between the structural elements- the beam and the soil bed. In most cases the contact is presented by replacing the elastic foundation with simple models, usually spring elements, because the main task is considered to be the analysis of the beam not the soil bed. The stiffness of the spring describes the behavior of the elastic foundation. A lot of methods are developed for determination of the spring stiffness and reduction of the 3-D problem to 2-D or 1-D.

In this case study, due to the large excavation depth, subsoils are under heavily over consolidated state. Installation of tunnel element, backfilling and siltation can be considered as a reloading procedure to the subsoils. Regarding this unique project, approximately 30 m- 40 m of overburden soils have been excavated, the subsoil stress state will not exceed the maximum previous stress during reloading procedure, therefore, the behavior of the subsoil is linear elastic. Thus, subsoils can be simulated by linear-elastic materials in “Beam-spring model”.

Foundation stiffness

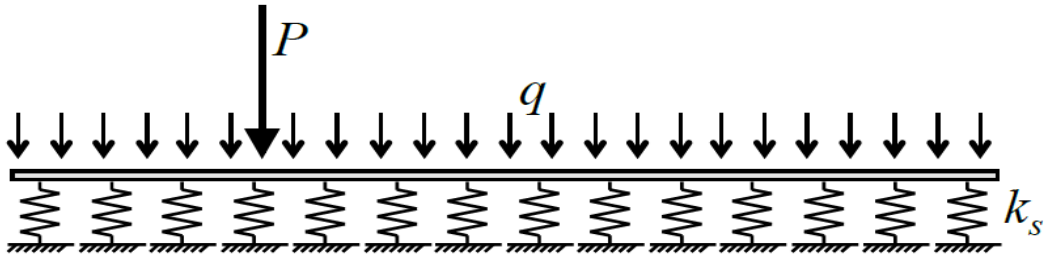

Figure 3.8 Beam on elastic foundation

The foundation stiffness, k_s, which is illustrated in Figure 3.8, is conceptually straightforward. When the beam displaces downwards, the foundation exerts an upward force. k_s has units of force per unit length along the beam.

Suppose the stiffness, k_s, is determined from soil testing. In particular, supposed a vertical load, P, is placed on an area with dimensions x and y, and that the vertical displacement, Δ, is measured. The relationship between distributed load and the displacement is written in terms of a distributed stiffness k_d:

$$\frac{P}{x \times y} = k_d \times \Delta \quad \Rightarrow k_d = \frac{P}{\Delta \times x \times y}\left[\frac{N}{m^3}\right] \tag{3.50}$$

While k_d is stiffness per unit area, k_s is stiffness per unit length. The sought value is obtained by multiplying k_d by the beam width, b:

$$k_s = b \times k_d \left[\frac{N}{m^2} \right] \tag{3.51}$$

If one assumes that the foundation material is linear elastic, there is no unique relationship between the Young's modulus, E, of the foundation material and the stiffness k_s. However, if one imagines that the soil underneath the beam is linear elastic with depth L to bedrock then the force-deformation relationship of the soil is

$$P = \frac{EA}{L} \times \Delta \tag{3.52}$$

Where $A = x \bullet y$ is the area loaded by P. Then the stiffness is

$$\frac{P}{x \bullet y} = k_d \bullet \Delta \Rightarrow k_d = \frac{E}{L} \left[\frac{N}{m^3} \right] \tag{3.53}$$

And

$$k_s = b \bullet k_d = \frac{b \bullet E}{L} \left[\frac{N}{m^2} \right] \tag{3.54}$$

4. Probabilistic Method on Settlement

In this chapter, firstly, based on relationship between CPT values and soil deformation factors, and the lab test results, the soil properties used in settlement calculation are determined. Secondly, the tunnel elements are assumed placing directly on the natural subsoil without manmade foundation layer. A deterministic approach on settlement has been performed based on design values, followed by stochastic analysis, Point estimate method, has been performed to investigate the effect of the intrinsic variability and uncertainty of the soil parameters on the calculated settlements. Then a Monte Carlo Simulation is carried out, for the settlement determination along the tunnel alignment. The results from deterministic method and probabilistic methods (PEM and MCS) are compared, the pros and cons of these two probabilistic methods are briefly discussed.

The influence of gravel bed on immersed tunnel settlement is investigated by a second Monte Carlo simulation. In this simulation, a 1.3 m thick gravel bed is firstly installed on the subsoil and then, tunnel elements are placed on the gravel layer. The results of settlement in this condition are compared with the condition that without gravel bed.

Finally, according to the distribution of settlement results, the equivalent stiffness of subsoil is back calculated, which are used as input variable in soil-structure interaction model in the next chapter.

The flow chat of this chapter are shown below：

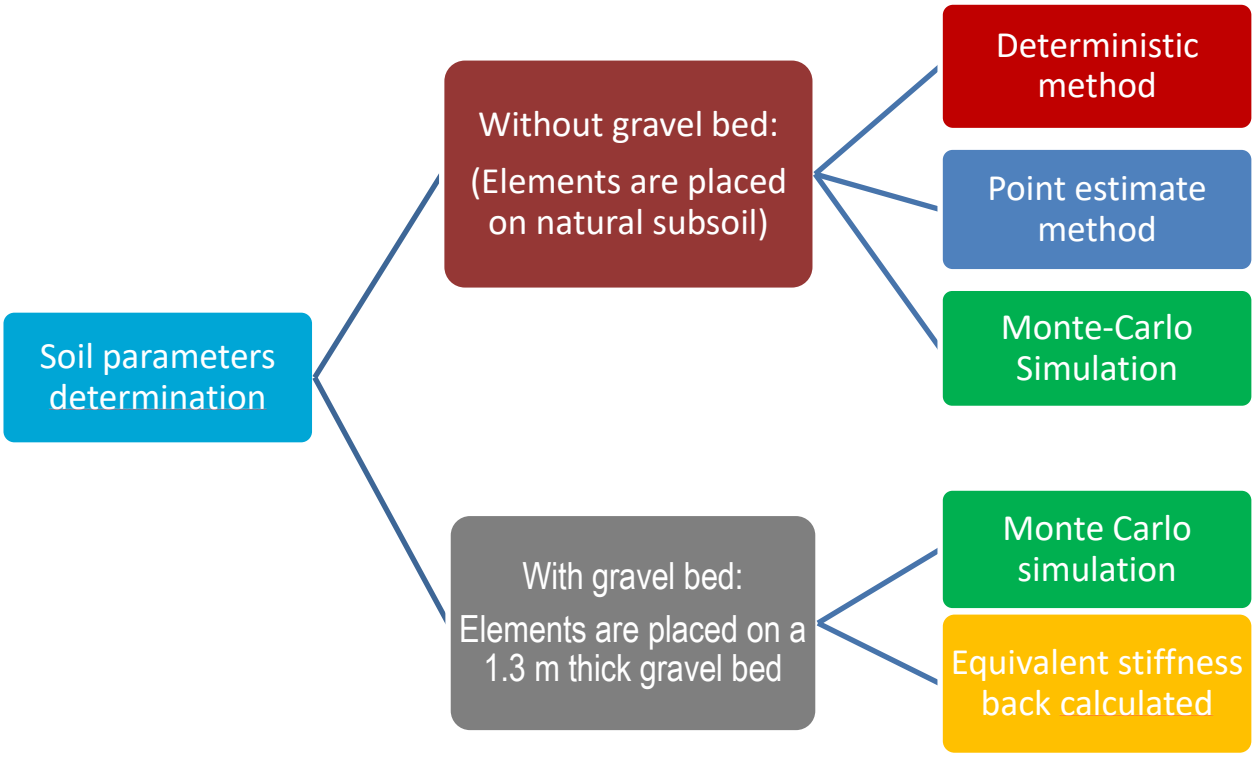

4.1 Soil parameter determination

Soils in project area can be divided into two main units, clayey soil and sandy soil. And these clayey soils and sandy soils can be further divided into subunits. Properties of different subgroups have considerable differences.

Figure 4.1 illustrates the geological profile in longitudinal direction of the immersed tunnel. The blue dashed line represents the bottom of the excavated trench, while solid lines stand for tunnel bottom. The research area is in the middle of this picture (E10-E24), from right to left, one can clearly find that Element 10 to Element 12 are placed directly on the yellow material, which mainly consists of coarse sand and fine sand. And in the middle, the subsoils beneath E14 to E20 are clay layers which are more compressible. Then to the left end, the subsoils condition below Element 24 is multiple, where “red pocket” can be found, representing the possible weakest zone in this area.

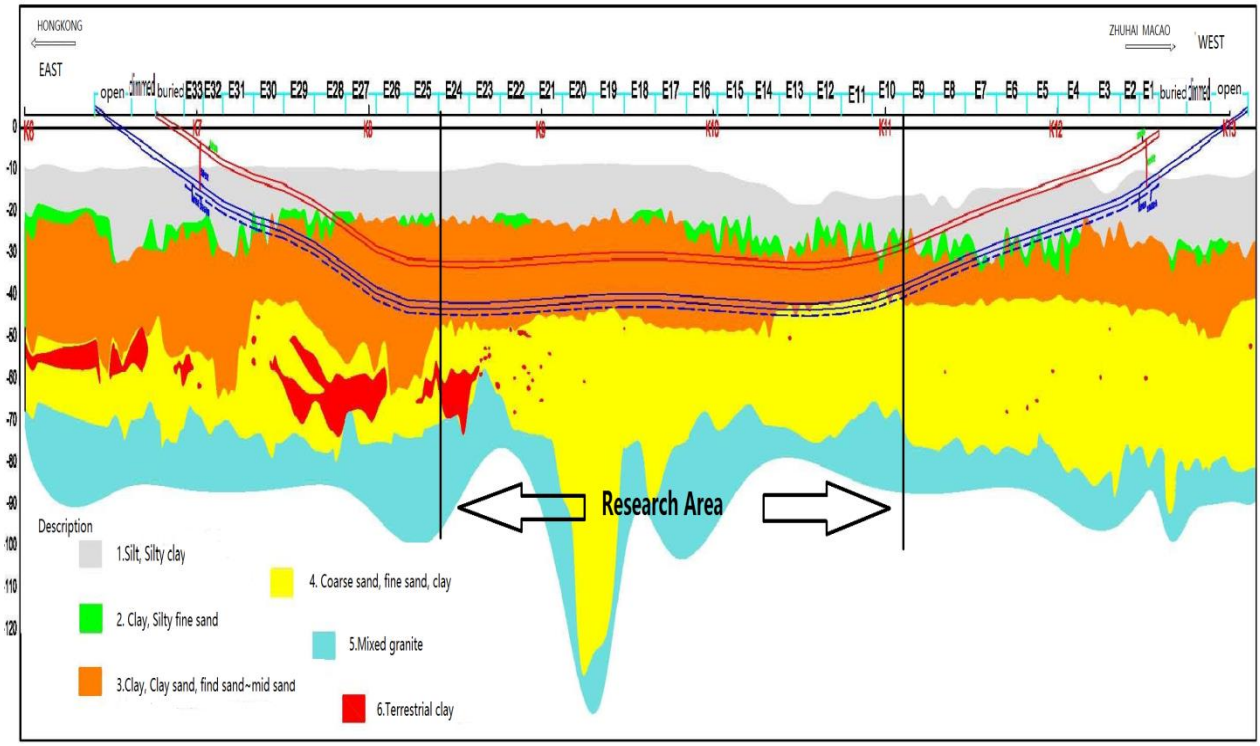

Figure 4.1 Soil strata and research area

In this section, CPT results are analyzed from investigation report. For sandy layers, the deformation factors are calculated based on the relationship between cone resistance and Young’s modulus. For clay layers, parameters for settlement calculation are obtained from lab test report. Figure 4.2 indicates the location for CPT boreholes in tunnel construction area.

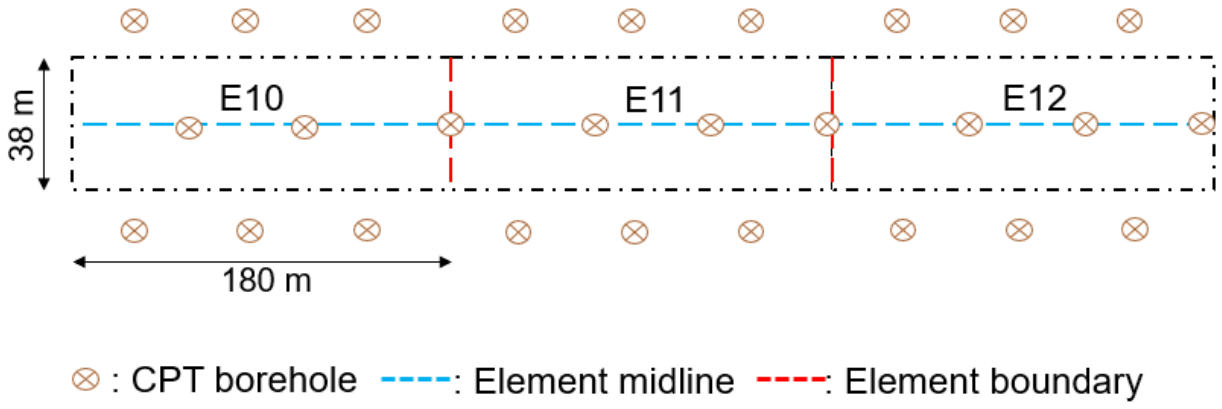

Figure 4.2 Top view of locations of CPT boreholes in tunnel construction area

As illustrated in the figure, there are around 8-10 CPT boreholes for each tunnel element, during the research, detailed information for an individual CPT borehole is not available, while, a summary including the means, maximum and minimum of CPT values base on every element can be obtained from soil investigation report. The data for lab test summary can be found in **APPENDIX A.**

4.1.1 Sand layer properties determination

Based on the Schmertmann's method, which is introduced in Chapter 3, to calculate the settlement of sand layer in the subsoil the following formula is used:

$$S = C_1 C_2 \Delta_p \sum_0^{2B} \frac{I_z}{E_s} \Delta_z \tag{4.1}$$

Where

C_1 = depth correction factor

C_2 = creep factor

Δ_p = net increase of load on soil at foundation level due to applied loading

B = width of loaded area

I_z = vertical strain influence factor

E_s = a secant modulus

Δ_z =thickness of soil layer

$$C_1 = 1 - 0.5\left(\frac{\sigma'_{vo}}{\Delta_p}\right) \tag{4.2}$$

$$C_2 = 1 + 0.2\log_{10}\left(\frac{time_{years}}{0.1}\right) \tag{4.3}$$

As can be seen in this formula C_1, I_z, and C_2 are fixed in this case and can be directly determined from the known data, but the value of E modulus is not comprehensive from the soil investigation report and should be determined from the relationship between CPT values and soil deformation factors. (Schemertmann, 1970) suggested that this could be done using the cone penetration resistance of the soils at the site. In the case of normally loaded cohesionless materials, the modulus of the sand E is related to the cone end resistance qc for each soil layer by $\mathrm{Es} = \alpha \mathrm{qc}$

Where

α=2.5 for a square foundation (L/B = 1)

α= 3.5 for a strip foundation (L/B>10)

The α values above are quoted for normally consolidated sands. For over consolidated sands (Meigh, 1987) suggested that the modulus values could be doubled.

In the case of HZMB immersed tunnel, the excavation depth for the trench is approximately 20-30 meters from the see bed, thus foundation layers are under heavily over consolidated state, and even after the placement of tunnel element and siltation, the stress path of subsoil is still on the unloading-reloading line. Therefore, for determination the settlement in sand layer, the term E in initial equation (4.1) is replaced by E_{ur}, which is the unloading-reloading modulus.

Thus, the equation can be rewritten as:

$$S = C_1 C_2 \Delta_p \sum_0^{2B} \frac{I_z}{E_{ur}} \Delta_z \tag{4.4}$$

Where $E_{ur} \approx 4E_{50}^{ref} \approx 4Es$, and E_{50}^{ref} is the secant modulus at 50% failure stress.

The values and distributions of unloading-reloading modulus of sand layer below each element are determined from the relationship mentioned above, and are listed in Table 4.1.

4.1.2 Clay layer properties determination

The analytical method for determination the settlement of clay layer is discussed in Chapter 3 and related equations are listed below:

1) If the soil is normally consolidated (OCR=1), the primary consolidation settlement is

$$S = \frac{H_0}{1+e_0} Cc \log \frac{\sigma'_{fin}}{\sigma'_{z0}} \tag{4.5}$$

2) If the soil is over-consolidated and $\sigma'_{fin} < \sigma'_{zc}$ (the maximum effective stress before unloading) the primary consolidation settlement is

$$S = \frac{H_0}{1+e_0} Cr \log \frac{\sigma'_{fin}}{\sigma'_{z0}} \tag{4.6}$$

3) If the soil is over-consolidated and $\sigma'_{fin} > \sigma'_{zc}$, the primary consolidation settlement is

$$S = \frac{H_0}{1+e_0}(Cr \log \frac{\sigma'_{zc}}{\sigma'_{z0}} + Cc \log \frac{\sigma'_{fin}}{\sigma'_{zc}}) \quad (4.7)$$

Where

H_0 = the thickness of the soil layer.

Cc = compression index

Cr = recompression index

σ'_{fin} = final vertical effective stress

σ'_{z0} = current vertical effective stress

σ'_{zc} = Maximum vertical effective stress ever

As mentioned in Section 4.1.1, the subsoils are under over consolidated state, so in this case equation (4.6) is used for generating the settlement of clay layers. In this equation, vertical stress can be directly calculated based on the unit weight and layer thickness from the soil investigation report. While, recompression index and void ratio are obtained from lab test in soil investigation report of this project.

4.1.3 Collection of soil parameters in tunnel area

The relationship between soil parameters and CPT values are studied in previous section (4.1.1 and 4.1.2). And general soil stratigraphy has been given in Chapter 3. There are seven different subunits in the research area, for simplicity, the subsoil units are numbered as (Sand 1-5, Clay 1-2).

In this section the parameters used for calculating settlement for each tunnel element are organized and listed in Table 4.1, including the means and standard deviations ("Std" in the table).

Element Number	Underlying layer	Layer Thickness (m)	Std (m)	Unit weight(kN/m3)	Void ratio	Std (-)	Cr	Std (-)	Eur (MPa)	Std (MPa)
10	Clay1	0.47	0.12	18.7	0.958	0.10	0.034	0.01		
	Sand1	0.44	0.1	18.8	0.826				179.6	15.7
	Sand4	19.57	3	19.9	0.470				310.0	14.7
	Sand3	5.63	1.2	19.6	0.650				292.4	28.1
	Sand5	3.00	0.2	20.9	0.460				251.2	27.8
11	Sand4	16.90	3.5	19.9	0.470				193.2	14.7
	Sand3	14.24	3	19.6	0.650				147.6	13.8

12	Sand4	15.78	3.2	19.9	0.470				252.5	24.3
	Sand3	5.21	1.2	19.6	0.650				173.4	15.1
	Sand5	4.9	1	20.1	0.460				215.2	16.8
13	Clay1	2.56	0.3	18.1	0.958	0.10	0.034	0.01		
	Sand4	15.28	3	19.9	0.470				241.2	28.6
	Clay2	0.88	0	18.6	0.827		0.032	0.01		
	Sand3	20.58	4	19.6	0.650				147.6	12.5
14	Clay1	3.83	0.5	18.1	0.958	0.10	0.034	0.01		
	Sand2	0.89	0.1	18.8	0.700				253.2	21.1
	Sand3	3.28	0.5	19.6	0.650				60.4	6.1
	Sand4	10.48	2	19.9	0.470				162.4	14.2
	Sand5	2.4	0.3	20.1	0.460				152.4	11.2
15	Sand2	1.3	0.1	18.8	0.700				253.2	20.8
	Clay1	3.29	0.5	18.1	0.958	0.08	0.034	0.01		
	Clay2	2.7	0	18.6	0.827	0.04	0.032	0.01		
	Sand4	8.98	1.5	19.9	0.470				112.8	9.0
	Sand3	14.66	3	19.6	0.650				60.4	6.1
16	Clay1	3.7	0.5	18.1	0.958	0.11	0.034	0.01		
	Sand1	2.05	0.2	18.8	0.826				123.2	19.1
	Sand2	0.85	0.1	18.8	0.700				253.2	32.4
	Sand4	12.8	2	19.9	0.470				170.4	20.1
	Sand3	0.85	0.1	19.6	0.650				61.2	6.5
	Sand5	7.2	1.5	20.1	0.460				106	10.1
17	Clay1	4.69	0.5	18.1	0.958	0.09	0.034	0.01		
	Sand4	30	2.5	19.9	0.470				219.2	21.8
18	Clay1	2.78	0.2	18.1	0.958	0.10	0.034	0.01		
	Sand1	0.96	0	18.8	0.826				161.2	14.5
	Sand2	11.73	2	19.9	0.470				142	13.7
	Sand4	0.62	0	19.6	0.650				147.6	12.9
	Sand3	20.0	3	20.1	0.460				141.2	9.5

19	Clay1	0.69	0.1	18.1	0.958	0.10	0.034	0.01		
	Sand1	0.58	0	18.8	0.826				164	14.5
	Sand3	1.85	0.3	20.1	0.460				454	53
	Sand2	4.77	1	19.9	0.470				291.6	28.1
	Clay2	0.43	0	18.6	0.827	0.04	0.032	0.01		
	Sand4	38.50	4	19.6	0.650				147.6	13.4
20	Clay1	1.83	0.1	18.1	0.958	0.10	0.032	0.01		
	Sand2	15.07	3	19.8	0.470				173.6	14.9
	Sand4	1.12	0	19.6	0.650				147.6	12.9
	Clay2	0.47	0	18.6	0.827	0.04	0.033	0.01		
	Sand3	29.0	3	20.1	0.460				502	53
21	Clay1	1.02	0	18.1	0.958	0.10	0.033	0.01		
	Sand1	0.6	0	18.8	0.826				198	14.5
	Sand2	15.78	2.8	19.9	0.470				185.2	20.6
	Sand4	1.24	0.2	19.6	0.650				72	6.0
	Clay2	0.74	0.1	18.6	0.827	0.04	0.033	0.01		
22	Clay1	3.39	0.34	18.1	0.958	0.10	0.034	0.01		
	Sand2	10.49	2.1	19.8	0.470				139.2	13.2
	Clay2	1.26	0	18.6	0.827		0.032	0.01		
	Sand4	6.57	1.2	19.6	0.650	0.04			108.8	8.1
23	Clay1	2.75	0.35	18.1	0.958	0.1	0.032	0.01		
	Sand1	0.94	0	18.8	0.826				113.6	14.9
	Sand2	9.55	2.1	19.9	0.470				236.8	28.1
	Sand3	9.6	0	20.0	0.460				205.6	20.0
	Clay2	1.46	0.3	18.6	0.827	0.04	0.033	0.01		
	Sand4	1.08	0.1	19.6	0.650				165.2	16.8
24	Clay1	2.6	0.5	18.1	0.958		0.033			
	Sand1	0.84	0	18.8	0.826				161.2	15.1
	Sand2	0.45	0	18.8	0.700				253.2	21.3
	Sand3	1.52	0.3	19.6	0.650				147.6	12.9
	Sand4	7.23	1.2	19.9	0.470				146.8	14.5
	Clay2	7.84	1.3	18.6	0.827		0.034			
	Sand5	1.20	0	20.0	0.460				205.6	20.0

Table 4.1 Subsoil parameters for each layer in construction area

4.2 Deterministic method on settlement

To start with, a deterministic method on settlement is carried out based on the design value of each soil property. The relative results are listed in Table 4.2 and Plotted in Figure 4.3. These results are considered as reference in comparison with the results from probabilistic methods in the next sections.

Element No.	Settlement (mm)	Element No.	Settlement (mm)
10	20	**18**	79
11	13	**19**	49
12	14	**20**	59
13	61	**21**	43
14	81	**22**	91
15	114	**23**	78
16	88	**24**	118
17	95		

Table 4.2 Settlement results based on the design values

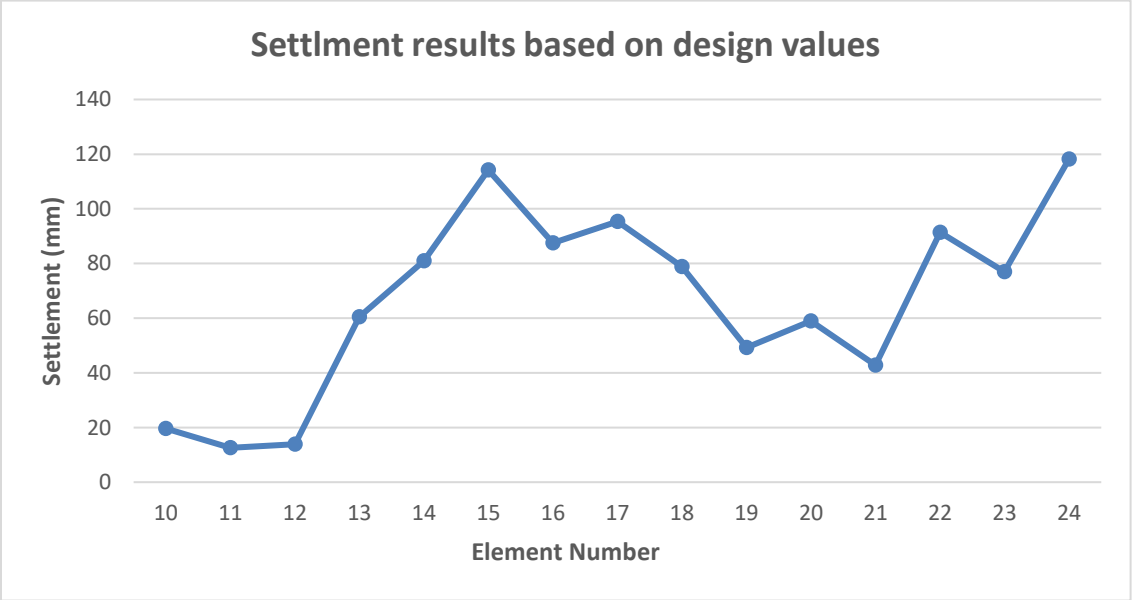

Figure 4.3 Settlement results based on design values

4.3 Point Estimate Method on settlement

The basic principle of Point Estimate Method has been described in Chapter 3, in this section, the calculation of settlement along tunnel line is firstly performed using Point estimate method (PEM), in the case that elements are directly installed on the bottom of trench. the results of PEM will be compared with Monte Carlo Simulation method, and the main procedures are listed as follow:

1. Determine the numbers of input variable

For each variable, two evaluation points need to be determined based on the mean value, as X+ and X-, which are one standard deviation on either side of the mean value.

2. Calculate for all combinations

For each tunnel element, settlement calculation times is equal to 2^n, where n is the number of variables. For example, as indicated in Table 4.1, Element 11 is placed on a soil layer consists of two sublayers (Sand4, Sand3), the variables for each sand layer are thickness (hsand4 and hsand3), unloading-reloading modulus (Eur4 and Eur3), that results in a calculation times of 16 (2^4).

The settlement results for each element from PEM are indicated in Table 4.3.

Element No.	Max value(mm)	Min value(mm)	Mean value (mm)	Standard deviation(mm)	COV
10	26	14	20	5	0.27
11	15	11	13	2	0.16
12	17	12	14	3	0.21
13	86	38	61	20	0.34
14	112	54	69	19	0.28
15	154	79	115	31	0.27
16	120	59	88	26	0.30
17	133	63	96	30	0.31
18	106	55	80	21	0.27
19	64	36	50	10	0.20
20	80	40	60	17	0.28

21	59	29	43	12	0.28
22	138	66	99	31	0.31
23	106	51	80	23	0.29
24	163	77	111	35	0.32

Table 4.3 Settlement results from PEM

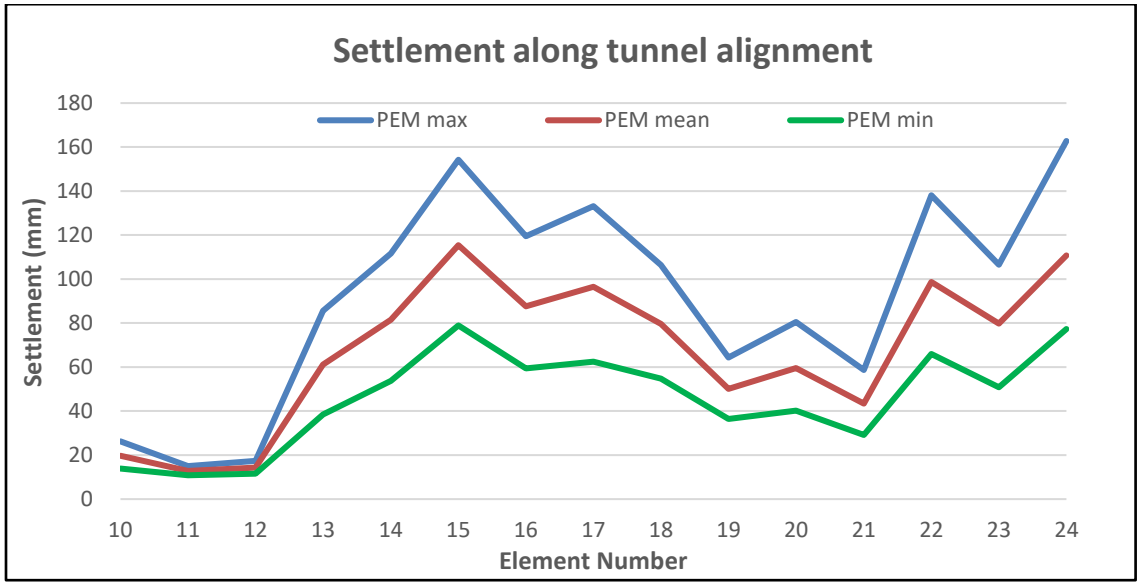

Figure 4.4 Settlement along tunnel line (PEM)

As illustrated in Table 4.3 and Figure 4.4 , the two biggest settlement occur at Element 15 and Element 24, assumption can be made that the subsoil closed to these two areas are relatively weak and more compressible. The averaged coefficient of variation of settlement is 0.27.

From the output of PEM, one can hardly define the distribution type of settlement, especially in some cases the number of variable is small (n is small), resulting in a limited number of output (2^n). Distribution of input variables can be determined from data obtained with the use of soil investigation or lab tests. However, it cannot be stated that when all input variables are normally distributed, the output distribution also follows a normal distribution. Due to the non-linear relationship between inputs and outputs, it is possible that output distribution deviates significantly from a normal distribution.

The exact output distribution can be defined from Monte Carlo simulation which is performed in next section, and the accuracy of the results form PEM can be further checked by Monte Carlo simulation.

4.4 Monte Carlo Simulation on Settlement

In this section, Monte Carlo Simulation is performed based on the soil properties determined from section 4.1. Input variables are divided for two main groups consist of clay layers and sand layers, and are determined for each sublayer.

According to the analytical method for settlement calculation, in clay layers, variables are **thickness of the layer** $(\mathbf{hc})$**, recompression modulus**$(\mathbf{Cr})$**, void ratio**$(\mathbf{e})$. In sand layers variables are **thickness**$(\mathbf{hs})$ and **unloading-reloading modulus**$(\mathbf{Eur})$. The results from 1st Monte Carlo simulation are compared with those from PEM in section 4.2, and then the influence of gravel bed on settlement is analyzed in the 2nd Monte Carlo simulation.

4.4.1 Main approach

The main aspects of Monte Carlo simulation are described below:

a) Define the stochastic input variables.

b) Define the stochastic distribution of the input variables

c) Define the correlation matrix of the input variables

   i. By combining the probability distribution of the input parameters and the correlation matrix, a covariance matrix is created.

   ii. From the covariance matrix the Cholesky decomposition matrix is created, which is in turn used to create a random sample set of correlated input variables.

d) Create a random (size 1000) sample set of input parameters based on the probability distribution and mutual correlations.

e) Run (N=1000) settlement simulations for each of the 15 locations below 15 tunnel elements along the immersed tunnel alignment.

f) From the output, the results are plotted along the tunnel alignment.

Mutual correlation

The mutual correlations between the different input variables are assumed constant for each soil layer. And the correlations are estimated based on expert judgment. Detailed correlation among parameters is shown in the correlation matrix (Table 4.4). (Rebonato, 1999)

ρ	Dry unit weight	Saturated unit weight	Voids Ratio	OCR	Hydraulic conductivity	Cα	Cr	Cc
Dry unit weight	1.00	1.00	0.00	0.00	0.00	0.00	0.00	0.00
Saturated unit weight		1.00	-0.79	0.00	-0.70	-0.40	-0.65	-0.67
Voids Ratio			1.00	0.00	0.67	0.31	0.65	0.87
OCR				1.00	0.00	0.00	0.00	0.00
Hydraulic conductivity					1.00	0.49	0.50	0.53
Cα						1.00	0.70	0.66
Cr							1.00	0.80
Cc								1.00

Table 4.4 Correlation matrix

4.4.2 1st Monte Carlo simulation (without gravel bed)

In the first Monte Carlo simulation, construction condition is the same as that in PEM, assumed that tunnel elements are placed directly on the bottom of the pre-excavated trench (lying on the top of nature subsoil). Following the approaches from section 4.2.1, the main results of settlement along the tunnel line are generated by Matlab coding. For each element, settlement calculation is performed 1000 times, the histograms (frequency versus settlement) for each element are in **Appendix B**, and the stochastic characteristics (including max value, mean value, mean value, standard deviation and coefficient of variation) are listed in Table 4.5.

Element No.	Max value (mm)	Min value (mm)	Mean value (mm)	Standard deviation(mm)	COV	Distribution type
10	35	7	19	5	0.25	Normal
11	22	7	13	2	0.19	Normal
12	33	9	15	3	0.19	Normal
13	102	14	62	14	0.23	Normal
14	152	23	81	20	0.25	Normal
15	202	40	115	23	0.20	Normal
16	159	16	88	20	0.23	Normal
17	207	27	95	28	0.29	Normal
18	132	20	80	15	0.19	Normal
19	89	28	50	9	0.17	Normal

20	93	25	60	12	0.20	Normal
21	98	6	43	10	0.23	Normal
22	160	26	91	20	0.22	Normal
23	141	8	77	18	0.23	Normal
24	298	16	119	33	0.28	Normal

Table 4.5 Settlement results from 1st Monte Carlo simulation

For engineering design, the mean values are commonly of most interests. As seen from Table 4.5, in 1000 generations, the mean values of settlement of Element 24 and Element 15 are the biggest two among the total fifteen elements, while the first three elements, from Element 10 to Element 12, settle less than any others and the settlements are all smaller than 20 mm. That means the subsoils below Element 10 to Element 12 are much stiffer than those in other locations of this area. The results are plotted along the tunnel line in Figure 4.5

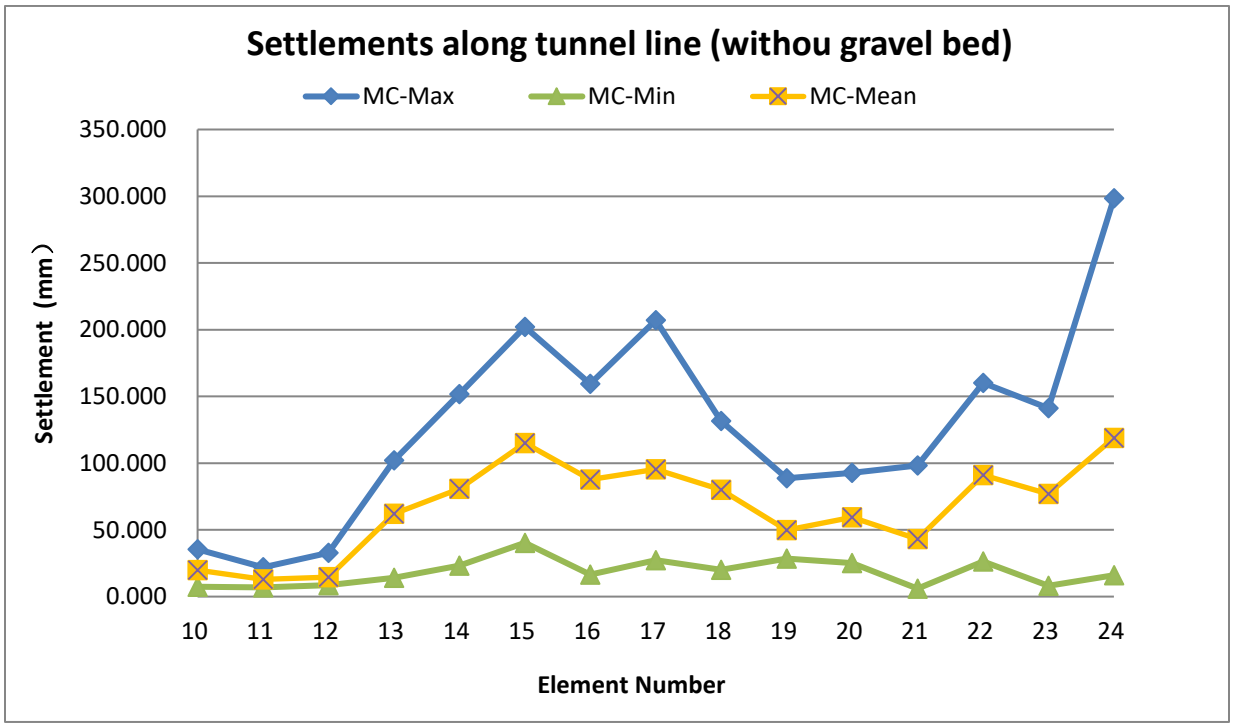

Figure 4.5 Spatial distribution settlement (without gravel bed) along the tunnel line

Figure 4.5 shows the possible settlement along the tunnel alignment, the topper blue line and the lower green line represent the maximum and minimum probable settlement respectively. In another word, nearly all the possible settlement will occur in the area between these two lines. Because the settlement for each element is distributed normally, the values closed to the mean value will take the most portions in the 1000 generations. In another word, the mean value is the most representative in the real construction.

The settlement spatial distribution will be affected by the soil strata in construction area, which is

shown in Figure 4.1. Comparing the geological profile and the determined results, it is easily to understand the reason that settlements fluctuate along the tunnel alignment, and the maximum settlement occurs in Element 24, beneath where, the “red pocket” (weak zones) can be found.

Comparison of deterministic results and probabilistic results

As described in Section 4.2, a deterministic method is performed based on the design values of soil properties. A comparison of the settlement results between deterministic method and two probabilistic methods (PEM and MCS) is made in this section.

In Figure 4.6, the mean values of two PEM and MCS are plotted together with deterministic results. As demonstrated in the graph, the Monte-Carlo Simulation perfectly match the deterministic method while small differences can be found in PEM. This phenomenon confirmed that in MCS, a number 1000 simulation times is sufficient to get convergent results with a significant accuracy in settlement determination.

Although, small differences can be found in PEM results, overall, it can still provide high similarity and considerable accuracy in this comparison.

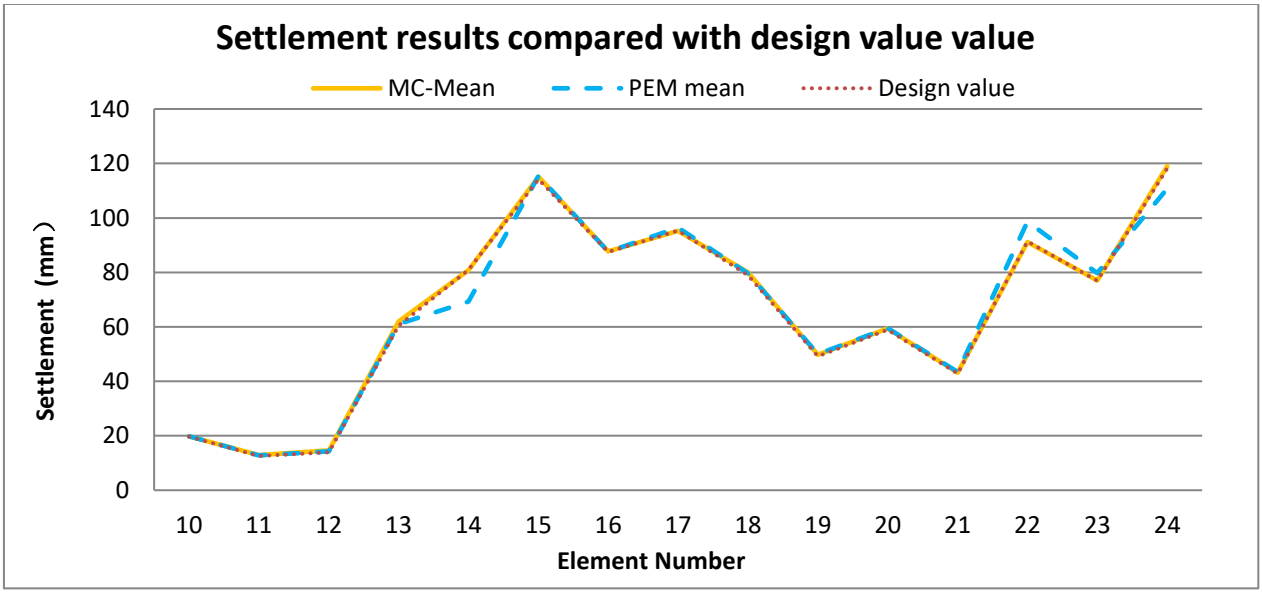

Figure 4.6 Comparison between deterministic method and probabilistic methods in settlement results

Comparison of Monte Carlo Simulation and Point Estimate Method

The settlement and COV from two methods (MCM and PEM) are plotted together in Figure 4.7 and Figure 4.8.

Figure 4.7 demonstrates the comparison of settlement between the range ($\mu \pm \sigma$) in Monte Carlo Simulation and Point Estimate Method. As shown in graph, results from the two different approaches show high similarity in mean values of settlement. While, the fluctuation range of settlement in PEM is slightly wider than in MCS, which means, the maximum and minimum values of PEM are slightly higher and lower than those ($\mu \pm \sigma$) in MCS, respectively. This can be caused by limitation of input variable combinations and discontinuous variable selection.

The input for each variable in PEM are selected only at two points ($\mu \pm \sigma$), because of which,

possibility of the values that exist out of the range ($\mu \pm \sigma$) are not involved. Thus, the maximum and minimum values from PEM are not particularly significant, as that they cannot represent the entire distribution of output. This problem can be easily solved in Monte Carlo simulation where nearly all the possibilities ($\mu \pm \mathbf{3\sigma}$) of input variables can be generated from enough calculation times.

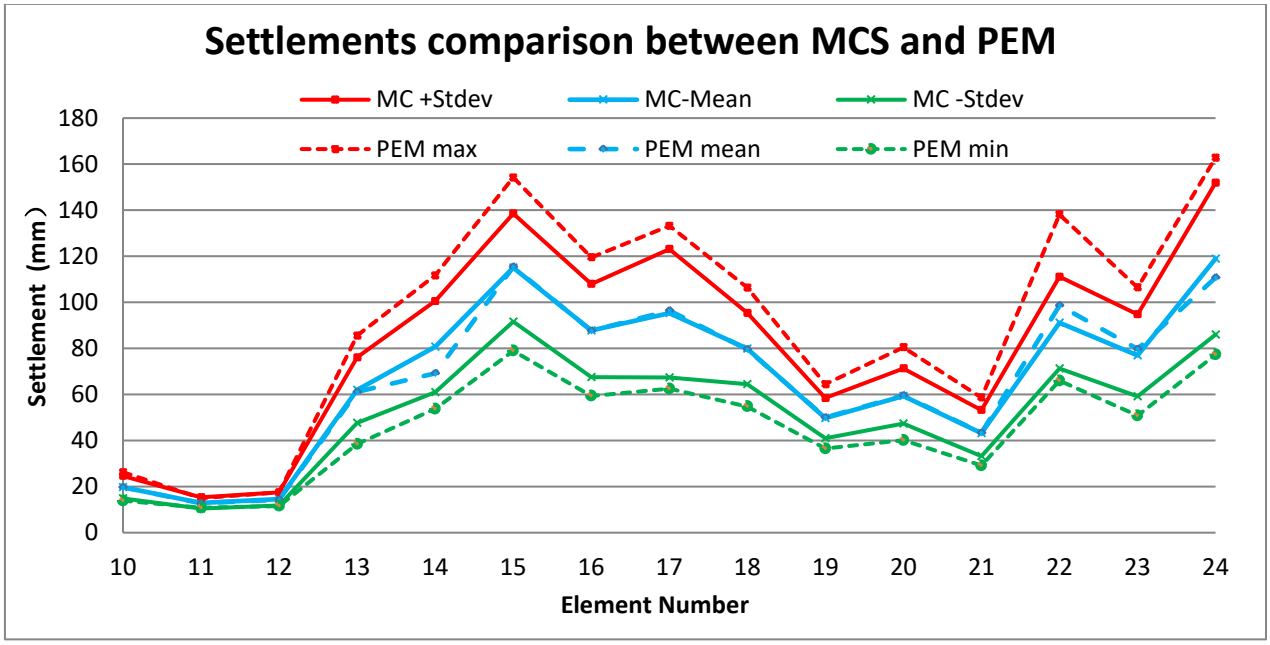

Figure 4.7 Settlement comparison between MCS and PEM

The coefficient of variation of the settlement results from these two methods are presented in Figure 4.8. Visible difference can be found in the graph, for most tunnel elements, the COV from PEM are larger than those from Monte Carlo simulation. One possible cause is that in PEM, the number of calculations totally depend on the number of variables, thus the output results are discretely generated based on the combinations (2^n). While in MCS, for sufficient simulations, the output results are approximately continuous, including nearly all the possibilities of input variables from their distribution.

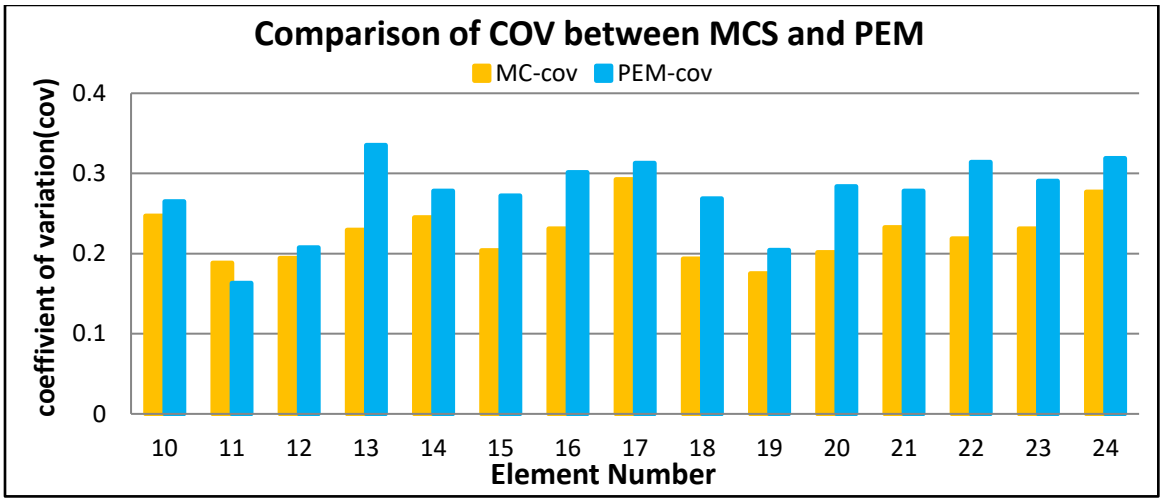

Figure 4.8 COV comparison between MCS and PEM

Advantages and disadvantages for MCS and PEM

Methods	Advantages	Disadvantages
Monte Carlo simulation	High accuracy	High computational cost
	Provide complete output distribution	
	Require little knowledge about probabilistic theory	
PEM	Considerable accuracy	Less accurate than Monte Carlo
	Lower computational cost	Does not provide complete output distribution
	Requite little knowledge about probabilistic theory	Not accurate in the "tails", which are out of the range $(\mu \pm \sigma)$

Table 4.6 Pros and Cons for MCS and PEM

As shown in Table 4.6, both pros and cons for those methods are clearly listed, the chosen of method depends on the engineering requirements including required accuracy level, computational costs and the expectation from the output.

4.5 Influence of gravel bed on settlement

2nd Monte Carlo simulation (with gravel bed)

In order to have an understanding of the influence of gravel bed on immersed tunnel settlement, a second Monte Carlo simulation is performed. In this condition, firstly, a 1.3 m thick gravel bed is installed on the subsoil with a unit weight of 21 kN/m^3 and a Young's Modulus of 50 MPa. Then the tunnel elements are placed on the gravel bed.

In 2nd Monte Carlo simulation, the unit weight and Young's Modulus of gravel bed are considered as constant values instead of variables. After the installation of gravel bed, subsoil stress has been changed due to additional weight of gravel and then recalculated, simultaneously the settlement of gravel bed itself is also counted in the total settlement for each element.

The settlement results from 2nd Monte Carlo simulation for each element are listed in Table 4.7. The comparison between these two Monte Carlo simulations (with and without gravel bed) for settlement spatial distribution is plotted in Figure 4.9.

Element No.	Max value (mm)	Min value (mm)	Mean value (mm)	Standard deviation (mm)	COV	Distribution type
10	27	9	17	3	0.16	Normal
11	28	13	18	2	0.13	Normal
12	40	14	20	3	0.14	Normal
13	84	21	54	10.	0.20	Normal
14	126	19	71	15	0.21	Normal
15	189	51	110	20	0.19	Normal
16	128	38	78	16	0.20	Normal
17	201	33	87	23	0.27	Normal
18	115	29	71	12	0.17	Normal
19	82	28	46	7	0.14	Normal
20	87	19	52	9	0.18	Normal
21	65	17	39	7	0.17	Normal
22	141	30	82	16	0.20	Normal
23	115	21	69	14	0.20	Normal
24	199	36	107	28	0.26	Normal

Table 4.7 Settlement results from 2nd Monte Carlo Simulation (with gravel bed)

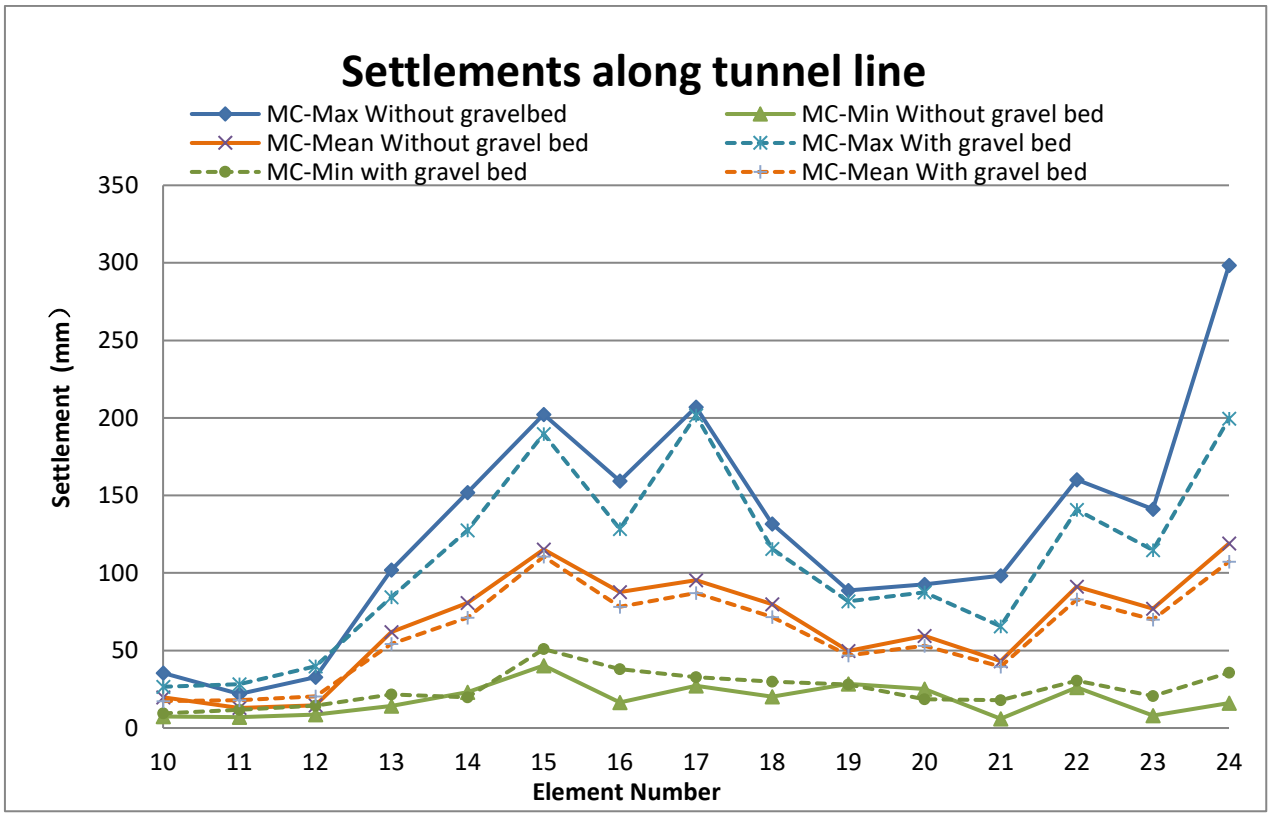

Figure 4.9 Comparison of settlement for conditions with and without gravel bed

Figure 4.9 presents the difference between the settlement results for two conditions, with and without gravel bed. The dashed lines represent the settlement of tunnel element placed on gravel bed, whereas solid lines represent the settlement of tunnel element placed directly on the subsoil.

Influence on settlement magnitude

As illustrated in this graph, considering the mean values, the orange dashed line is mostly below the orange solid line, which means that the settlement results for elements with gravel bed are smaller than in the case without gravel bed, the averaged reducing settlement is approximately 9%.

Therefore, the gravel bed can be considered as an improvement to the subsoil. However, for the Element 11 and Element 12, the settlements are higher than those without gravel bed. That is because, even gravel bed can to some extent densify the whole soil column below these elements, the subsoil below E10 and E11 are already stiff enough, and original settlement will not be influenced that much by gravel bed installation, while on the other hand, the gravel bed itself will settle for a certain value, thus after taking the settlement of gravel bed into account, the total settlement for E10 and E11 are even more than before.

What is more, the green dashed line and solid line represent the minimum of settlement. As a possible function of gravel bed mentioned above, settlement with gravel bed should be lower than those with gravel bed. However, the results in two green lines give an opposite trend. The reason is that for all minimum settlement values, the input parameters with lowest compressibility are occasionally selected from the input variable data base, resulting in minimum settlement values among the 1000 realizations. While the stiffness and thickness of gravel bed are constant in this

case, the combination of the settlement makes these values bigger than those without gravel bed.

Influence on COV (coefficient of variation)

As discussed in the previous section, after the installation of gravel bed, the maximum values of settlement along tunnel alignment are mainly decreased and minimum values are increased. Consequently, the range of fluctuation of settlement reduces. The coefficient of variation for each element can be responsible for the range of fluctuation.

The COVs are plotted in two conditions in Figure 4.10

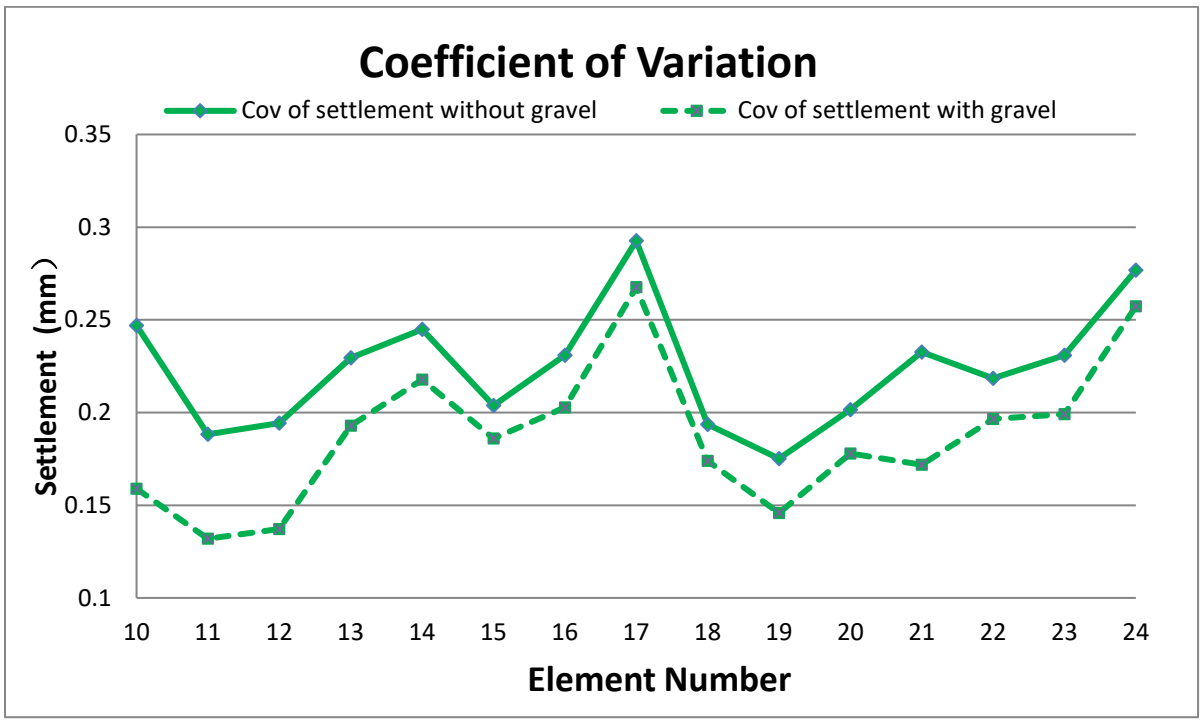

Figure 4.10 Comparison of coefficient of variation of settlement

This figure intuitively represents that in the condition with gravel bed, coefficient of variations (COVs) are decreased, averaging 16%. In another word, the installation of gravel bed reduces the probability of occurrences of limit values, as well as the possibility of potential failure.

4.6 Stiffness back calculated from settlement distribution

On purpose of setting up soil structure model to generate the shear force in tunnel joints, a beam-spring structural model will be built in Chapter 5, and in the model, each “spring” is simulated by soil column combined with gravel bed below each element. As shown in Figure 4.11 the original sublayers are then simulated by an equivalent soil column. Then, the stiffness of each soil column is back calculated based on the settlement results from previous section and is considered as the input variable in beam-spring model.

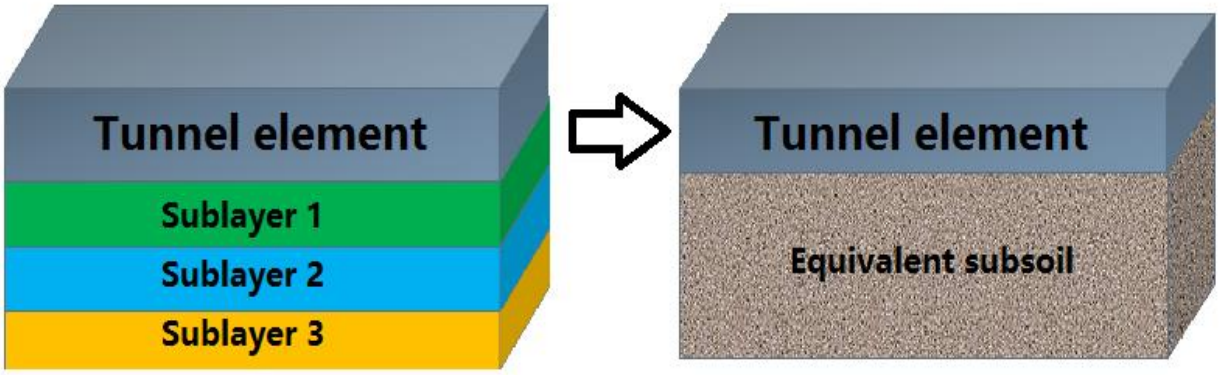

Figure 4.11 Determined the equivalent stiffness of subsoil

The equivalent stiffness distribution for each soil column is back calculated from the settlement distribution and thickness of entire column.

$$E = \frac{P \times H}{S} \tag{4.8}$$

Where

E = equivalent stiffness for soil column

P = acting load

H = equivalent thickness of soil column

S = displacement of the soil column

In this section, to facilitate the establishment of the model in PLAXIS, the equivalent H, is fixed as 30 meters and equals to each other.

Stiffness as well as its stochastic characteristics for each soil column are listed in Table 4.8.

Element No.	Max value (MPa)	Min value (MPa)	Mean value (MPa)	Standard deviation (MPa)	COV	Distribution type
10	601.29	185.83	334.30	54.06	0.161	Normal
11	560.49	232.90	372.47	47.93	0.128	Normal
12	473.02	171.05	338.64	43.55	0.128	Normal
13	290.03	74.30	120.49	26.69	0.221	Normal
14	348.36	54.14	102.32	26.88	0.262	Normal
15	145.12	38.93	69.30	14.18	0.204	Normal
16	201.47	59.55	102.18	22.76	0.222	Normal
17	236.61	38.52	95.97	27.89	0.290	Normal
18	259.28	67.12	111.88	21.81	0.194	Normal
19	276.29	94.66	168.69	24.69	0.146	Normal
20	414.68	88.38	151.15	30.97	0.204	Normal
21	443.52	120.77	205.52	37.28	0.181	Normal
22	268.24	58.11	103.08	23.31	0.226	Normal
23	394.30	71.23	122.01	27.80	0.227	Normal
24	221.36	39.64	79.21	23.49	0.296	Normal

Table 4.8 Equivalent stiffness distribution for each soil column with gravel bed

5. Soil structure interaction and reliability analysis

5.1 Introduction

A general soil-structure interaction analysis method, beam-spring model, is introduced in Literature study. In this model, soil is considered as linear elastic material and the key approach is to determine the soil reaction modulus (stiffness modulus). In chapter 4, the settlement distributions for each tunnel element are generated by Monte Carlo simulation and the corresponding stiffness distributions are back calculated.

In this chapter, firstly, the scale of fluctuation of soil stiffness is determined by Space Average Method. Based on theory in literature study and the settlement results from Chapter 4, three PLAXIS models with different purposes are set up to evaluating the shear forces along the tunnel alignment. The first two models are carried out in the condition that the stiffness of soil units is independent from each other. In the 3rd model, the determined SOF (scale of fluctuation) of stiffness is applied and the impact of stiffness correlation on shear force is analyzed.

In order to achieve the efficiency and save calculation costs, a Python script is written in cooperation with PLAXIS to perform Monte Carlo Simulation with 1000 iterations. The outputs form PLAXIS will be automatically stored by coding.

Finally, reliabilities against shear force SLS for all these models are generated and compared the relative differences of the results are discussed.

5.2 Stiffness scale of fluctuation determination

The stiffness distribution for subsoil below each element is determined in Chapter 4 and will be used as input variable in soil-structure model.

Reliability of a structure is considered as a function of both point statistics (COV, mean, discussed in previous section) and a spatial correlation property or autocorrelation function (scale of fluctuation). In this case study, the length (2700m) of the research area is much bigger than the soil depth (approximately 30m). The shear behavior of tunnel joints is influenced by different settlement between elements, caused mainly by spatial variability of stiffness in horizontal direction. Thus, the scale of fluctuation in horizontal direction (θ_h) is of more interests than in vertical direction (θ_v). Therefore, in this section, only θ_h is determined and applied in the 3rd model.

The Space average method described in Literature study is used to determine θ_h of the stiffness, the main approaches are as follow:

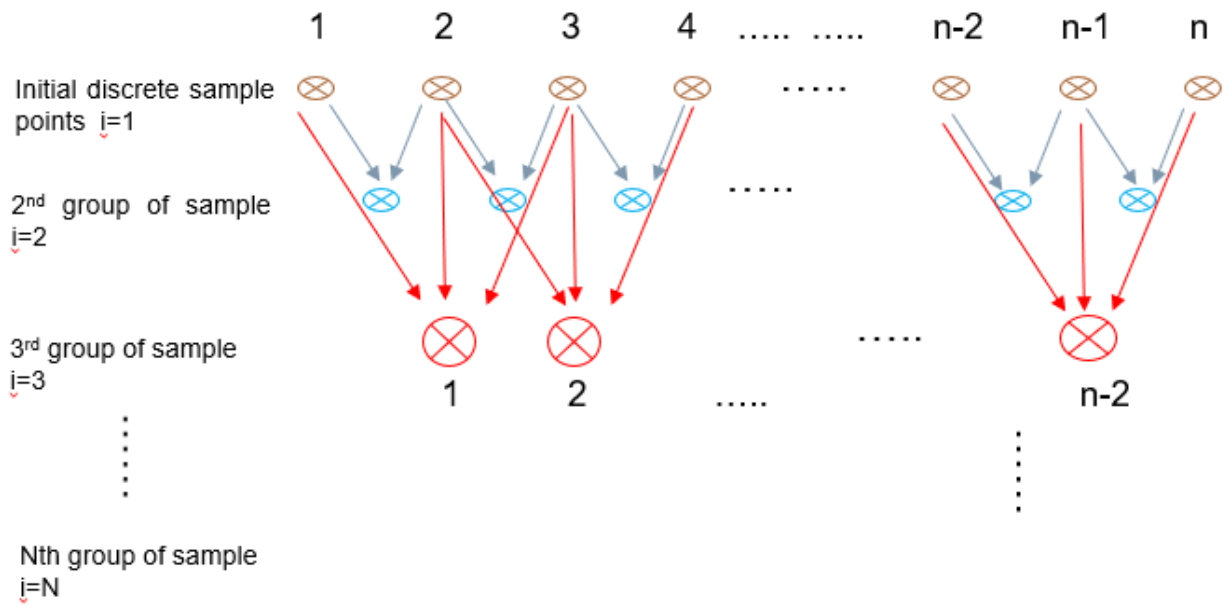

1. The initial discrete sample points are selected, with a horizontal distance (Δ_h) between each other, calculate the point statistic value, initial mean (μ) and initial standard deviation (σ);
2. Let $i = 2$, build new a set of data based on the mean values of every two adjacent points. Determine the standard deviation of the built data, ($\sigma_{(2)}$);
3. Calculate $\Gamma(2) = \frac{\sigma_{(2)}}{\sigma}$;
4. Sketch the points $(2, \Gamma(2))$, on the plot of $\Gamma(i) \sim i$;
5. Let $i = 3, 4, \ldots$, repeat step 2, 3, and 4, continuously add points on plot $\Gamma(i) \sim i$;
6. Find the stable point of (n*, $\Gamma(n^*)$), the scale of fluctuation can be determined as

$$\theta = n^* \cdot \Delta_h \Gamma^2(n^*)$$

Scale of fluctuation based on tunnel element

Firstly, to determine the value of θ_h, the initial discrete sample points are selected from the subsoil beneath each tunnel elements separately (Figure 5.1), resulting in a total number of 15 points (from Element 10 to Element 24), and a distance (Δ_h) of 180 m from each other.

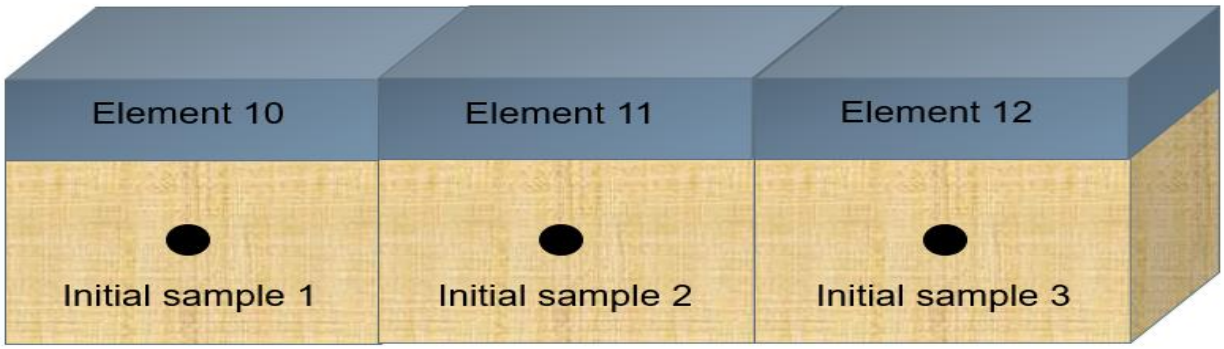

Figure 5.1 Initial sample points selected based on element

The results and plot of $\Gamma(\mathrm{i})\sim\mathrm{i}$ are shown in Figure 5.2

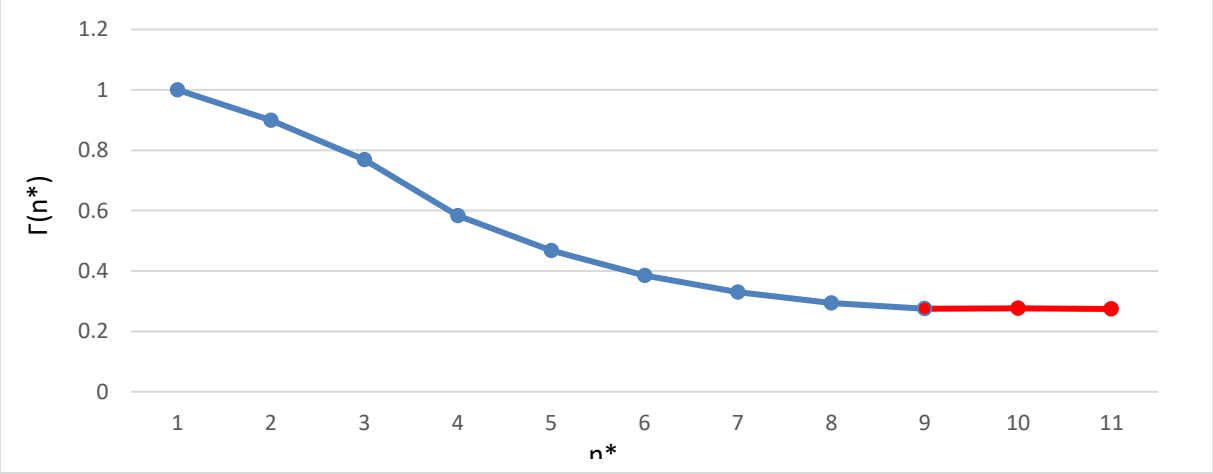

Figure 5.2 Γ(n*) vs n*

As illustrated in Figure 5.2, the stable point for $\Gamma(n*)$ is n* = 9, then

$$\theta_h = n^* \cdot \Delta_h \Gamma^2(i) = 9 \times 180 \times \Gamma^2(9) = 118.1m$$

Previous publications indicated that, a range of θ_h of soil stiffness is approximately from 3 m to 80 m (Phoon, 1995). According to the calculation method, the value of scale of fluctuation is significantly influenced by the number of original sample points and the interval distance between each point, since the number of sample (n^*=15) is relatively small and an interval distance of 180 m is way larger than those used in most engineering cases to determine θ_h . Even a stable point can be found from the plot, the value is to some extent unrealistic compared with published literatures.

However, because of the limitation of available data points, it is impossible to generate an accurate in-situ scale of fluctuation. Thus, $\theta_h = 118$m is used in this paper to analyze the impact of stiffness correlation to the tunnel joints shear behavior in a qualitative way other than quantitative.

5.3 Model description

In this section, three different “beam-spring” models are carried out, 1st model is only focusing on the shear forces in element joints. 2nd model is considering the shear forces in all segment joints, and the 3rd model shares the same domain with 2nd model, while in this case, the correlation length of subsoil stiffness is taken into account.

1st Model

This model is set up in Plaxis2D, as shown in, the tunnel elements are simulated by “Plates” placing on the top of soil polygons, the yellow points in between are “connections”, and the subsoils are modeled by using “Soil polygon” in Plaxis2D. On the purpose of analyzing the reliability of shear force in tunnel element joints against Serviceability Limit State (SLS), the model is set up elementally consisting of 15 elements. The soil domain is divided into 15 soil polygons below each element, each soil polygon has a normal distributed stiffness values with different means $(\mathrm{u}_i, i = 1,2, \dots 15)$ and standard deviations $(\sigma_i, i = 1,2, \dots 15)$,and they are independent from each other. Shear forces are calculated for each element joints. Each soil polygon has a dimension of 30 meters in depth and 180 meters in length as shown in Figure 5.3

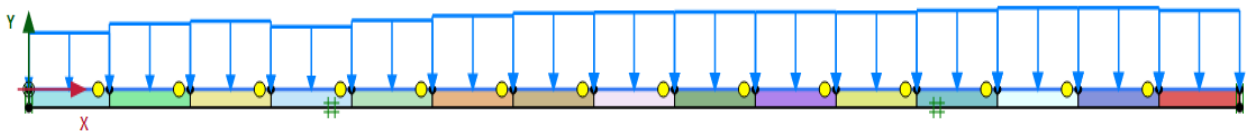

Figure 5.3 1st Soil-structure interaction model in PLAXIS

2nd Model

To avoid the possibilities of bending failure during transportation process, immersed tunnel elements are mostly product segmentally. In HZBM immersed tunnel, each element consists of 8 segments with 22.5 m in length (Figure 5.4). And they are connected by segment joints, in which shear failure may possibly occur. Thus, it is necessary to set up a detailed soil-structure interaction model based on the tunnel segment joints.

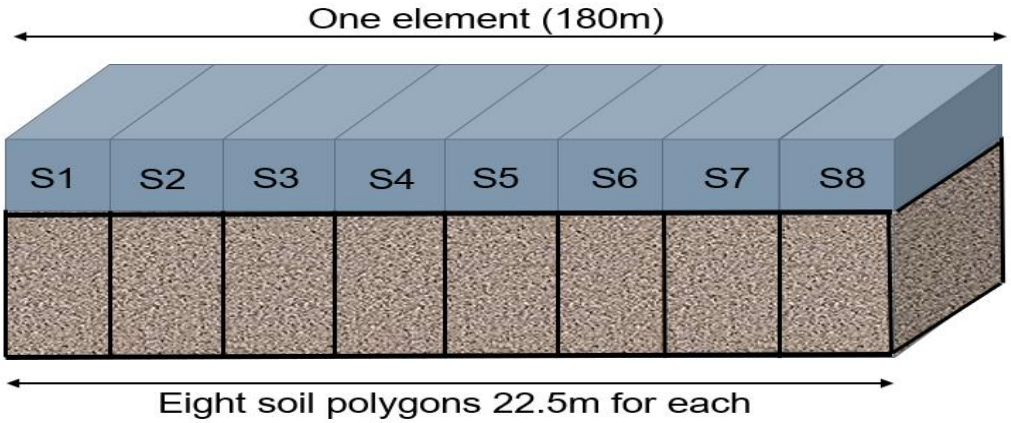

Figure 5.4 Eight segments in one element

In the 2nd PLAXIS model (Figure 5.5), on behalf of analyzing the shear forces occurring in segment joints, the soil domain is further subdivided based on the location of each segment,

result in 120 soil polygons in total, every 8 soil polygons share the same stiffness distribution. In every generation, the input stiffness for each soil polygon is random selected from the corresponding distributions.

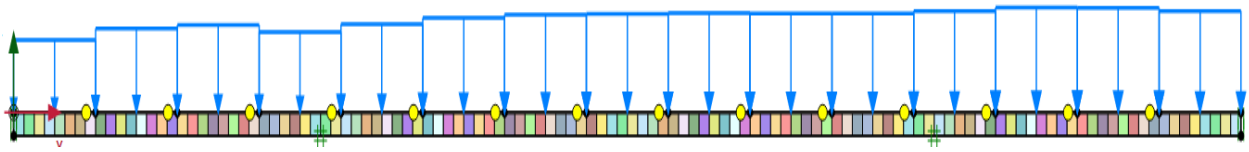

Figure 5.5 2nd Soil-structure interaction model in PLAXIS

3rd Model

The third model has the same domain with the 2nd one, as shown in Figure 5.6, the only different is that in this case, the spatial correlation of stiffness is taken into consideration. The value of scale of fluctuation is determined in Section 5.2, and correlation coefficient matrix of the input stiffness is set up with the use of an exponentially decaying Markovian correlation function (Griffiths, 1999).

$$\rho(\tau) = e^{-(2\tau/\theta h)}$$

Where, ρ is the familiar correlation coefficient and τ is the absolute distance between two points in the middle of different segments. θh is the horizontal scale of fluctuation of stiffness which equals to 79.2 m.

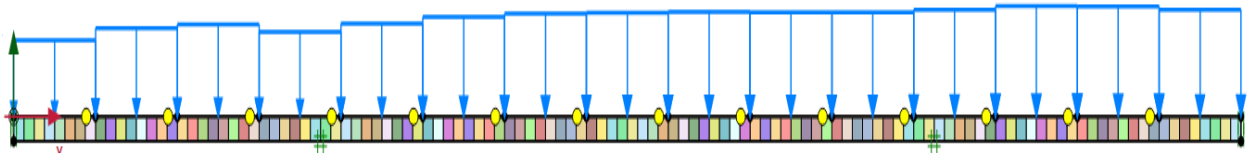

Figure 5.6 3rd Soil-structure interaction model in PLAXIS

5.3.1 Model type

As mentioned before, in HZMB immersed tunnel project, the subsoils are under over consolidated state due to large excavation depth. Even after installation of tunnel elements, backfilling and siltation, the soil stress will still not exceed the previous stress state. Thus, the deformation, in this case, can be considered as purely elastic behavior, and in material set window of PLAXIS, 'Soil Model' is chosen as 'Linear Elastic'. Since, this research is based on the behavior at 100 years after construction, the main soil material is sand, therefor 'Drainage Type' is set as 'Drained'. The tunnel element is simulated by "Plate" in PLAXIS, and "Connection" is used to model tunnel joint (yellow points shown in Figure 5.3). Parameters of "Plate" are introduced in next section.

5.3.2 Input parameters

The detailed input variable for soil is stiffness, and the values for each element are determined in Chapter 4. On purpose of simulating the spring behavior in "Beam-spring" model, here Poison's ratio is set as zero.

The parameters for 'Plate' are listed in Table 5.1

Parameter	Name	Value
Normal Stiffness	EA	5.24E9
Flexural Rigidity	EI	99.5E9

Table 5.1 Parameters for Plate

5.3.3 Boundary conditions

Location	Displacement horizontal direction	Displacement vertical direction
Both ends	Fixed	Free
Bottom	Fixed	Fixed

Table 5.2 Boundary conditions

5.4 Python scripting

Since in the PLAXIS input windows, the input for each soil property can only be a single value (Figure 5.7), it is impossible to change soil properties for every generation manually in Monte Carlo Simulation. Furthermore, number of soil polygons in the 2nd and 3rd model is 120 (Figure 5.5 and Figure 5.6), it is time consuming to create these polygons by hand.

Thus, a Python script is written to post PLAXIS creating soil domain, selecting parameter and storing output data from each generation, automatically

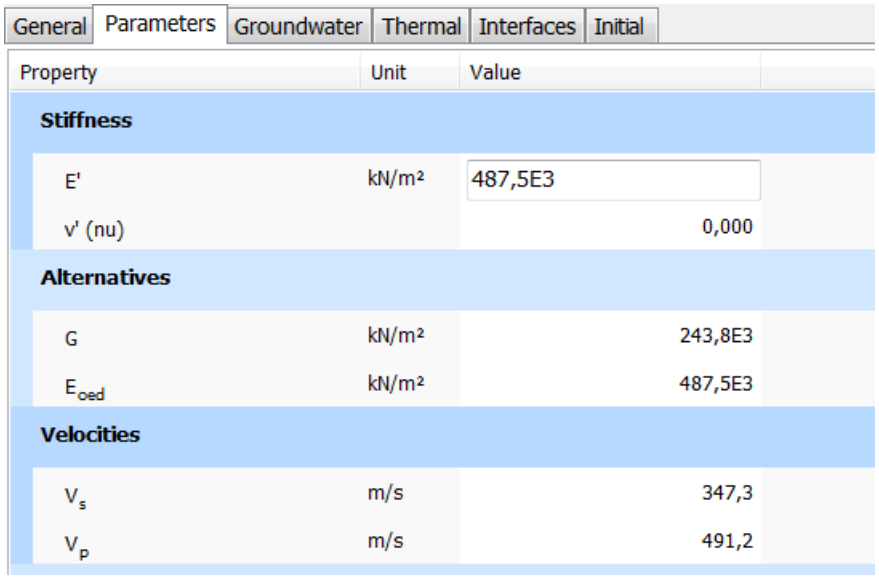

Figure 5.7 Parameters input window in PLAXIS

The main working procedures of Python scripts are listed as follow.

Step 1: Connect PLAXIS with Python

a) Starting the scripting sever

b) Connection to a remote PLAXIS application

c) Creating a project

The detailed information for how to get Python scripts connected to PLAXIS is described in PLAXIS 2D Reference (Ronald, 2016).

Step 2: Create soil domains and structures

In the soil structure interaction model, for each soil polygon, stiffness is the only variable. Thus, fixed values, such as properties of the tunnel element, the size of soil polygon, the acting load and boundary conditions, are created first and saved as default to reduce computational costs.

Step 3: Create stiffness matrix

In order to let PLAXIS select properties automatically, a stiffness data base has to be created in advance. In the first model, the size of stiffness matrix is 15*1000, for fifteen soil polygons and 1000 simulation times while in the 2nd and 3rd model, the matrix has a size of 120*1000. To understand the influence of correlation length on the shear forces, the scale of fluctuation is applied to create a correlated stiffness matrix in the 3rd model.

Step 4: **Store the results**

In PLAXIS, the results are coming from PLAXIS Output window, the output file opens automatically after each simulation. There is a threshold on the numbers of active projects can be opened at the same time in Output. Due to that 1000 is exceeding this threshold, the software will be crashed after a certain time or error will occur. Thus, a command is written in the scripts to close the active model each time after storing the results.

The relative codes including PLAXIS-Python connection and creation of stiffness matrix and shown in **APPENDIX C**.

5.5 Results from Monte-Carlo simulation

In this section, the results from Monte-Carlo simulations in 3 models are discussed and compared. The output has positive and negative values due to the direction of shear force. In the reliability analysis, only the magnitude of the value is taken into consideration, thus the output shear forces are transferred to absolute values.

5.5.1 Shear forces in tunnel element joints

1st Model

From 1000 calculation times, the stochastic values of each joint are listed in Table 5.3 and plotted in Figure 5.8.

In the table, “Joint No.1” means the first joint between the first two tunnel elements (Element 10 and Element 11), as a total number of elements is 15, results in 14 joints in between.

Joint number	max (kN)	min (kN)	mean (kN)	std (kN)	COV
1	3779.86	0.26	569.51	467.98	0.82
2	2517.58	0.33	532.84	412.74	0.77
3	15798.27	398.82	3486.37	1293.72	0.37
4	15117.17	1.67	1436.87	1249.49	0.87
5	9211.34	2.27	2857.89	1720.19	0.60
6	10187.34	3.28	2646.04	1738.06	0.66
7	6607.49	4.65	1703.95	1284.96	0.75
8	7322.12	4.24	1595.17	1271.86	0.80
9	9202.83	1.75	2090.90	1366.11	0.65
10	8736.71	2.21	1467.39	1173.66	0.80
11	7942.75	0.70	2053.81	1337.19	0.65
12	13251.32	28.52	4120.25	1894.06	0.46
13	12411.89	0.66	2317.20	1881.24	0.81
14	18871.59	14.99	2740.93	2032.59	0.74

Table 5.3 Stochastic values for element joints

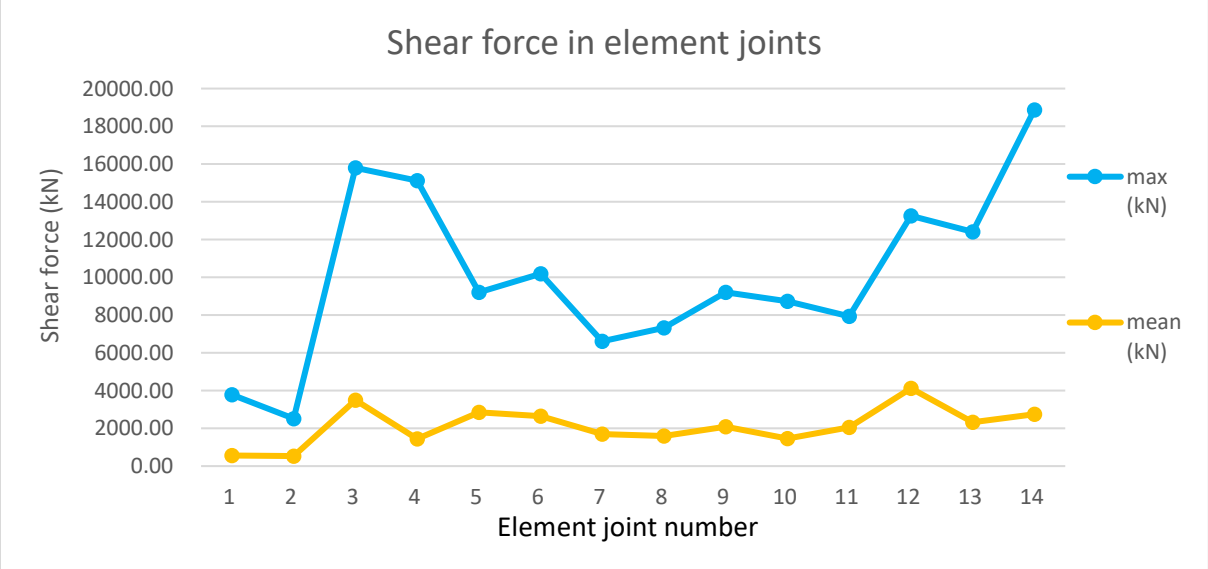

Figure 5.8 Shear force in element joints

In this graph, the minimum shear forces are not shown, one of the reason is that as shown in Table 5.3, they are relatively small and can be negligible in the graph, another reason is minimum values are of less interests of determination of the probability of failure.

5.5.2 Shear forces in segment joints (without correlation length)

2nd Model

In the second Monte Carlo simulation, all shear forces are determined on segment joints and the correlation length is not taken into account in this case. For 120 segments, there are 119 joints in between, due to the large amount of values, the results are listed in **APPENDIX C,** the trend of shear forces for each segment joints are indicated in Figure 5.9 and compared with 1st model in Figure 5.10.

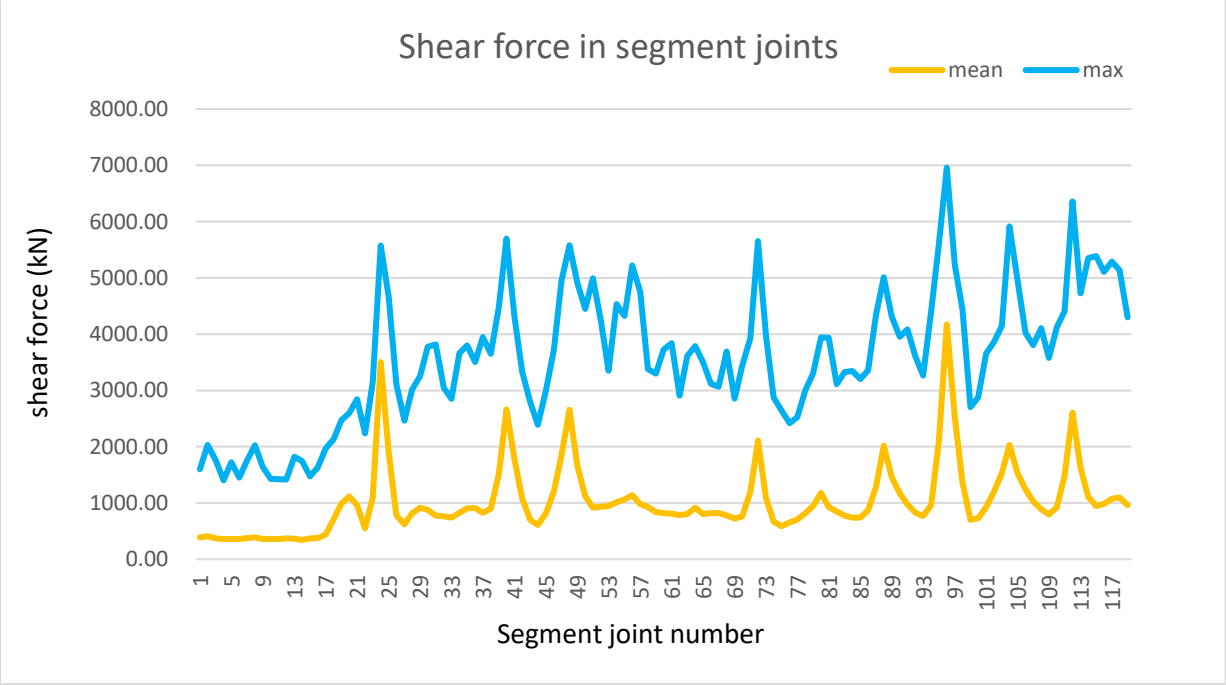

Figure 5.9 Shear force in segment joints

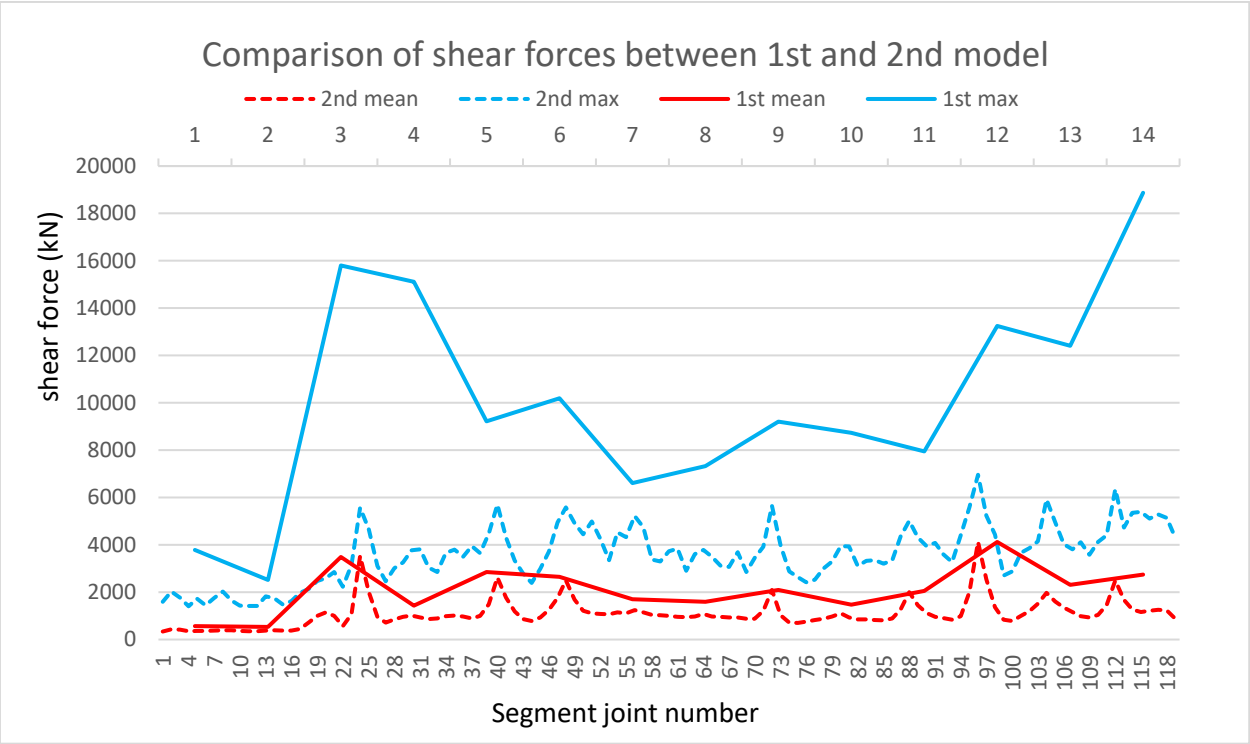

Figure 5.10 comparison of shear forces between 1st and 2nd model

As shown in Figure 5.10, generally, the maximum shear forces in 2nd model are way smaller than those in 1st model, the reason is in the 2nd model, due to subdivision of the soil unit, shear forces are transferred to the tunnel structure to some extent instead of concentrating in the tunnel joints. While the peak values of shear forces in both models occur approximately at the element joints instead of segment joints. That is because the within one element, the subsoil shares a same distribution of stiffness, and for two adjacent elements the subsoil may have significant different distributions leading to a "jump" in the shear forces.

5.5.3 Shear forces in segment joints (with correlation length)

3rd Model

In the 3rd model, the scale of fluctuation is applied, as shown in Figure 5.11. The mean values from 2nd model and 3rd model are exactly alike, in this point of view, two hypotheses have been made that, firstly, the correlation length (scale of fluctuation) does not significantly influence the mean values of shear forces in segment joints, or the correlation determined from $\theta h = 120 m$ is not high enough to be able to exert an considerable influence. These hypotheses are being proved in next section by applying larger values of θh.

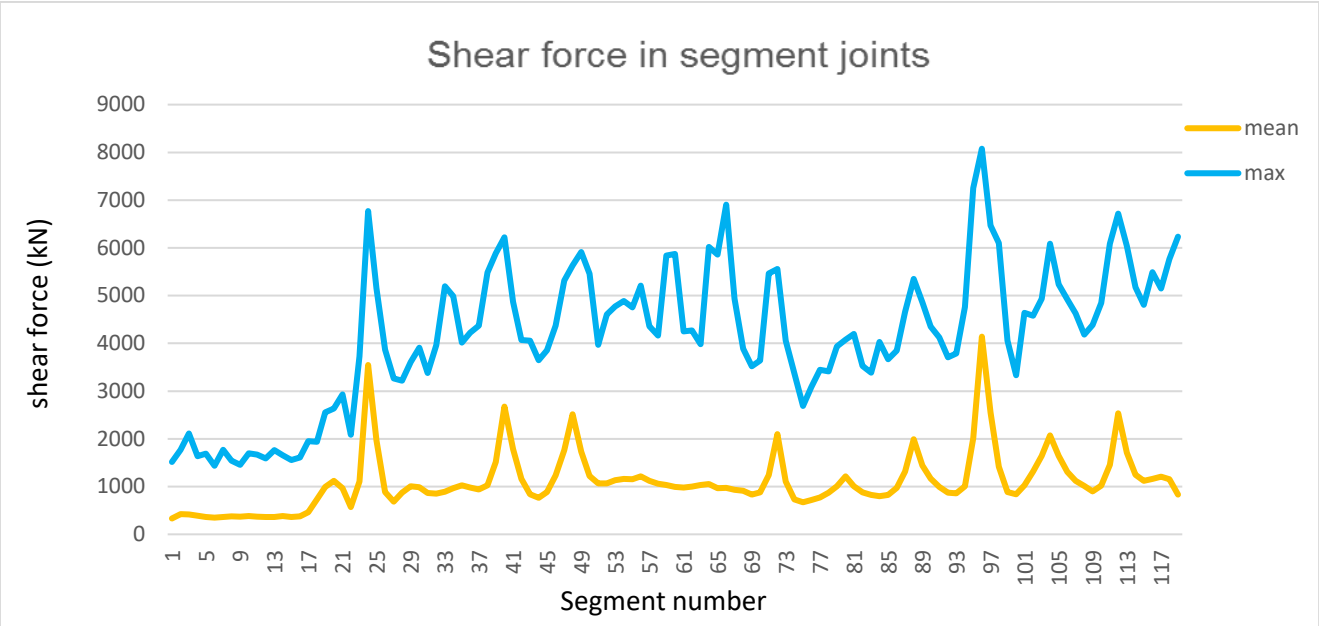

Figure 5.11 Shear force in segment joints (with correlation length)

Applying higher scale of fluctuation

From the comparison between the mean values of shear forces in 2nd Model and 3rd Model, no significant differences can be found. This may due to that the values of input scale of fluctuation (Sof), $\theta h = 120$m is not high enough. In this section, different values of θh are chosen and the corresponding mean values are plotted together in Figure 5.12.

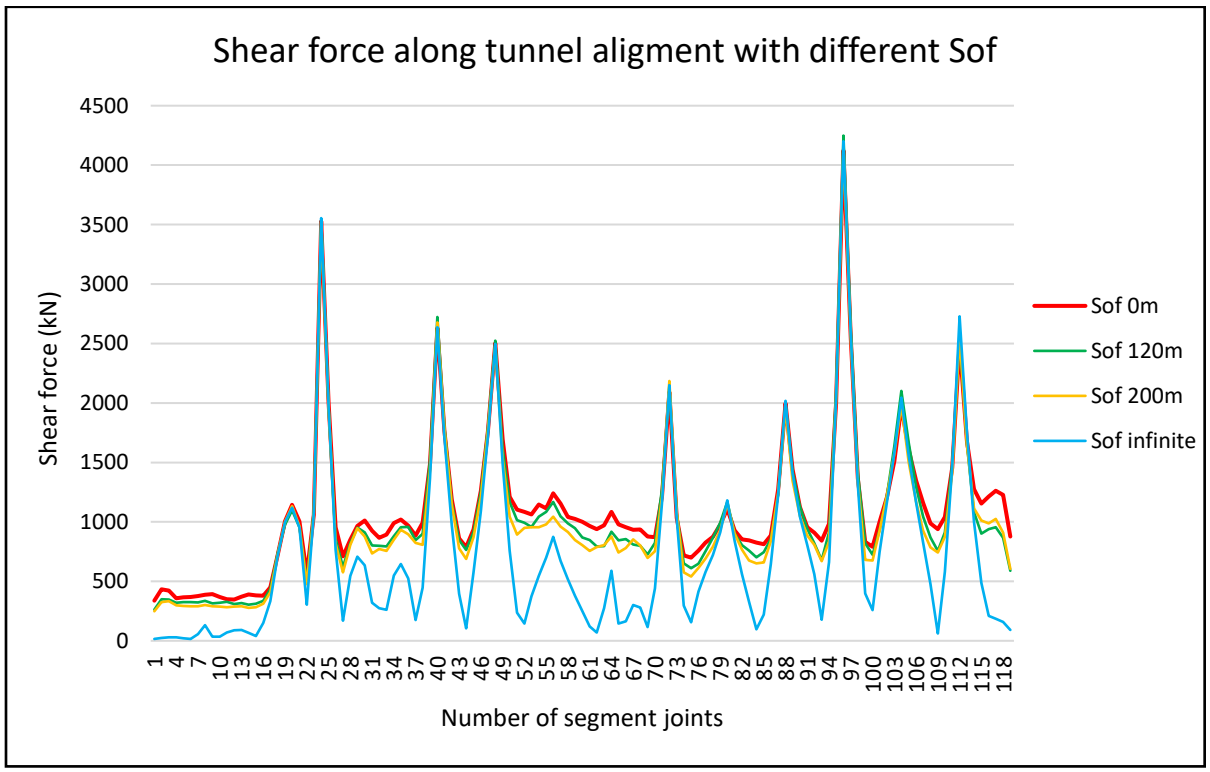

Figure 5.12 Mean values of Shear force for segment joints with different Sof

As shown in the graph, the mean values of shear forces decrease slightly with increasing scale of fluctuation ($\theta h = 0\ m, 120\ m, 200\ m$). Only when Sof is chosen as infinite, significant differences can be obtained at the segment joints except the peak values at element joints.

While in this analysis, a trial value of $\theta h = 200$ m is already unrealistic, thus there is no more engineering practical sense to apply values of θh larger than 200 m. To conclude, the magnitude of scale of fluctuation of stiffness does not has a strong impact on the mean values of shear forces.

One uncommon phenomenon is that, after application of the correlation length, the peak shear forces still occur at the same location with the similar magnitude. This is mainly caused by the condition in which that two soil polygons underneath adjacent segments have considerably different stiffness distribution. This phenomenon is unrealistic, since the soil properties within correlation length will not vary that much in real engineering project. Thus, the stiffness distribution is then corrected in the next section, to avoid the peak values and obtain reasonable results.

Correction of stiffness distribution

Theoretically, the magnitude of shear forces of one joint depends on the difference of the loads (ΔP) acting on the two adjacent segments, and the difference of stiffness (ΔE) of the subsoil below the two closed segments (Figure 5.13). Since in this project, loads are assumed to be constant (ΔP is constant), therefore, the difference of stiffness (ΔE) is the only factor influencing on the shear forces.

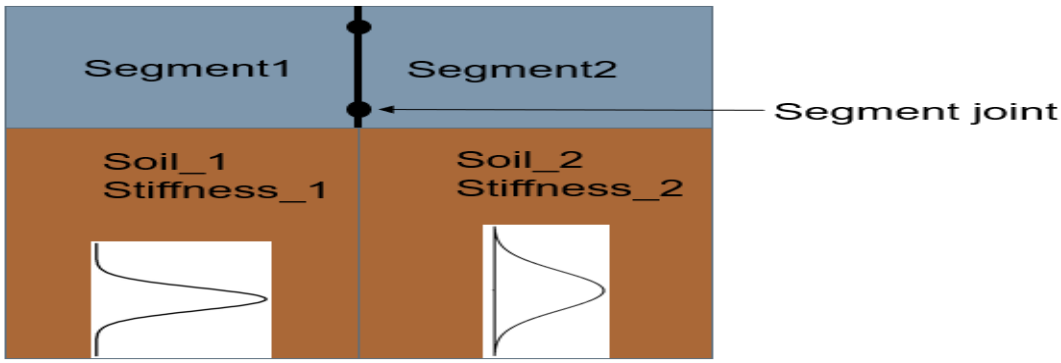

Figure 5.13 Segment joint in two elements with significant different stiffness distribution

In the case that, the distributions of the stiffness of two closed soil columns significantly differ from each other, the peak values of shear force will occur, even after applying scale of fluctuation, the mean values of shear forces in the corresponding joint are still approximately the same.

Figure 5.14 illustrates that the comparison of mean difference of stiffness (ΔE) between the cases with and without application of Sof. Although a value of $\theta h = 8000\ m$ is applied, mean values of ΔE are nearly the same resulting in 217803 kPa and 218391 kPa respectively.

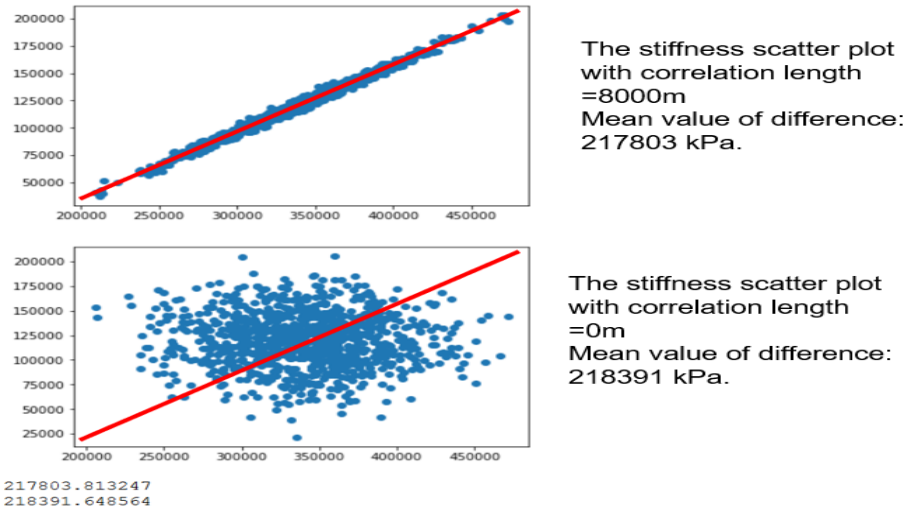

Figure 5.14 Comparison of mean differences of stiffness between Sof=0 and Sof=infinite

To avoid this unrealistic phenomenon, a corrected distribution of stiffness is shared by two closed soil polygons, which initially have significantly different distribution. As shown in Figure 5.13, for example, the soil polygon_1 has a distribution of stiffness_1, and the soil polygon_2 has a distribution of stiffness_2, and the corrected stiffness distribution, with an updated mean value and standard deviation are generated from the two original distributions as shown in Figure 5.15.

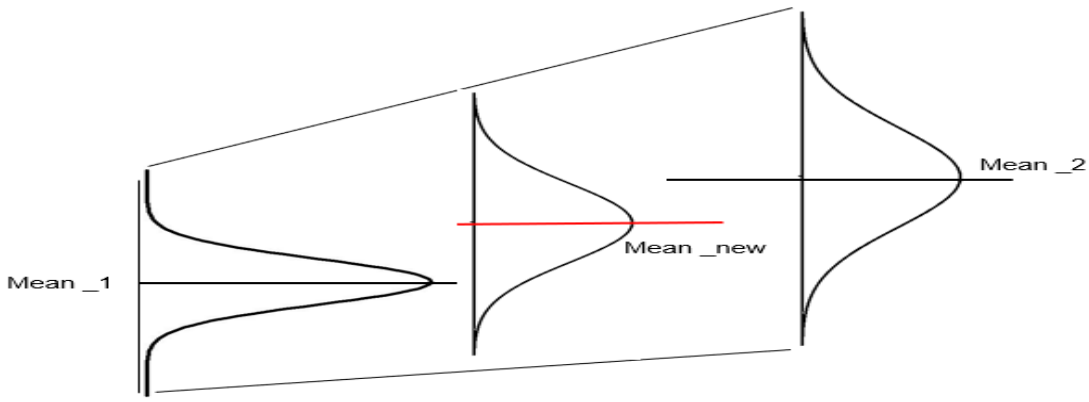

Figure 5.15 Uniformized distribution

After correlation of the stiffness distribution, another Monte-Carlo Simulation has been performed in the 3rd model and the results are indicated in Figure 5.16.

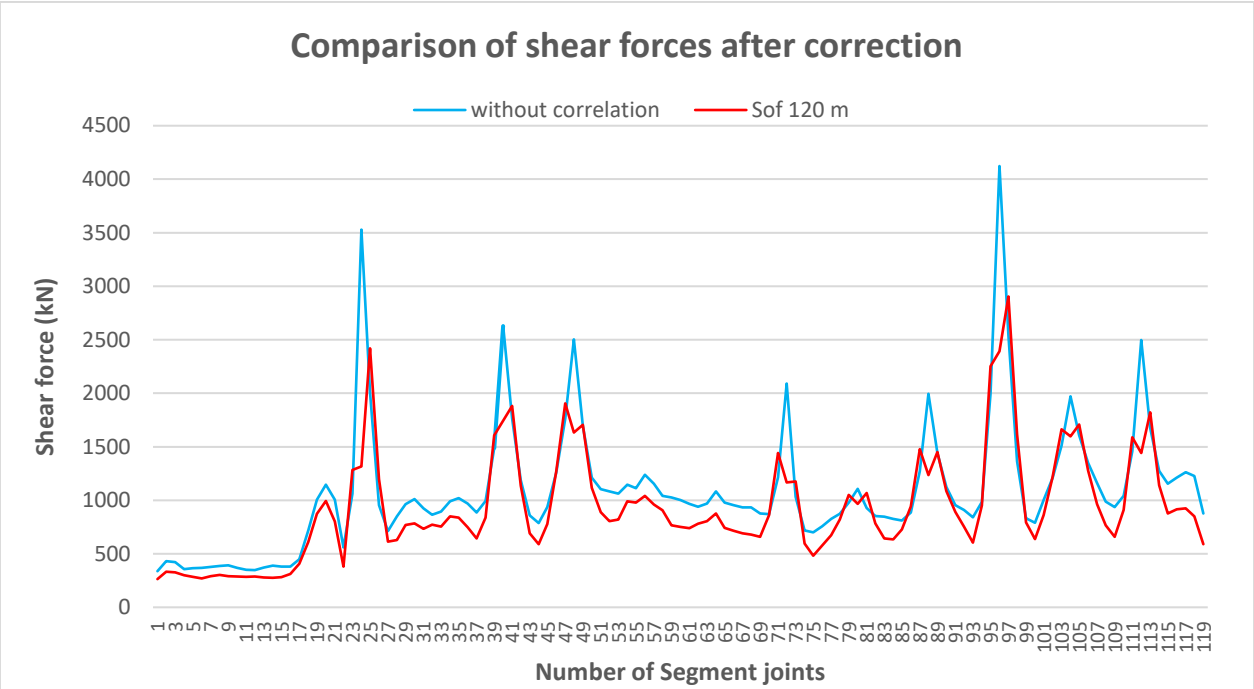

Figure 5.16 Comparison of mean shear forces along tunnel alignment

In the graph, the peak values are visually reduced after correction of the stiffness distribution, which results in more realistic and reasonable shear forces along the tunnel alignment.

However, the comprehensive shear forces can be only determined by detailed soil data with a relative small distance, e.g. every 20 meters. In this research, the soil properties are summarized based on elements with distance of 180 meters from each other. Thus, shear forces in each segment joint cannot be precisely defined. The reliability of this model is analyzed and compared with the former 2 models in the next section.

5.6 Reliability analysis of shear forces

In this section, reliability analysis is performed in all three models. The Serviceability Limit State (SLS) of shear capacity for tunnel joints are defined by the number of shear keys and the shear capacity of each shear key.

In HZMB immersed tunnel, each joint has four shear keys. And the capacity for each shear key is 6 MN and 8 MN for SLS and ULS (Ultimate Limit State)，respectively. Which means the SLS of shear force in the joints is 24 MN (6MN*4).

The probability of failure is determined as

$$P_f = \frac{nf}{n}$$

Where P_f is the probability of failure, nf is the number of failure times and n is the total simulations times. The reliability then equals to (1-P_f).

In immersed tunnel joints design, the required reliability is 95% (Richard, 2013). As clearly indicated in section 5.3, even the maximum values of shear forces among all three models are

much lower SLS (24MN), which means that in this case study, the reliability is 100%. In this point of view, the SLS can be reduced until 95% of reliability is achieved.

Error from the output

As mentioned before, Monte Carlo Simulation is a method with high accuracy and high computational costs when number of iterations is sufficient. In this case, 1000 times is applied in reliability analysis, and the corresponding accuracy and error is discussed.

As a thrum of rule, the standard deviation of output from Monte Carlo Simulation can be determined by the equation:

$$\sigma_{P_f} = \sqrt{\frac{P_f(1-P_f)}{N}} \tag{5.1}$$

Where, σ_{P_f} is the standard deviation of probability of failure, and N is the numbers of simulation times.

In Monte Carlo simulations, the 95% confidence interval for the probability of failure performance ($P_f \pm 1.96\sigma_{P_f}$) is required, the absolute error can be estimated from the following equation.

$$|\varepsilon| = \left|P_f - P\right| \leq 1.96\sigma_{P_f} = 1.96\sqrt{\frac{P_f(1-P_f)}{N}} \tag{5.2}$$

Table 5.4 illustrates the results of new thresholds and errors for each model to reach a reliability of 95%.

Number of Model	Serviceability Limit State (kN)	Reliability against SLS (%)	Reduced threshold (kN)	Updated Reliability (%)	Stand deviation (%)	Error (%)
Model 1	24000	100	8219	95	0.6	1.35
Model 2	24000	100	5629	95.1	0.6	1.35
Model 3	24000	100	5023	95.1	0.6	1.35

Table 5.4 Reduced threshold for 3 models

As shown in the table, the error of reliability in 1000 simulations is 1.35%. Based on the Equation (5.2), if an error of 1% is required, then, calculation times N can be recalculated equals to 1824. Since negligible increase in accuracy will lead to much more extra generation times. Due to high computation costs, in this research, an error of 1.35% is accepted. Furthermore, even the mean values of shear forces in the joints of all three models are similar with each other, the reduced threshold values vary significantly among different models.

The CDF (cumulative density function) plots of the reliability against reduced threshold of shear forces are shown below.

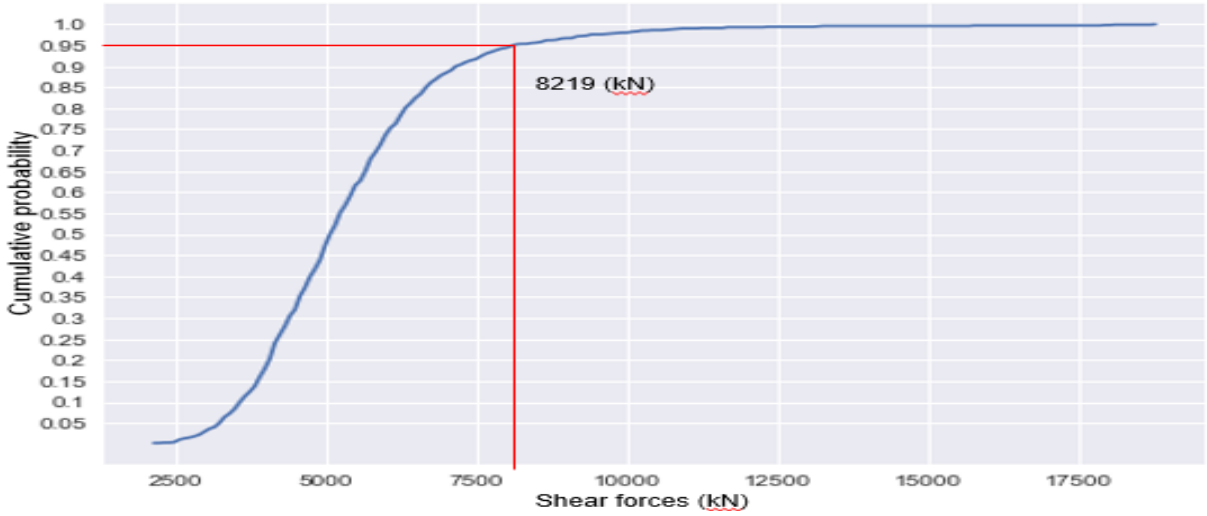

Figure 5.17 Cumulative density function plot of reliability against reduced threshold in 1st model

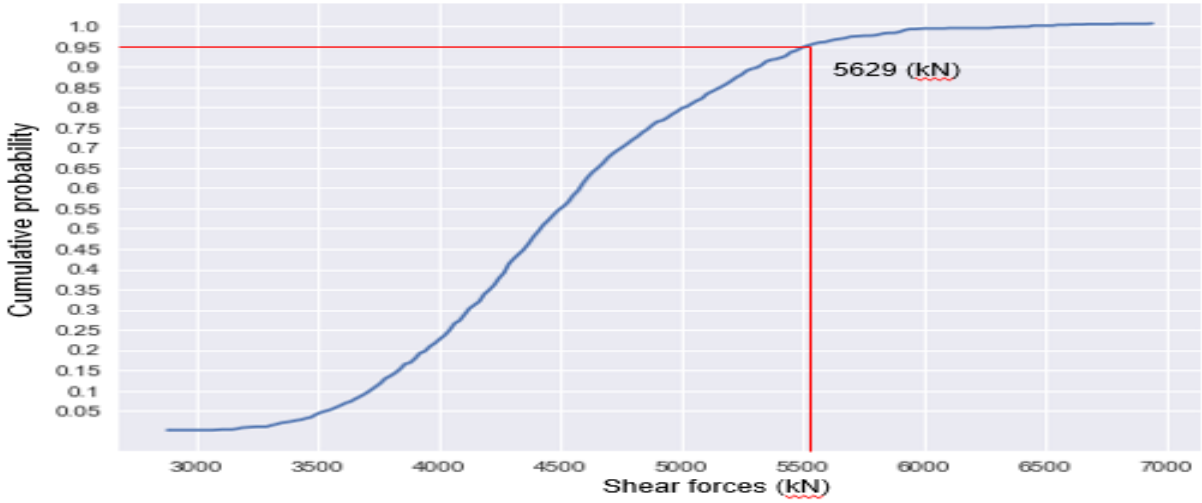

Figure 5.18 Cumulative density function plot of reliability against reduced threshold in 1st model

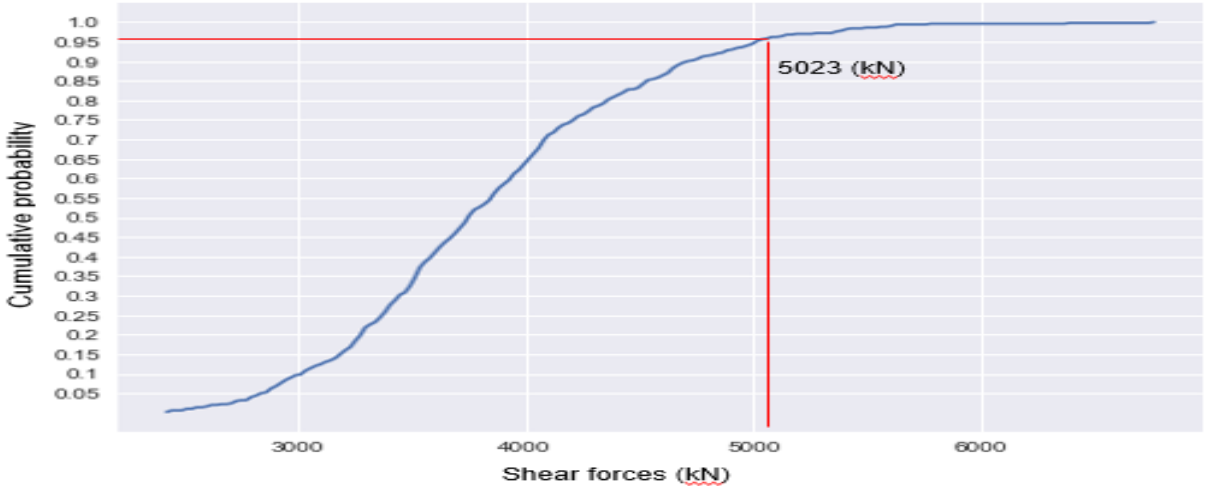

Figure 5.19 Cumulative density function plot of reliability against reduced threshold in 1st model

Discussion

In the 1st model, global soil domain is divided into 15 soil columns with a length of 180 meters. During one generation, there are 15 different input variables independent to each other. Since the loads are acting uniformly on each element and are considerably different from each other, resulting in peak values of shear forces in the element joints and trough values in the middle of every element (Figure 5.20). Furthermore, the tunnel structure itself will bare less shear forces compared with joints.

Figure 5.20 Shear force distribution along tunnel line in 1st model from PLAXIS Output in one generation

In the 2nd model, soil column underlying each element is further classified into 8 soil polygons, and there are 120 (15*8) input variables in one generation. Consequently, the potential differential settlement is uniformized and shear forces can be somehow transferred to concrete structure (Figure 5.21), thus the number of generation with higher shear forces is also to some extent reduced.

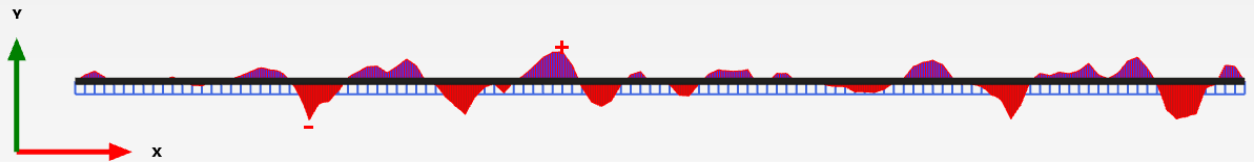

Figure 5.21 Shear force distribution along tunnel line in 2nd model from PLAXIS Output in one generation

In the 3rd model, the number of input variables within one generation is the same as that in the 2nd model, while the difference is they are correlated to each other rather than independent. In this condition, the output of shear force leads to a more uniformed distribution compared with the former two models. Furthermore, correction of stiffness plays an important role in reducing peak values of shear forces. And that is one of the reason that the 3rd model has the lowest threshold value to achieve a reliability of 95%.

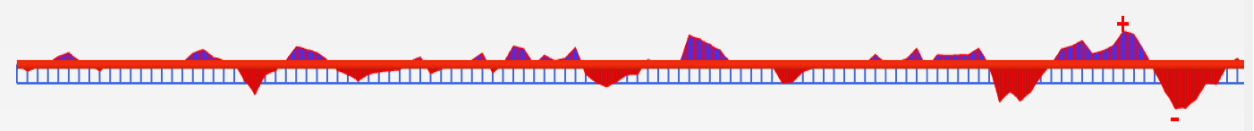

Figure 5.22 Shear force distribution along tunnel line in 3rd model from PLAXIS Output in one generation

6. Conclusion and Recommendations

6.1 Answering to the research questions

1. What are the influence factors of differential settlement in immersed tunnel foundation?

The differential settlement between one part on a structure and another is of greater significance to the stability of the structure than the magnitude of the total settlement. If there is relative movement between various parts of the tunnel, stresses are set up in the structure. Serious cracking, damaging of the tunnel joints, may occur while the differential movements are excessive. Differential settlements between parts of an immersed tunnel may occur as results of the following:

a) Variations in strata.

One elements of the tunnel may be placed on a compressible soil and the other on incompressible or relative stiffer material.

In areas of irregular bedrock surface, parts of a tunnel may be founded on shallow rock and others on soil or compressible weathered rock. Or the layer thickness between the element bottom and the bedrock may also be different.

b) Variations on foundation loading.

In ideal condition, the load acting on tunnel elements are similar with each other. While in the reality, the tunnel line is not paralleled to the sea level, which means, those elements with deeper elevation, will suffer larger siltation after construction. Then the load acting on these elements are obviously larger than others.

c) Variation in site conditions.

One part of the tunnel area may have been occupied by a heavy structure which had been removed or demolished; or on a sloping site it may be necessary to remove a considerable thickness of overburden to form a level site. These variations result in different stress state both before and after loading with consequent differential settlement or swelling.

2. How uncertainties of soil stiffness will impact on differential settlement?

Generally, the different settlement occurs in the condition that structure is placed on inhomogeneous soil layer, the heterogeneity includes the thickness of soil layers and the properties of the soil.

In conventional method, the settlement calculation is a deterministic approach based on the average values of soil properties, as well as the layer thickness. While in most cases due to inherent spatial variability, the soil properties might vary from one site point to another. And these points may have the same mean values, thus, resulting in the same settlement magnitude in conventional method, which is unrealistic in practical engineering condition. On behalf of

understanding the real impact of these uncertainties on different settlement, probabilistic methods are applied in determination of settlement based on the stochastic characteristics (distribution type, mean values μ, standard deviation σ, coefficient of variation cov) of the parameters instead of mean values only.

Consequently, the settlement results also follow a certain type of distributions other than a single value. Thus, the possibility of potential different settlement caused by soil spatial variability can be defined as discussed in Chapter 4.

3. What is the criterion of tunnel joints design regarding shear force?

Limit state design requires the structure to satisfy two principal criteria: the ultimate limit state (ULS) and the serviceability limit state (SLS). A limit state is a set of performance criteria (e.g. vibration levels, deflection, strength, stability, buckling, twisting, collapse) that must be met when the structure is subject to loads. Any design process involves numbers of assumptions. The loads to which a structure will be subjected must be estimated, sizes of members to check must be chosen and design criteria must be selected. All engineering design criteria have a common goal: that of ensuring a safe structure and ensuring the functionality of the structure.

Ultimate Limit State (ULS) for tunnel joints regarding shear forces:

To satisfy the ultimate limit state, the structure most not collapse when subjected to the peak design load. A structure is deemed to satisfy the ULS criteria if all factored bending, shear and tensile of compressive stresses are below the factored resistance calculated for the section under consideration.

The ULS of shear force for tunnel joints depends on the number of shear keys within one joint, in HZMB project, there are four shear keys in one joint, and each shear key has a shear capacity 8 MN for ULS, resulting in the ULS for one tunnel joint is 8 MN*4 = 32 MN.

Serviceability Limit State (SLS) for tunnel joints regarding shear forces:

To satisfy the serviceability limit state criteria, a structure must remain functional for its intended use subject to routine loading, and such the structure must not cause occupant discomfort under routine conditions.

The SLS of shear force for tunnel joints also depends on the number of shear keys, and the shear capacity for each shear key in SLS is 6 MN, thus, the SLS of shear force for one tunnel joint is 6 MN*4 = 24 MN

4. What is the reliability of shear forces in tunnel joints against SLS, taking spatial variability of the soil into account?

The reliability analysis is performed in Chapter 5, for three different models, the first two models are set up without correlation length of soil stiffness, while in the third model a horizontal scale of fluctuation of stiffness ($\theta_h = 120\ m$) is applied. In all cases, probability of failure against SLS (24MN) are zero, and then updated threshold values are determined for three models to achieve a reliability of 95%, in another word, probability of failure of 5%. As shown in the Table 5.4, the updated threshold values are 8219 kN, 5629 kN and 5023 kN, respectively.

5. How gravel bed will influence on immersed tunnel settlement?

The influence of gravel bed on immersed tunnel settlement is analyzed in Chapter 4, a Monte

Carlo Simulation is performed on the settlement calculation in case that tunnel elements are placed on a 1.3 m gravel bed. The result is compared with the condition that without gravel, in which elements are installed directly on the natural subsoils. The comparison indicates that application of gravel bed will reduce the settlement for most elements, the averaged settlement reduction is approximately 9% among all elements.

While among the 1000 generations in Monte Carlo Simulations, the range of fluctuation of settlement result for each element decreases due to gravel bed. The coefficient of variation (COV) for each settlement decreases by 17% averagely.

6.2 Main Conclusions

1. Point Estimate Method is a computationally efficient probabilistic method that can be used to determine the approximate distribution of the output. However due to various assumptions made in PEM, the results may not be very accurate. In contrast, Monte Carlo Simulation can generate the exact distribution of the output, and the results is with high accuracy when calculation times are enough, whereas this method is not efficient due to high computational costs in the case that large numbers of calculation times is required.
2. The function of gravel bed is not only reducing the total settlement, but also uniformizing the settlement distribution along the tunnel alignment. In other words, the possibility of ultimate differential settlement can be reduced. The relative displacement of two adjacent settlements may cause potential high shear forces in the joint, which in this way can also be limited by installation of gravel bed.
3. The shear forces in element joints depends on two main factors:

   a) The difference of loads acting on two nearly element.

   b) The difference of stiffness of soil underneath two adjacent elements.

   In the case that values of loads are constant, peak values of shear forces in the joints occurs in between two elements with highly deviated stiffness distributions even they are correlated.
4. The shear forces in segment joints will decrease slightly along with increasing scale of fluctuation of subsoil stiffness, only when the value of SOF is chose as infinite, significant reduction of shear forces can be found except peak values.
5. In this project, the reliability against SLS is 100% in all three models (Chapter 5). To achieve a reliability of 95%, the model with correlation length (3rd model) has the lowest threshold of shear capacity.
6. 1000 iterations in Monte Carlo Simulation in reliability analysis is acceptable with an error of 1.35 %. To achieve a lower error, 1 %, larger amount of extra iterations is needed, leading to 1824 iterations. Thus, considering both accuracy and efficiency, using 1000 iterations in this research is more appropriate.

6.3 Recommendations

In this paper soil properties are modelled as variables and reliability of the tunnel joints against shear failure is analyzed by Monte Carlo Simulation in cooperation with PLAXIS. However, in order to fully establish the effectiveness and accuracy of such a method, further improvements

and investigations should be performed. Some recommendations and further research are summarized here.

1. Due to time limitation this thesis only focuses on the soil variability along the tunnel line, the uncertainties in transversal direction should be taken in to account and a 3-D model is required to set up to get a comprehensive understanding of the tunnel behavior.
2. The reliability analysis is performed only on shear forces of tunnel joints, due to the uncertainties in transversal direction, torque failure may occur, which can also be researched by a 3-D model.
3. Only two probabilistic methods (Point Estimate Method and Monte Carlo Simulation) are implemented in this paper, more suitable methods can be used in settlement calculation as well as reliability analysis. The results can be compared with each other and the most suitable method can be used in further research considering the accuracy and computational costs.
4. Due to limitation of the soil data, the scale of fluctuation of soil stiffness is determined in a simplified way (Space average method), while more detailed data and accurate methods should be applied in this approach, to generate the most realistic scale of fluctuation and define the influence on joints reliability.
5. Random Finite Element Method cannot be implemented in PLAXIS, this should be involved in the future. So far, users can only define the properties of “soil blocks” by programing in Python, which is time consuming and the software PLAXIS needs a lot of time to assign properties for each soil block.

Bibliography

Baecher, G. B. (2005). Reliability and statistic in geotechnical engineering.

Ching, J. (2011). Practical Monte Carlo based reliability analysis and design methods for geotechnical problems. In P. S. Mordechai, *Applications of Monte Carlo Method in Science and Engineering* (pp. 758-780).

Cornell. (1969). A probability-based structural code. *ACT-Journal*, pp. 974-985.

Gang, W. (2012, 11 29). Analysis of Settlement Reasons and Machanism in Immersed Tunnel. *Applied Mechanics and Materials*, pp. 803-807.

Griffiths. (1999). Slope stability analysis by finite elements. *Geotechnique,49*.

Hicks, M. (2016). *Lecture Notes cie4395.*

Hu, Z.-n. (2015). Challenges and strategies involved in designing and construction a 6 km immersed tunnel: A case study of the Hong Kong-Zhuhai-Macao Bridge. *Tunnelling and Underground Space Technology*, pp. 171-177.

Ingerslev. (2005). Considerations and strategies behind the design and construction requirements of the Istanbul Strait mmersed tunnel. *Tunnelling and Underground Space Technology. 20.*, pp. 604-608.

Kulhawy, E. (1992). On evaluation of static soil properties. *Stability and performance of slopes and embanckments.*

Lunniss&Baber. (2013). *Immersed Tunnels.*

Meigh. (1987). Cone penetration testing. In Meigh.

Phoon. (1995). Reliability-based design of foundations for transmission line structures. In *Computers and Geotechnics.*

Rebonato. (1999). The most general methodology to create a valid correlation matrix for risk management and option pricing purpose.

Richard, L. (2013). *Immersed Tunnels.*

Ronald. (2016). *PLAXIS 2D Reference Manual.*

Rosenblueth. (1975). Point estimates for probability moments. *Mathematics*, pp. 3812-3814.

S.P.Kamp. (2016). *Reliability-based ultimate limit state design in finite element methods.*

Schemertmann. (1970). Static cone to compute static settlement over sand. *ASCE Journal of Soil Mechnicas and Foundation Division*, pp. 1101-1043.

Schmertmann. (1978). Improved strain influence factor diagrams. *ASCE Journal of the Geotechnical Engineering Division*, pp. 1131-1135.

Schnerder. (2012). Dealing with uncertainties in EC7 with emphasis on determination of characteristic soil proerties. *IOS Press.* Rotterdam.

Tawfiq, K. (2010). *Soil Settlement. Lecture Notes.*

Tomlinson. (2001). *Foundation design and construction seventh edition.*

Vanmarcke. (1977). Probabilistic modeling of soil profiles. *Journal of the Geotechnical Engineering Divisions, ASCE*, pp. 1227-1246.

Walter. (2001). Immersed tunnel settlements Part 1: nature of settlements. *Tunnelling and Underground Space Technology*, pp. 195-201.

APPENDIX A

A.1 The Cone Penetration Test

The CPT procedure

In a CPT cone, connected by rods, will be pushed into soil with a certain constant penetration rate. During the penetration continuous measurements are made of penetration resistance of the cone and the sleeve. When using a piezocone, measurements of the pore pressure are registered as well. The definitions above are visualized in Figure 3.4. Standard electronic cones have a 60 degrees apex angle and a cross-section area of either $10cm^2$ or $15cm^2$ (Roberson and Cabal, 2015). The standard length for a rod is one meter.

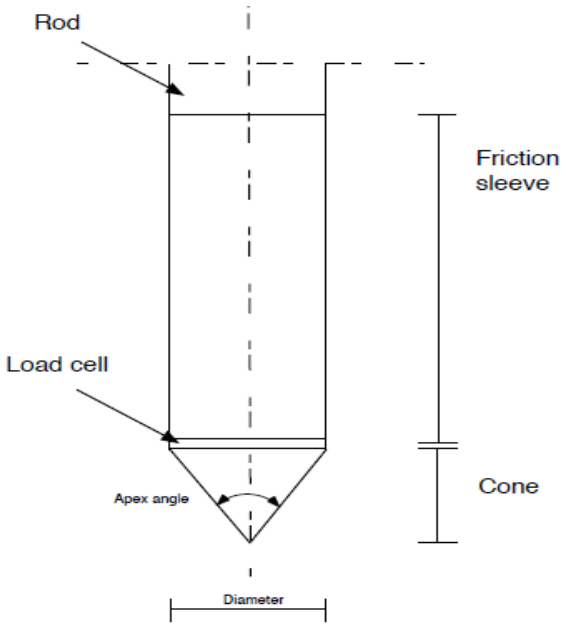

Figure A.1 CPT components

To obtain reliable results from field operations with cone penetrometers, well qualified operators and good technical back-up facilities for calibration and maintenance of the equipment are required. The test procedures are covered by the following sections, and the scientific background of CPT is described.

1. Pre-drilling

For penetration in fills or hard soils it may be necessary to pre-drill in order to avoid damaging the cone.

2. Verticality

The thrust machine should be set up so as to obtain a thrust direction as close as possible to vertical. The deviation of the initial thrust direction should not exceed 2 degrees. The deviation of the initial thrust direction from vertical should not exceed 2 degrees and push rods should be checked for straightness. Modern cones have simple slope sensors incorporated to enable a measure of the non-verticality of the sounding. This is useful to avoid damage to equipment and breaking of push rods

3. Rate of penetration

The standard rate of penetration is the standard rate of penetration is 2cm/sec (approximately 1 inch per

Second). The cone results are generally not sensitive to slight variations in the rate of penetration.

4. Interval of readings

Electric cones produce continuous analogue data. However, most systems convert the data to digital form at selected intervals. Most standards require the interval to be no more than 200 mm (8 inches). In general, most systems collect data at intervals of between 25-50 mm (1 to 2 inches).

5. Dissipation Tests

During a pause in penetration, any excess pore pressure generated around the cone will start to dissipate. The rate of dissipation depends upon the coefficient of consolidation, which in turn, depends on the compressibility and permeability of the soil. The rate of dissipation also depends on the diameter of the probe. A dissipation test can be done at any required depth by stopping the penetration and measuring the decay of pore pressure with time. It is common to record the time to reach 50% dissipation. Dissipation rate increases as probe size decreases.

6. Calibration and maintenance

Calibrations should be carried out at regular intervals based on the stabilities of the zero load readings. Typically, if the zero load readings remain stable, the load cells do not require check calibration. For major projects, check calibrations can be carried out before and after the field work, with functional checks during the work. Functional checks should include recording and evaluating the zero load measurements (baseline readings).

A.2 The Lab Test Results (in Chinese)

表 14.3.2.3 变形计算岩土参数建议值

	e	OCR	μ	Cc	Cs	Es	m_v				Cv				Caε			
单元层号	天然孔隙比	超固结比	泊松比	压缩指数	回弹指数	压缩模量(MPa)	加荷条件下体积压缩系数（MPa^{-1}）		卸载再加荷条件下体积压缩系数（MPa^{-1}）		加荷条件下固结系数（m^2/y）		卸载再加荷条件下固结系数（m^2/y）		加荷条件下次固结系数（‰）		卸载再加荷条件下次固结系数（‰）	
							(50~100) kPa	(100~200) kPa	(50~100) kPa	(100~200) kPa	(50~100) kPa	(100~200) kPa	(50~100) kPa	(100~200) kPa	(50~100) kPa	(100~200) kPa	(50~100) kPa	(100~200) kPa
11	1.723	0.94	0.328	0.69	0.03		1.42	0.71	0.23		1.842	2.322	8.669		8.013	7.281	1.947	
14		1.86				10												
21	0.866	1.52	0.315	0.27	0.03		0.19	0.13	0.09	0.12	3.360	3.390	5.857	3.342	1.081	1.646	0.385	1.365
22		1.40	0.250			21												
31	1.052	2.16	0.324	0.46	0.02		0.19	0.13	0.09	0.12	3.360	3.390	5.857	3.342	1.081	1.646	0.385	1.365
32	0.958	1.49	0.296	0.34	0.03		0.30	0.21	0.12	0.08	3.721	3.107	6.242	4.786	1.597	1.997	0.237	0.719
33	0.826	1.08	0.270			34.4												
34	0.700	1.40	0.290			62.0												
41	0.827	1.19	0.272	0.32	0.03		0.20	0.14	0.08	0.06	3.750	3.400	4.297	3.804	0.935	1.083	0.136	0.145
42	0.650	1.01	0.270			33.4												
44	0.470	1.25	0.290		0.006	68.7									0.462	0.549	0.077	0.121
45	0.460	1.42	0.300			41.0												

注：不同荷载阶段的体积压缩系数、固结系数和次固结系数详见附表 5；；不排水条件下细粒土的泊松比建议采用 0.5。

A.3 Summary of soil properties (English)

Number of Element	acting load	underlying layer	thickness	density(g/cm^3)	Unit weight kN/m3	e	OCR	Cc compresion index	Cr(回弹指数) recompression index	Es (Mpa)	Eur (Mpa)
E10		32	0.47	1.85	18.13	0.958	1.49	0.34	0.0300		
		33	0.44	1.92	18.82	0.826	1.08			44.9	179.6
		44	19.57	2.03	19.89	0.470	1.25		0.0060	77.5	310.0
		42	5.63	2.00	19.60	0.650	1.01			73.1	292.4
		45	3.0	2.05	20.09	0.460	1.42			62.8	251.2
Number of Element		underlying layer	thickness	density(g/cm^3)	Unit weight kN/m3	e	OCR	Cc compresion index	Cr(回弹指数) recompression index	Es (Mpa)	Eur (Mpa)
E11		44	16.9	2.03	19.89	0.470	1.25		0.0060	48.3	193.2
		42	14.24	2.00	19.60	0.650	1.01			36.9	147.6
Number of Element		underlying layer	thickness	density(g/cm^3)	Unit weight kN/m3	e	OCR	Cc compresion index	Cr(回弹指数) recompression index	Es (Mpa)	Eur (Mpa)
E12		44	15.78	2.03	19.894	0.470	1.25			51.1	204.4
		42	5.21	2.00	19.6	0.650	1.01		0.0060	36.9	147.6
		45	4.9	2.05	20.09	0.460	1.42			45.6	182.4
Number of Element		underlying layer	thickness	density(g/cm^3)	Unit weight kN/m3	e	OCR	Cc compresion index	Cr(回弹指数) recompression index	Es (Mpa)	Eur (Mpa)
E13		32	2.56	1.85	18.13	0.958	1.49	0.34	0.0260		
		44	15.28	2.03	19.894	0.470	1.25		0.0060	60.3	241.2
		41	0.88	1.90	18.62	0.827	1.19	0.32	0.0300		
		42	20.58	2.00	19.6	0.650	1.01			36.9	147.6
Number of Element		underlying layer	thickness	density(g/cm^3)	Unit weight kN/m3	e	OCR	Cc compresion index	Cr(回弹指数) recompression index	Es (Mpa)	Eur (Mpa)
E14		32	3.83	1.85	18.13	0.958	1.49	0.34	0.0300		
		34	0.89	1.92	18.82	0.700	1.40			63.3	253.2
		42	3.28	2.00	19.60	0.650	1.01			15.1	60.4
		44	10.48	2.03	19.89	0.470	1.25		0.0060	40.6	162.4
		45	2.4	2.05	20.09	0.460	1.42			38.1	152.4
Number of Element		underlying layer	thickness	density(g/cm^3)	Unit weight kN/m3	e	OCR	Cc compresion index	Cr(回弹指数) recompression index	Es (Mpa)	Eur (Mpa)
E15		34	1.3	1.92	18.816	0.700	1.40			63.3	253.2
		32	3.29	1.85	18.13	0.958	1.49	0.34	0.0300		
		41	2.7	1.90	18.62	0.827	1.19	0.32	0.0300		
		44	8.98	2.03	19.894	0.470	1.25		0.0060	28.2	112.8
		42	14.66	2.00	19.6	0.650	1.01			15.1	60.4

Number of Element		underlying layer	thickness	density(g/cm^3)	Unit weight kN/m3	e	OCR	Cc compresion index	Cr(回弹指数) recompression index	Es (Mpa)	Eur (Mpa)
E16		32	3.7	1.85	18.13	0.958	1.49	0.34	0.0300		
		33	2.05	1.92	18.816	0.826	1.08			30.8	123.2
		34	0.85	1.92	18.816	0.700	1.40			63.3	253.2
		44	12.8	2.03	19.894	0.470	1.25		0.0060	42.6	170.4
		42	0.85	2.00	19.6	0.650	1.01			15.3	61.2
		45	7.2	2.05	20.09	0.460	1.42			26.5	106
Number of Element		underlying layer	thickness	density(g/cm^3)	Unit weight kN/m3	e	OCR	Cc compresion index	Cr(回弹指数) recompression index	Es (Mpa)	Eur (Mpa)
E17		32	4.69	1.85	18.13	0.958	1.49	0.34	0.0300		
		44	30	2.03	19.894	0.470	1.25		0.0060	54.8	219.2
Number of Element		underlying layer	thickness	density(g/cm^3)	Unit weight kN/m3	e	OCR	Cc compresion index	Cr(回弹指数) recompression index	Es (Mpa)	Eur (Mpa)
E18		32	2.78	1.85	18.13	0.958	1.49	0.34	0.0300		
		33	0.96	1.92	18.816	0.826	1.08			40.3	161.2
		44	11.73	2.03	19.894	0.470	1.25		0.0060	35.5	142
		42	0.62	2.00	19.6	0.650	1.01			36.9	147.6
		45	20.0	2.05	20.09	0.460	1.42			35.3	141.2
Number of Element		underlying layer	thickness	density(g/cm^3)	Unit weight kN/m3	e	OCR	Cc compresion index	Cr(回弹指数) recompression index	Es (Mpa)	Eur (Mpa)
E19		32	0.69	1.85	18.13	0.958	1.49	0.34	0.0300		
		33	0.58	1.92	18.816	0.826	1.08			41.0	164
		45	1.85	2.05	20.09	0.460	1.42			113.5	454
		44	4.77	2.03	19.894	0.470	1.25		0.0060	72.9	291.6
		41	0.43	1.90	18.62	0.827	1.19	0.32	0.0300		
		42	40.00	2.00	19.6	0.650	1.01			36.9	147.6
Number of Element		underlying layer	thickness	density(g/cm^3)	Unit weight kN/m3	e	OCR	Cc compresion index	Cr(回弹指数) recompression index	Es (Mpa)	Eur (Mpa)
E20		32	1.83	1.85	18.13	0.958	1.49	0.34	0.0300		
		44	15.07	2.03	19.894	0.470	1.25		0.0060	43.4	173.6
		42	1.12	2.00	19.6	0.650	1.01			36.9	147.6
		41	0.47	1.90	18.62	0.827	1.19	0.32	0.0300		
		45	30.0	2.05	20.09	0.460	1.42			125.5	502
Number of Element		underlying layer	thickness	density(g/cm^3)	Unit weight kN/m3	e	OCR	Cc compresion index	Cr(回弹指数) recompression index	Es (Mpa)	Eur (Mpa)
E21		32	1.02	1.85	18.13	0.958	1.49	0.34	0.0300		
		33	0.6	1.92	18.816	0.826	1.08			49.5	198
		44	15.78	2.03	19.894	0.470	1.25		0.0060	46.3	185.2
		42	1.24	2.00	19.6	0.650	1.01			18.0	72
		41	0.74	1.90	18.62	0.827	1.19	0.32	0.0300		

Number of Element		underlying layer	thickness	density(g/cm^3)	Unit weight kN/m3	e	OCR	Cc compresion index	Cr(回弹指数) recompression index	Es (Mpa)	Eur (Mpa)
E21		32	1.02	1.85	18.13	0.958	1.49	0.34	0.0300		
		33	0.6	1.92	18.816	0.826	1.08			49.5	198
		44	15.78	2.03	19.894	0.470	1.25		0.0060	46.3	185.2
		42	1.24	2.00	19.6	0.650	1.01			18.0	72
		41	0.74	1.90	18.62	0.827	1.19	0.32	0.0300		
Number of Element		underlying layer	thickness	density(g/cm^3)	Unit weight kN/m3	e	OCR	Cc compresion index	Cr(回弹指数) recompression index	Es (Mpa)	Eur (Mpa)
E22		32	3.39	1.85	18.13	0.958	1.49	0.34	0.0300		
		44	10.49	2.03	19.894	0.470	1.25		0.0060	34.8	139.2
		41	1.26	1.90	18.62	0.827	1.19	0.32	0.0300		
		42	6.57	2.00	19.6	0.650	1.01			27.2	108.8
Number of Element		underlying layer	thickness	density(g/cm^3)	Unit weight kN/m3	e	OCR	Cc compresion index	Cr(回弹指数) recompression index	Es (Mpa)	Eur (Mpa)
E23		32	2.75	1.85	18.13	0.958	1.49	0.34	0.0300		
		33	0.94	1.92	18.816	0.826	1.08			28.4	113.6
		44	9.55	2.03	19.894	0.470	1.25		0.0060	59.2	236.8
		45	9.6	2.05	20.09	0.460	1.42			51.4	205.6
		41	1.46	1.90	18.62	0.827	1.19	0.32	0.0300		
		42	1.08	2.00	19.6	0.650	1.01			41.3	165.2
Number of Element		underlying layer	thickness	density(g/cm^3)	Unit weight kN/m3	e	OCR	Cc compresion index	Cr(回弹指数) recompression index	Es (Mpa)	Eur (Mpa)
E24		32	2.6	1.85	18.13	0.958	1.49	0.34	0.0300		
		33	0.84	1.92	18.816	0.826	1.08			40.3	161.2
		34	0.45	1.92	18.816	0.700	1.40			63.3	253.2
		42	1.52	2.00	19.6	0.650	1.01			36.9	147.6
		44	7.23	2.03	19.894	0.470	1.25		0.0060	36.7	146.8
		41	7.84	1.90	18.62	0.827	1.19	0.32	0.0300		
		45	1.20	2.05	20.09	0.460	1.42			51.4	205.6

APPENDIX B

Histograms of settlement form Monte Carlo Simulations

The X-axial represents settlement values and Y-axial stands for frequency in 1000 calculations.

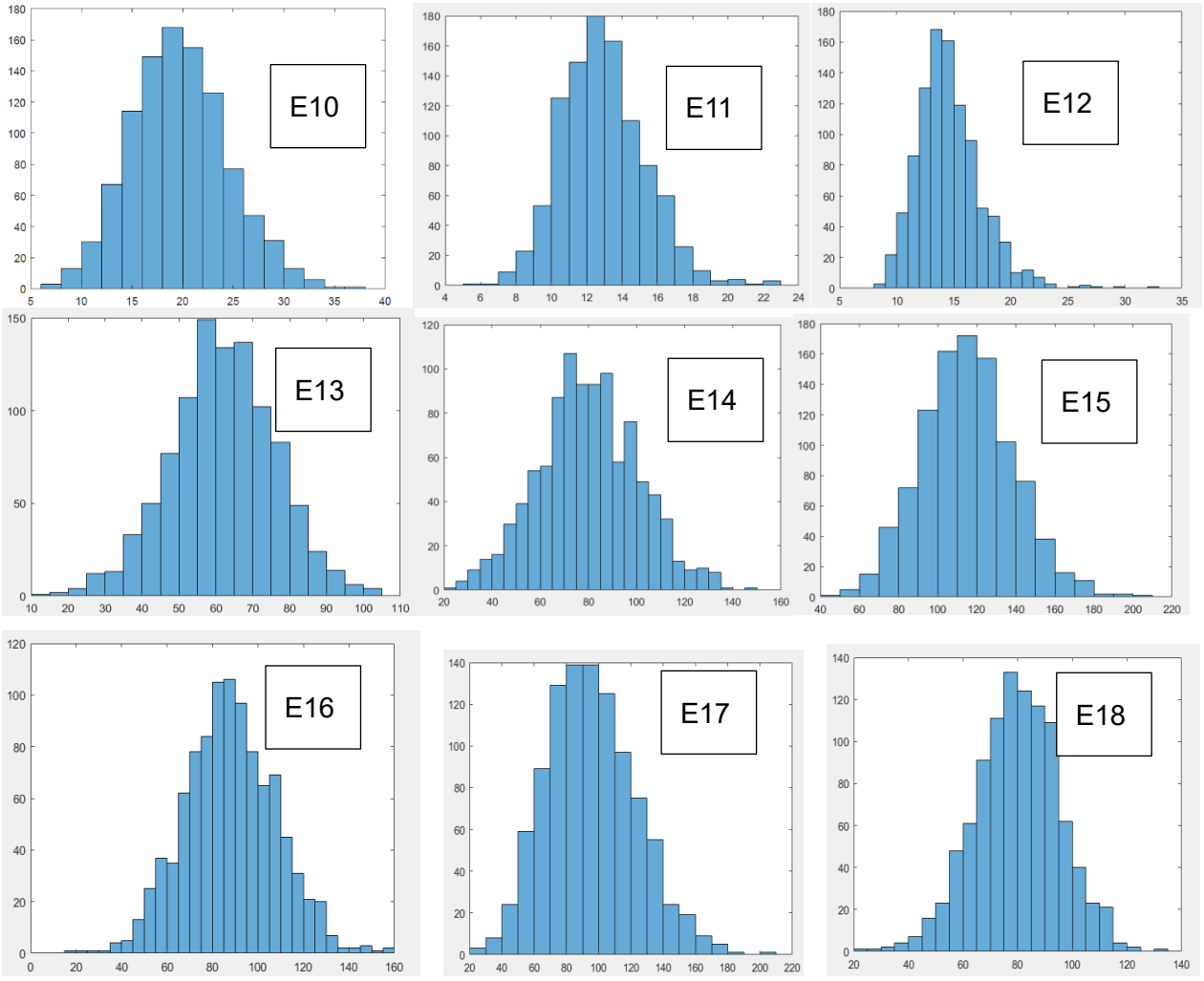

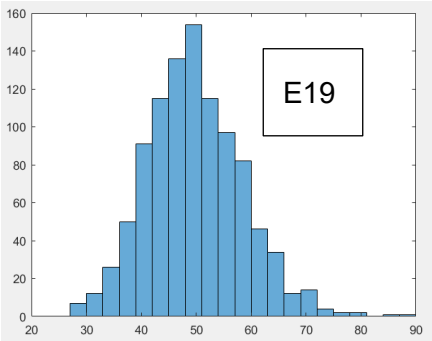
E19

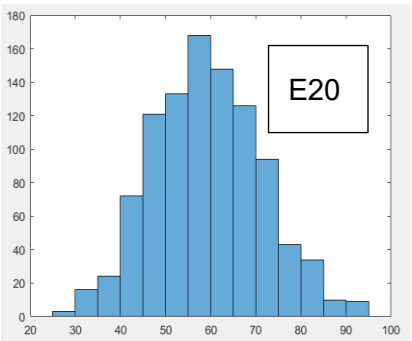
E20

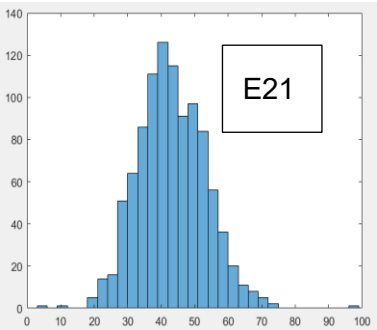
E21

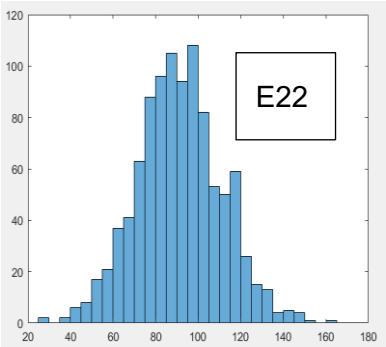
E22

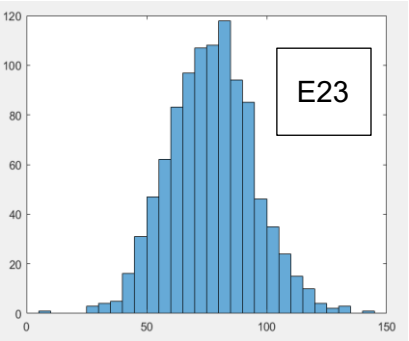
E23

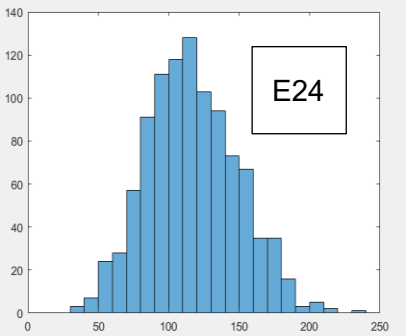
E24

APPENDIX C

Python Scripts

1. Connection

```
# %%%%%%The connection code for python scripts connceting to a certain port number%%%%%
from random import randint
# input port number in PLAXIS 2D application
localhostport_input = 10000 Port number
localhostport_output = 10001
plaxis_path = r'C:\Program Files (x86)\Plaxis\PLAXIS 2D' #no trailing backslash!
import imp
found_module = imp.find_module('plxscripting', [plaxis_path])
plxscripting = imp.load_module('plxscripting', *found_module)
from plxscripting.easy import *
s_i, g_i = new_server('localhost', localhostport_input)
```

Tips: the input port number should be the same as that in PLAXIS server

2. Create Soil domain and Structures

```
#creat soil polygon
soil=[]
for i in range(0,120):
    soil.append(g_i.polygon(((22.5*i),-30),(22.5*(i+1),-30),(22.5*(i+1),0),((22.5*i),0)))

soil_1=g_i.polygon((0,-30),(22.5,-30),(22.5,0),(0,0))
```

3. Create stiffness distribution

```
# Create stiffness distributions for soil below each element
import numpy as np
import math

mu_1,sigma_1 = 334.30E3 , 50.06E3
mu_2,sigma_2 = 372.47E3 , 47.91E3
mu_3,sigma_3 = 338.64E3 , 43.54E3
mu_4,sigma_4 = 120.49E3 , 26.69E3
mu_5,sigma_5 = 102.49E3 , 20.88E3
mu_6,sigma_6 = 69.29E3 , 12.18E3
mu_7,sigma_7 = 102.18E3 , 22.76E3
mu_8,sigma_8 = 95.97E3 , 19.89E3
mu_9,sigma_9 = 111.88E3 , 21.81E3
mu_10,sigma_10 = 168.69E3 , 24.68E3
mu_11,sigma_11 = 151.14E3 , 30.96E3
mu_12,sigma_12 = 205.52E3 , 37.28E3
mu_13,sigma_13 = 103.08E3 , 18.31E3
mu_14,sigma_14 = 122.01E3 , 21.80E3
mu_15,sigma_15 = 79.21E3 ,15.49E3
E10_stiffness = np.random.normal(mu_1,sigma_1,1000)
E11_stiffness = np.random.normal(mu_2,sigma_2,1000)
E12_stiffness = np.random.normal(mu_3,sigma_3,1000)
E13_stiffness = np.random.normal(mu_4,sigma_4,1000)
E14_stiffness = np.random.normal(mu_5,sigma_5,1000)
E15_stiffness = np.random.normal(mu_6,sigma_6,1000)
E16_stiffness = np.random.normal(mu_7,sigma_7,1000)
E17_stiffness = np.random.normal(mu_8,sigma_8,1000)
E18_stiffness = np.random.normal(mu_9,sigma_9,1000)
E19_stiffness = np.random.normal(mu_10,sigma_10,1000)
E20_stiffness = np.random.normal(mu_11,sigma_11,1000)
E21_stiffness = np.random.normal(mu_12,sigma_12,1000)
E22_stiffness = np.random.normal(mu_13,sigma_13,1000)
E23_stiffness = np.random.normal(mu_14,sigma_14,1000)
E24_stiffness = np.random.normal(mu_15,sigma_15,1000)
E_stiffness=[E10_stiffness,E11_stiffness,E12_stiffness,E13_stiffness,E14_stiffness,
           E15_stiffness,E16_stiffness,E17_stiffness,E18_stiffness,E19_stiffness,
            E20_stiffness,E21_stiffness,E22_stiffness,E23_stiffness,E24_stiffness ]
```

4. Create correlated stiffness matrix

```
##creating correlated stiffness matrix##
import pprint
import scipy
import scipy.linalg
a=np.zeros(shape=(120,120)) #empty matrix with shpe of(120, 120)
distance=22.5
sof=120
for i in range(len(a)):
    for j in range(len(a[i])):
        co = math.exp(-distance*abs(j-i)*2/sof)
        if co < 0.1:
            co=0
        a[i][j]=co

Upper = scipy.linalg.cholesky(a, lower=False)
y=[]
for i in range(120):
    y.append(np.random.normal(0,1,1000))
q=list(map(list,zip(*y)))

x=np.matrix(q)*np.matrix(Upper)
x = np.transpose(x)
x = np.asarray(x)

stiffness = [[(each*sigma[int(index/8)]+mu[int(index/8)]) for each in row] for index, row in enumerate(x)]
np.shape(stiffness)
for i in range(len(stiffness)):
    if(i>0)&(i<len(stiffness)-1)&(i%8==0):
        tmp = [(stiffness[i-1][ind]+stiffness[i][ind])/2 for ind,value in enumerate(stiffness[i])]
        stiffness[i-1] = np.random.normal(np.mean(tmp),np.std(tmp),1000)
        stiffness[i] = np.random.normal(np.mean(tmp),np.std(tmp),1000)
Shape of stifnees[] is (120, 1000)
```

Tips: The detailed information of create correlated property matrix in Monte Carlo simulation can be found in Chapter 3 Literature Study.

5. Store data and Open stored data

```
output=list(map(list,zip(*results)))
import json
data = {'data':x}
with open('shearforces.json','w') as output:
    json.dump(data,output)
```

```
with open('shearforces.json','r') as file:
    data_dict = json.load(file)
```

6. Determine the stochastic values from output

```
: import pandas as pd
  shear = [[abs(float(x)) for x in y] for y in shear]
  max_min = np.array(list(map(lambda x:[max(x),min(x),np.mean(x),np.std(x)], shear)))
  header = ['max','min','mean','std']
  df=pd.DataFrame(max_min,columns = header)
  print(df)
  df.to_csv('shearforces.xls',sep="\t", encoding='utf-8',columns=header)
```

The results will be printed on the screen as follow and an excel file will be built for storing the results:

```
              max          min         mean          std
0     1518.410882     0.906270   343.808213   255.940041
1     1655.467448     0.713923   438.107329   311.139457
2     2110.015214     3.174296   429.507966   333.620875
3     1633.300993     0.394389   409.256969   303.653938
4     1688.040349     2.093950   363.436011   279.915732
5     1281.182768     0.233842   348.987103   266.663902
6     1543.390724     0.615515   355.835848   278.699689
7     1340.664709     0.026240   390.279362   298.379380
8     1457.814718     0.225139   383.981645   301.846219
9     1700.166796     0.935776   383.690799   294.716011
10    1529.277590     0.944059   349.641717   281.630560
11    1475.441490     0.223526   354.723650   270.727981
12    1761.406510     0.809685   359.949161   284.948955
13    1512.046959     1.045655   373.443642   285.639596
14    1419.179535     0.523226   355.024811   289.867341
15    1500.827629     1.657733   379.802983   284.540131
16    1641.722512     1.876020   454.139067   345.118120
17    1910.367501     1.216276   743.083765   416.779772
18    2551.676566    16.222265   991.670964   470.658894
19    2635.934657     0.771977  1117.041131   508.187970
20    2931.172561     6.060470   969.329324   517.748732
21    1956.427976     1.527473   583.375439   413.642187
22    3666.748507     7.590188  1101.908649   662.375678
23    6163.860326  1141.384566  3534.035701   808.057847
24    4613.912761   135.506438  1963.662538   774.597492
25    3308.484646     5.653407   881.873170   629.650151
26    2952.913710     2.877389   663.890233   510.088841
27    3216.492115     1.374463   876.445952   618.141255
28    3604.311759     4.084791   994.356754   704.197821
29    3911.897207     0.553406   947.848393   705.177231
..            ...          ...          ...          ...
89    4350.890114     6.793273  1160.365109   806.895984
90    3463.099946     3.723829   980.820950   721.034566
91    3707.404440     2.679773   881.843248   650.076469
92    3044.042010     0.629069   848.111891   625.589945
93    4762.825924     3.327931   982.035957   772.263403
94    5216.784901     4.847484  1972.580561   964.422216
95    6815.037333  1569.257378  4156.820258   979.691586
96    6163.587285    92.243881  2559.489413   991.281990
97    4519.886692     3.349725  1416.619134   858.267530
98    4056.162794     0.444687   895.597998   727.211478
99    3317.746060     2.218131   816.870345   648.175692
100   3860.343921     1.709956  1051.852974   698.112975
101   4023.320578     0.526372  1336.454680   816.564539
102   4562.335010     9.440448  1649.193194   939.293092
103   5815.330239     0.844521  2068.669080  1044.478389
104   5232.853635    13.563592  1665.533365   991.315653
105   4620.631808     1.008982  1323.566672   929.010242
106   4625.549164     5.619582  1106.086551   863.645027
107   4183.275223     0.527492  1032.006755   781.421936
108   4036.527269     6.912170   923.221691   710.243256
109   4844.120322     7.014015  1009.118193   784.668591
110   5255.969341     0.746703  1433.833814   993.163881
111   6713.774300    16.458071  2548.874740  1167.388271
112   6041.923339     0.934375  1749.663363  1079.067977
113   5144.108845     5.857756  1289.408863   935.509570
114   4555.976218     1.816369  1141.825222   873.897808
115   5491.933050     1.553012  1165.190660   955.067786
116   5149.632542     2.608153  1216.142986   959.848935
117   5260.010762     3.326100  1178.337506   947.106181
118   4945.949780     0.298805   836.083179   693.570753

[119 rows x 4 columns]
```

7. Reliability analysis function based on the shear forces

```
def transpose(data):
    data =list(map(list,zip(*data)))
    print(np.shape(data))
    return data

def get_abs(data):
    data = [[abs(float(e)) for e in each] for each in data ]
    return data

def get_proba(data,threshold):
    beyond_proba = [0 for x in range(len(data))]
    for index, value in enumerate(data):
        for each in value:
            if each >= threshold: beyond_proba[index]+=1
    count = 0
    for each in beyond_proba:
        if each >0:count+=1
    proba = count/len(data)
    return proba

def get_threshold(data,num):
    max_values = sorted([max(each) for each in data],reverse=True)
    return max_values[num-1]
```

The output includes reliability against SLS, reduced threshold of shear forces.

```
shear_new=data_dict['data']
np.shape(shear_new)

shear_new = get_abs(shear_new)
shear_new=np.transpose(shear_new)

proba = get_proba(shear_new_,24000)
print(proba)
threshold = get_threshold(shear_new_,50)
print(threshold)
new_proba = get_proba(shear_new_80,threshold)
print(new_proba)
print (np.shape(shear_new_80))
```

```
0.0
5023.05516479
```

Here, value “0.0” is the probability of failure against SLS, and “5023.055 (kN)” is the reduced threshold to achieve a reliability of 95%.